AD-A170 474 WORLD ATLAS OF TOTAL SKY-COVER(U) AIR FORCE GEOPHYSICS 1/2
LAB HANSCOM AFB MA C F BURGER 04 SEP 85
AFGL-TR-85-0198

UNCLASSIFIED F/G 4/2 NL

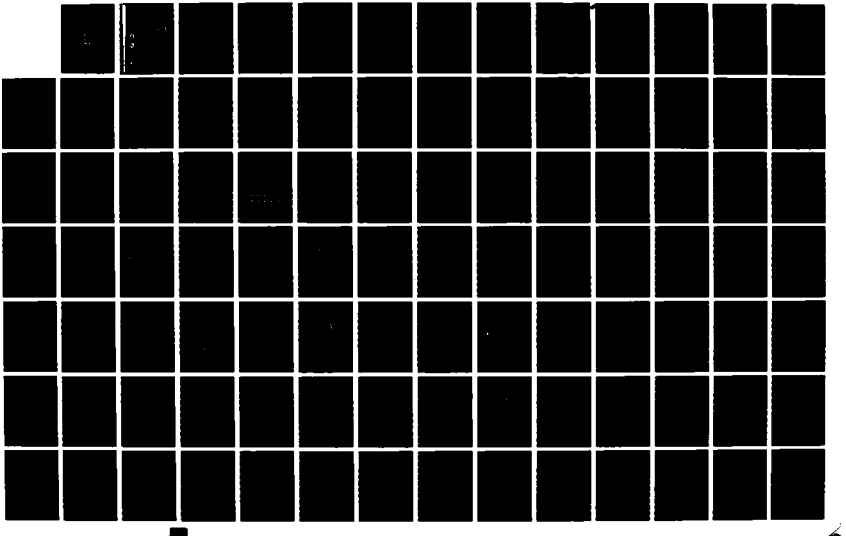

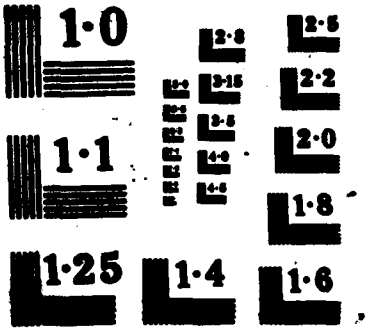
1·0
1·1
1·25
1·4
1·6
1·8
2·0
2·2
2·5

AFGL-TR-85-0198
ENVIRONMENTAL RESEARCH PAPERS, NO. 927

World Atlas of Total Sky-Cover

CHARLES F. BURGER

4 September 1985

ATMOSPHERIC SCIENCES DIVISION PROJECT 6670
AIR FORCE GEOPHYSICS LABORATORY
HANSCOM AFB, MA 01731

This report has been reviewed by the ESD Public Affairs Office (PA) and is releasable to the National Technical Information Service (NTIS).

"This technical report has been reviewed and is approved for publication"

FOR THE COMMANDER

DONALD D. GRANTHAM
Chief, Atmospheric Structure Branch

ROBERT A. McCLATCHEY
Director, Atmospheric Sciences Division

Qualified requestors may obtain additional copies from the Defense Technical Information Center. All others should apply to the National Technical Information Service.

If your address has changed, or if you wish to be removed from the mailing list, or if the addressee is no longer employed by your organization, please notify AFGL/DAA, Hanscom AFB, MA 01731. This will assist us in maintaining a current mailing list.

Do not return copies of this report unless contractual obligations or notices on a specific document requires that it be returned.

UNCLASSIFIED

SECURITY CLASSIFICATION OF THIS PAGE

AD-A170 474

REPORT DOCUMENTATION PAGE

1a. REPORT SECURITY CLASSIFICATION: Unclassified	1b. RESTRICTIVE MARKINGS
2a. SECURITY CLASSIFICATION AUTHORITY	3. DISTRIBUTION/AVAILABILITY OF REPORT: Approved for public release; distribution unlimited.
2b. DECLASSIFICATION/DOWNGRADING SCHEDULE	
4. PERFORMING ORGANIZATION REPORT NUMBER(S): AFGL-TR-85-0198 ERP, No. 927	5. MONITORING ORGANIZATION REPORT NUMBER(S)
6a. NAME OF PERFORMING ORGANIZATION: Air Force Geophysics Laboratory; 6b. OFFICE SYMBOL (If applicable): LYA	7a. NAME OF MONITORING ORGANIZATION
6c. ADDRESS (City, State and ZIP Code): Hanscom AFB, Massachusetts 01731	7b. ADDRESS (City, State and ZIP Code)
8a. NAME OF FUNDING/SPONSORING ORGANIZATION; 8b. OFFICE SYMBOL (If applicable)	9. PROCUREMENT INSTRUMENT IDENTIFICATION NUMBER
8c. ADDRESS (City, State and ZIP Code)	10. SOURCE OF FUNDING NOS.

PROGRAM ELEMENT NO.	PROJECT NO.	TASK NO.	WORK UNIT NO.
62101F	6670	09	12

11. TITLE (Include Security Classification): World Atlas of Total Sky-Cover

12. PERSONAL AUTHOR(S): Burger, Charles F.

13a. TYPE OF REPORT	13b. TIME COVERED	14. DATE OF REPORT (Yr., Mo., Day)	15. PAGE COUNT
Scientific Interim	FROM _____ TO _____	1985 September 4	120

16. SUPPLEMENTARY NOTATION

17. COSATI CODES			18. SUBJECT TERMS (Continue on reverse if necessary and identify by block number)
FIELD	GROUP	SUB. GR.	Global Cloud Climatology; Scale Distance; Boehm Sawtooth Wave Model; Frequency Distribution; Simulation; Mean Sky-Cover
		0402	

19. ABSTRACT (Continue on reverse if necessary and identify by block number)

The purpose of this atlas is to establish a global cloud climatology that details seasonal and diurnal variations. The Boehm Sawtooth Wave (BSW) simulation model is used to devise a method for describing the frequency distribution of total sky-cover. Two parameters, scale distance and mean sky-cover, permit the calculation of the sky-cover distribution from clear to overcast. This is an efficient means of data storage, since two numbers define the entire frequency distribution. Hence, the frequency distribution of sky cover can be found for locations world-wide using the global analyses of mean sky-cover and scale distance given in the atlas. Twenty maps are presented for each of these parameters – one set 4 times daily (0000-0200, 0600-0800, 1200-1400, 1800-2000 LST), for each midseason month (January, April, July, and October), and another set of monthly means for all hours for each midseason month.

20. DISTRIBUTION/AVAILABILITY OF ABSTRACT	21. ABSTRACT SECURITY CLASSIFICATION
UNCLASSIFIED/UNLIMITED ☐ SAME AS RPT ☒ DTIC USERS ☐	Unclassified

22a. NAME OF RESPONSIBLE INDIVIDUAL	22b. TELEPHONE NUMBER (Include Area Code)	22c. OFFICE SYMBOL
Charles F. Burger	(617) 861-5956	LYA

DD FORM 1473, 83 APR EDITION OF 1 JAN 73 IS OBSOLETE

UNCLASSIFIED

SECURITY CLASSIFICATION OF THIS PAGE

Preface

The author wishes to thank Mr. Irving I. Gringorten and Maj. Albert R. Boehm of AFGL who provided valuable guidance. I commend the efforts of Systems and Applied Sciences Corporation and students at Regis College, both under contract, in compiling and computerizing the large volume of climatological data. Finally, I also extend my thanks to Mrs. Helen Connell who typed several drafts of the text and tables.

Contents

Illustrations

Illustrations

Tables

World Atlas of Total Sky-Cover

1. INTRODUCTION

The realistic evaluation of weapon system performance is a critical element in DoD decision making. Since many sensors and systems cannot operate in clouds, the assessment of cloud limitations on their performance plays a key role in the evaluation process. Therefore, the DoD needs cloud models to support the operational evaluation, acquisition, studies and analysis, and war gaming communities. The development of reliable cloud models requires accurate cloud climatologies. The purpose of this atlas is to establish a global cloud climatology that details seasonal and diurnal variations.

Since cloud climatologies are critical elements in global climate modeling, monitoring of climatic variability, and earth-oriented space experiments, a broad spectrum of the non-DoD meteorological community has been interested in this topic in recent years. The establishment of the International Satellite Cloud Climatology Project (ISCCP) indicates wide recognition of the need for an accurate global cloud climatology. According to Schiffer and Rossow,[1] the goal of ISCCP

(Received for Publication 26 August 1985)

1. Schiffer, R. A., and Rossow, W. B. (1983) The International Satellite Cloud Climatology Project (ISCCP): The first project of the World Climate Research Programme, Bull. Am. Meteorol. Soc. 64:779-784.

is to estimate the global distribution of cloudiness by collecting and analyzing satellite data.

2. BACKGROUND

2.1 Previous Work

A variety of global and regional atlases have already been compiled using numerous data sources. The Handbook of Meteorology[2] contains global analyses of monthly mean cloudiness for every other month starting with January. London[3] compiled a mean seasonal global cloud climatology for the Northern Hemisphere based on surface observations taken at 1200 LST. Sadler[4] used satellite data to estimate the average monthly cloud-cover for the tropics. Sherr et al[5] compiled a master file of tabulated cloud statistics and cloud distributions on a world-wide basis, including diurnal and seasonal changes. They defined 29 large-scale homogeneous cloud regions such that the statistics from a single station within the region would adequately represent the entire region. Satellite imagery was included among the data sources. Hall[6] analyzed cloud characteristics at 32 locations in Russia. Frequencies of coverage were given by cloud types – low, middle, and high. Miller and Feddes[7] compiled monthly, seasonal, semiannual, and annual global charts of relative cloud-cover using meteorological satellite data acquired during the period 1 January 1967 through 31 December 1970. Malberg[8]

---

2. Berry, F. A., Jr., Bollay, E., and Beers, N. R. (1945) Handbook of Meteorology, McGraw-Hill Book Company, Inc., New York, pp. 988-996.
3. London, J. (1957) A Study of the Atmospheric Heat Balance, AFCRC-TR-57-287, Final Report, Contract No. AF 19(122)-165, New York University, ASTIN No. 11 7227.
4. Sadler, J. C. (1966) Average Monthly Cloud Cover for the Global Tropics as Determined from Satellite Observations, Preprint Pamphlet, Contract No. AF 19 (628)-3860, Hawaii Institute of Geophysics, University of Hawaii.
5. Sherr, P. E., Glasen, A. H., Barnes, J. C., and Willand, J. H. (1968) World-Wide Cloud Cover Distribution for Use in Computer Simulations, NASA CR-61226, Final Report, Contract No. NAS 8-21040, Allied Research Associates, Inc., Concord, Mass.
6. Hall, R. J. (1969) Cloud Cover of the USSR, SAMSO-TR-69-147, Vol. 1, Contract No. F04701-68-C-0200, Aerospace Corp.
7. Miller, D. B., and Feddes, R. G. (1971) Global Atlas of Relative Cloud Cover 1967-70, NOAA/NESS, USAFETAC.
8. Malberg, H. (1973) Comparison of mean cloud cover obtained by satellite photographs and ground-based observations over Europe and the Atlantic, Mon. Wea. Rev. 101:893-897.

compared satellite and ground-based observations of mean cloud-cover for Europe and the Atlantic. Berlyand and Strokina[9] present a world atlas of mean monthly cloud amounts for every other month starting with January, with data taken from approximately 3400 surface stations and from satellite observations. The maps represent cloud-cover distributions for daylight hours only. Hahn et al[10] published an atlas of co-occurrence of different cloud types over the ocean. Ship observations were used, and the clouds grouped into six types. The results are expressed as contingency probabilities at a resolution of 15° latitude × 30° longitude. They also published a subsequent atlas[11] on the co-occurrence of cloud types over land using a similar analysis procedure on land observations. Henderson-Sellers and Hughes[12] produced a one-year (1979) global cloud climatology using 3DNEPH data exclusively.

Several authors have modeled the frequency distribution of cloudiness as seen by the ground observer or satellite. Each model includes all fractions of coverage ranging from clear to overcast, and is claimed to have versatile statistical characteristics to simulate J- or U-shaped distributions of sky cover as well as more conventional bell-shaped distributions. Henderson-Sellers et al,[13] in explaining the need for a global-scale cloud archive, recommend the Beta distribution model as developed by Falls.[14, 15] Its density function is

$$f(x) = \frac{\Gamma(a+b)}{\Gamma(a)\Gamma(b)} x^{a-1}(1-x)^{b-1} \qquad a,b > 0 \ , \tag{1}$$

---

9. Berlyand, T. G., and Strokina, L. A. (1980) Global distribution of total cloud amount, Gidrometeoizdata, Leningrad (translated by S. Warren).

10. Hahn, C. J., Warren, S. G., London, J., Chervin, R. M., and Jenne, R. (1982) Atlas of Simultaneous Occurrence of Different Cloud Types Over the Ocean, NCAR Technical Note No. TN-201+STR, Atmospheric Analysis and Prediction Division, Boulder, Colo.

11. Hahn, C. J., Warren, S. G., London, J., Chervin, R. M., and Jenne, R. (1984) Atlas of Simultaneous Occurrence of Different Cloud Types Over Land, NCAR Technical Note No. TN-241+STR, Atmospheric Analysis and Prediction Division, Boulder, Colo.

12. Henderson-Sellers, A., and Hughes, N. A. (1984) Cloud Archiving Strategies, AFGL-TR-84-0166, Final Report, Contract/Grant No. AFOSR-83-0118, University of Liverpool, Liverpool, U. K.

13. Henderson-Sellers, A., Hughes, N. A., and Wilson, M. (1981) Cloud archiving on a global scale: a discussion of principles, Bull. Am. Meteorol. Soc. 62:1300-1307.

14. Falls, L. W. (1973) The Beta Distribution: A Statistical Model for World Cloud Cover, NASA Technical Memorandum No. 64714, Marshall Space Flight Center, Ala.

15. Falls, L. W. (1974) The beta distribution: a statistical model for world cloud cover, J. Geophys. Res. 79:1261-1264.

where Γ is the gamma function, x is the fraction of sky covered, and a and b are parameters whose values can vary to permit varying characteristics of the cloud-cover distribution. Falls assigned values to a and b in 29 regions of the world. While the density function is easy to compute, the cumulative probability is difficult to obtain since no succinct analytical expression exists. Therefore, tables, numerical integration, or other approximate methods are necessary to obtain cumulative probabilities.

Bean and Somerville[16] also used the Beta distribution to model cloud-cover distributions world-wide. They used the infrared measurements from a TIROS satellite taken over a period of approximately four years and determined the proportion of cloud cover world-wide over 2.5° latitude-longitude grids. Estimates of a and b were then obtained and grouped into homogeneous regions. Thus, the globe was divided into homogeneous cloud-cover regions for each season.

Somerville et al[17] used the Johnson S_B family of distributions to model total sky-cover for seven diverse locations. The S_B family is given by

$$Z = \gamma + \eta \ln [x/(1 - x)] \quad . \tag{2}$$

The variable x is equal to the fractional coverage, and the parameters γ and η are determined by the data. The variable Z is the equivalent normal deviate (END) of the cumulative probability of x. Z has a mean of zero and a standard deviation of 1. The solution gives the probability that the sky cover will be less than or equal to the fractional cover x. Somerville et al developed 96 pairs of values for γ and η for each station (8 times per day, 12 months) using simple linear regression. The root mean square (rms) error for all stations ranged from 0.0175 to 0.0595.

Somerville and Bean[18] developed another cloud model using the S-distribution, which is given by

$$F(x) = 1 - (1 - x^{\alpha})^{\beta} \quad \alpha, \beta > 0 \quad . \tag{3}$$

As in Eqs. (1) and (2), x is equal to the fractional coverage and F(x) is the probability that the sky cover is less than x. The parameters α and β can be estimated

---

16. Bean, S. J., and Somerville, P. N. (1981) Some new worldwide cloud-cover models, J. Appl. Meteorol. 20:223-228.

17. Somerville, P. N., Watkins, S., and Daley, R. (1978) Some Models for Sky Cover, AFGL-TR-78-0219, Scientific Report No. 2, Contract No. F19628-77-C-0080, Florida Technological University, Orlando, Fla., AD A062650.

18. Somerville, P. N., and Bean, S. J. (1979) A New Model for Sky Cover, AFGL-TR-79-0219, Scientific Report No. 5, Contract No. F19628-77-C-0080, University of Central Florida, Orlando, Fla., AD A078368.

iteratively using either the method of maximum likelihood or a nonlinear regression technique. Both methods are considerably more complicated than the simple linear regression used to obtain Eq. (2). Somerville developed 96 different pairs of values for α and β for 23 stations around the world. The rms errors ranged from 0.003 to 0.071. Strictly speaking, this model, as well as the previously described models, yields zero for the probability of all clear and full overcast; hence they cannot be theoretically accurate. The difficulty is overcome, in practice, by stipulating that the integration for clear be taken from 0 to 0.5 tenths, and for overcast from 9.5 to 10 tenths.

2.2 Current Work

This AFGL atlas uses a mathematical model that describes the frequency distribution of total sky-cover. The model, known as the Boehm Sawtooth Wave (BSW) simulation model, is explained in more detail in Section 3. Like the models of Falls and Somerville, the BSW model uses two parameters. Our model has several advantages over theirs, however. First, both parameters have physical meaning. One parameter is the mean sky-cover, which we identify as the single-point probability of a cloud. The other parameter, which we call scale distance, is the distance over which there is a correlation coefficient of 0.99. The correlation coefficient between points separated by greater distances can be found by Eq. (4) (Section 3). It has been found that the scale distance varies systematically with time of day and time of year, which enhances its choice as a parameter. The second advantage of the BSW model is that it can be extended to provide the distribution of cloud cover, from clear to overcast, over areas of varying sizes, from a few km^2 to 100,000 km^2. A third advantage is that conditions of absolute clear and full overcast have meaningful probabilities, estimated unequivocally by the model.

The scale distance, in combination with the mean sky-cover, permits the calculation of the sky-cover distribution from clear to overcast. Thus, the frequency distribution of sky cover can be found for locations world-wide using the global analyses of mean sky-cover and scale distance given in the atlas. Twenty maps are presented for each of these parameters, one set four times daily (0000-0200, 0600-0800, 1200-1400, and 1800-2000 LST) for each mid-season month (January, April, July, and October), and another set of monthly means for each mid-season month. The model provides for convenient data storage, since two numbers define the entire frequency distribution.

3. THE BSW MODEL

The Boehm Sawtooth Wave (BSW) simulation model was developed by Maj. Albert R. Boehm of AFGL. The model, described in detail in Burger and Gringorten,[19] generates fields (or maps) of normally distributed values called equivalent normal deviates (ENDs). An analytical solution has been found for BSW for the spatial correlation function $\rho(s)$ between points separated by distance (s), in units of the wavelength:

$$\rho(s) = 1 - (12/\pi)s + 3s^2 \quad \text{for } 0 \le s \le 1 \tag{4}$$

$$= 1 - (12/\pi)s + 3s^2 + (24/\pi)[\cos^{-1}(1/s) - \sqrt{s^2 - 1}] \quad \text{for } 1 < s \le 2,$$

where s is the standardized distance given by

$$s = s'/\Lambda \quad , \tag{5}$$

s' is the measured distance (km), and Λ is the wavelength (km). For $s > 2$, $\rho(s)$ oscillates between negative and positive values, converging on zero. The graph of $\rho(s)$ vs s is shown in Figure 1. The correlation is high for short distances, but

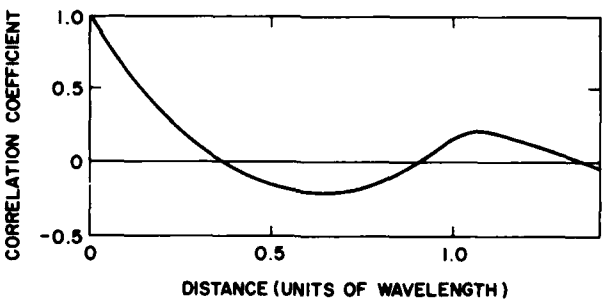

Figure 1. Distance vs Correlation Coefficient for BSW Model

drops monotonically to zero at s = 0.3684, becomes negative, and crosses zero again at s = 0.9049. The distance over which $\rho(s)$ decreases to 0.99 is the model parameter, scale distance (r/km). Eq. (4) yields $\rho(s) \cong 0.99$ over a distance of

---

19. Burger, C. F., and Gringorten, I. I. (1984) Two-Dimensional Modeling for Lineal and Areal Probabilities of Weather Conditions, AFGL-TR-84-0126, AD A147970.

1 km, (r = 1 km) if Λ = 340 km. The ratio between r and Λ is constant, chosen for this atlas to be 1/340. Thus,

$$r = (\Lambda/340) \text{ km} \quad . \tag{6}$$

As previously described,[19] an analytical solution for the probability of a maximum condition in an area or fraction of an area has not yet been found. Instead, we have obtained approximate solutions by a Monte Carlo method. The results were put in graphical form, one graph for each tenth of coverage, from 0 to 10 tenths. The graphs for 0 through 5 tenths are shown in Figures 2 through 7. The graphs for 6 through 10 tenths are not shown because they are merely the inverted mirror images of the graphs for 4 through 0 tenths, respectively. On the graphs, the vertical axes are uniform in the END (y) of the cumulative probability (P). The horizontal axis has a uniform z-scale, where

$$z = \frac{\ln\left(\frac{\sqrt{A}}{r}\right)}{\ln 2} \tag{7}$$

from which we obtain

$$r = \frac{\sqrt{A}}{2^z} \tag{8}$$

A is the area of interest.

The graphs were fitted by empirical equations, making it possible to obtain solutions quickly by computer. The solution is as follows:

$$y' = \alpha + \beta + \gamma + \delta \quad , \tag{9}$$

where y' is the END of the cumulative probability of sky cover for a given fractional coverage (F/10); y' will vary with r and mean sky-cover P_o. The terms α, β, γ, and δ are given in Table 1, and the associated constants in Tables 2 and 3. The variable y_o (from Table 1) is the END of 1 - P_o. When F > 5, the signs of y' and y_o are reversed, and F = 10 - F. In addition, when z > 7 and F is not an integer, $y' = y'[\text{INT}(F)] + [F - \text{INT}(F)]\{y'[\text{INT}(F) + 1] - y'[\text{INT}(F)]\}$.* These solutions are valid only within the bounds of the graphs, and therefore include the following restrictions: $|y'| \leq 3.72$, $|y_o| \leq 4.7$, and $-1 \leq z \leq 8$. Note that the formula permits solutions for any value of F instead of just the integer values, as with the graphs. In other words, the empirical solution interpolates between graphs, so that it is possible, for example, to use the model for eighths of cloud cover as well as tenths.

*INT is a function that acts to truncate any number to its integer value.

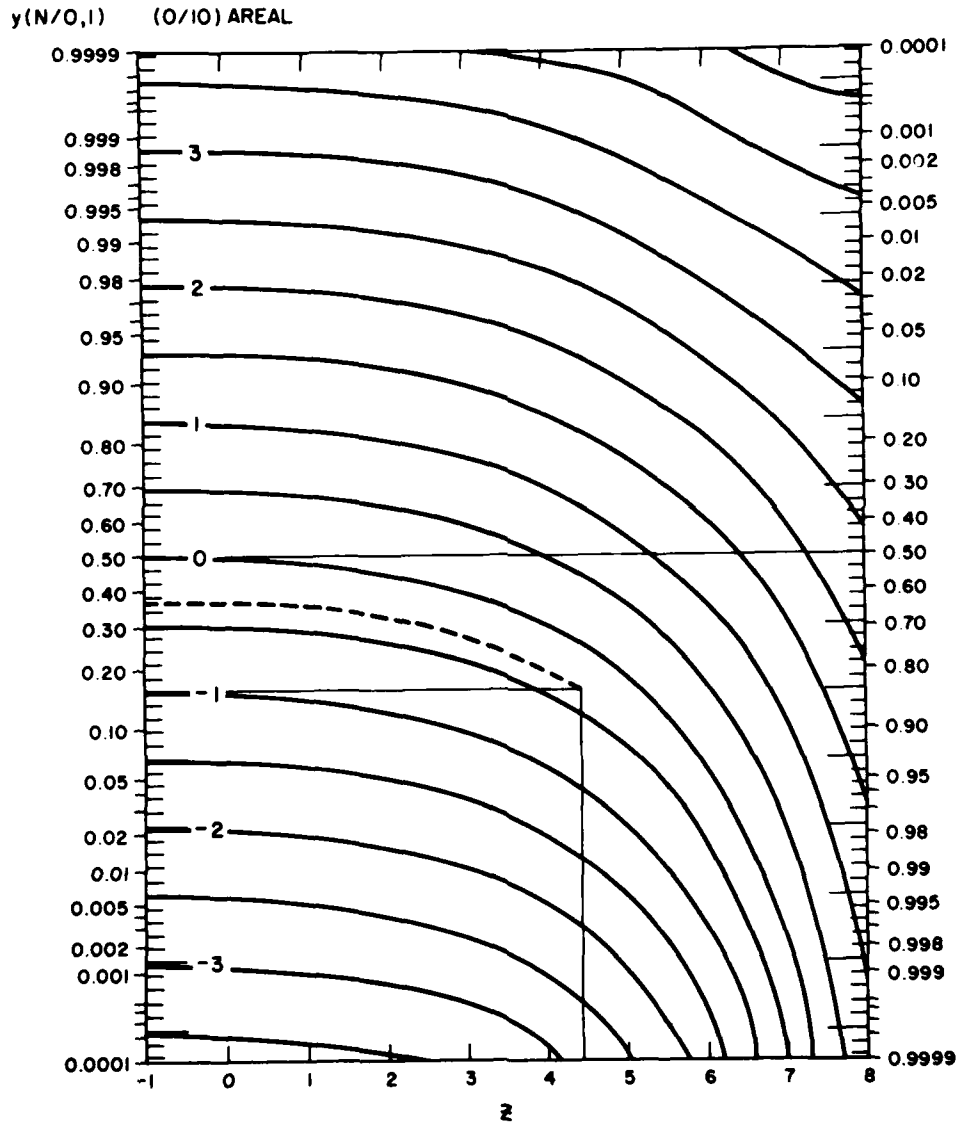

Figure 2. Graph for Estimating P(0/10) and P(< 10/10) Coverage. Each curve corresponds to a single y_0 value, and $z = \ln(\sqrt{A}/r)/\ln 2$. The additional solid lines and dashed curve illustrate an example from Section 3.1

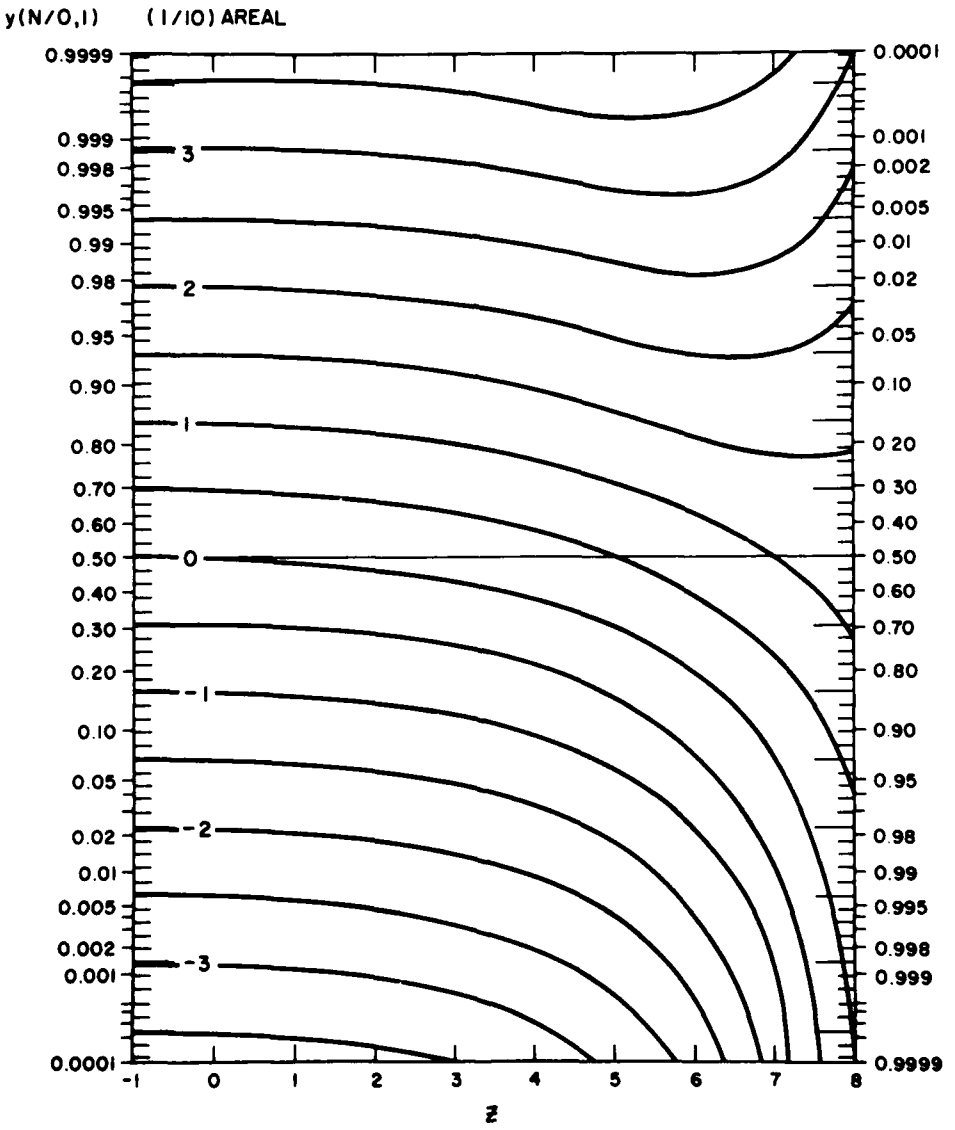

Figure 3. Graph for Estimating $P(\leq 1/10)$ and $P(\leq 9/10)$ Coverage. Each curve corresponds to a single y_o value, and $z = \ln(\sqrt{A}/r)/\ln 2$

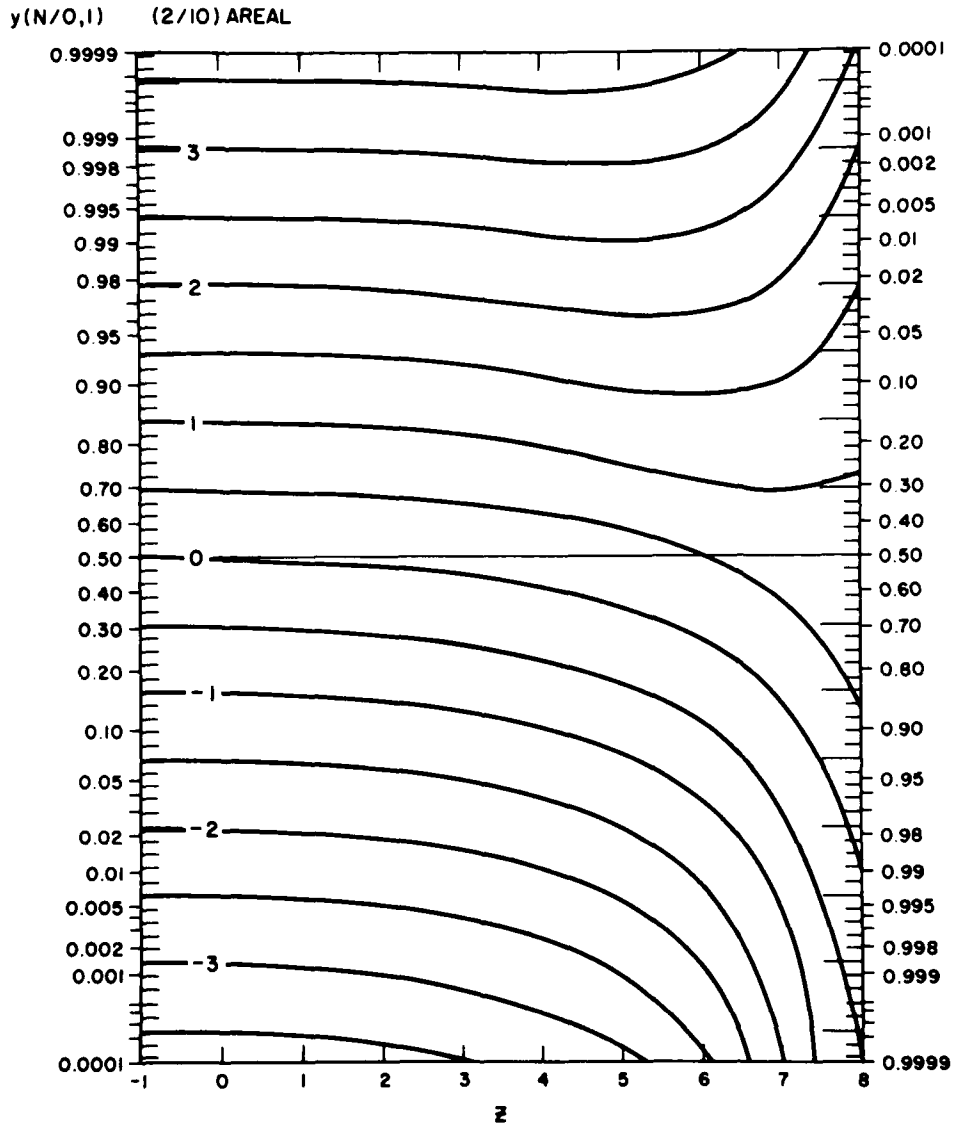

Figure 4. Graph for Estimating $P(\leq 2/10)$ and $P(\leq 8/10)$ Coverage. Each curve corresponds to a single y_o value, and $z = \ln(\sqrt{A}/r)/\ln 2$

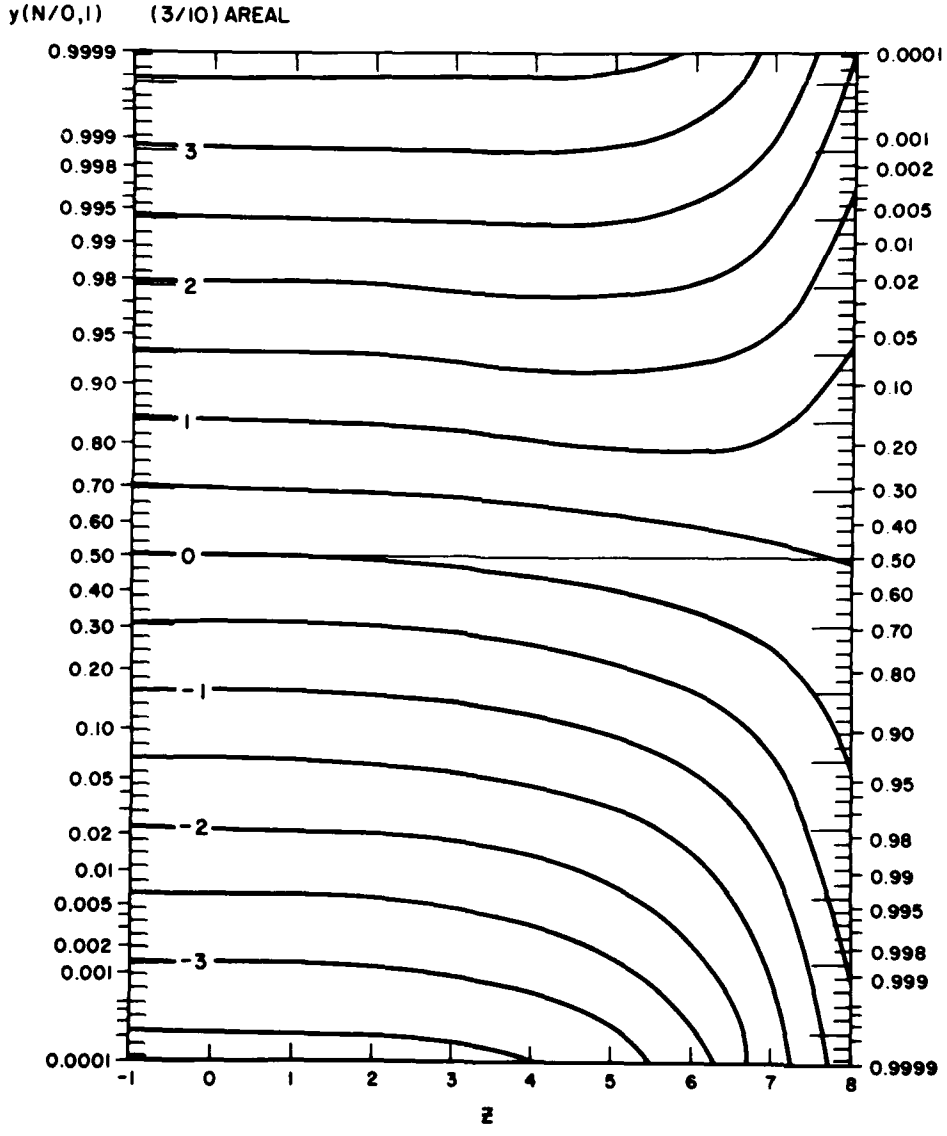

Figure 5. Graph for Estimating $P(\leq 3/10)$ and $P(\leq 7/10)$ Coverage. Each curve corresponds to a single y_o value, and $z = \ln(\sqrt{A}/r)/\ln 2$

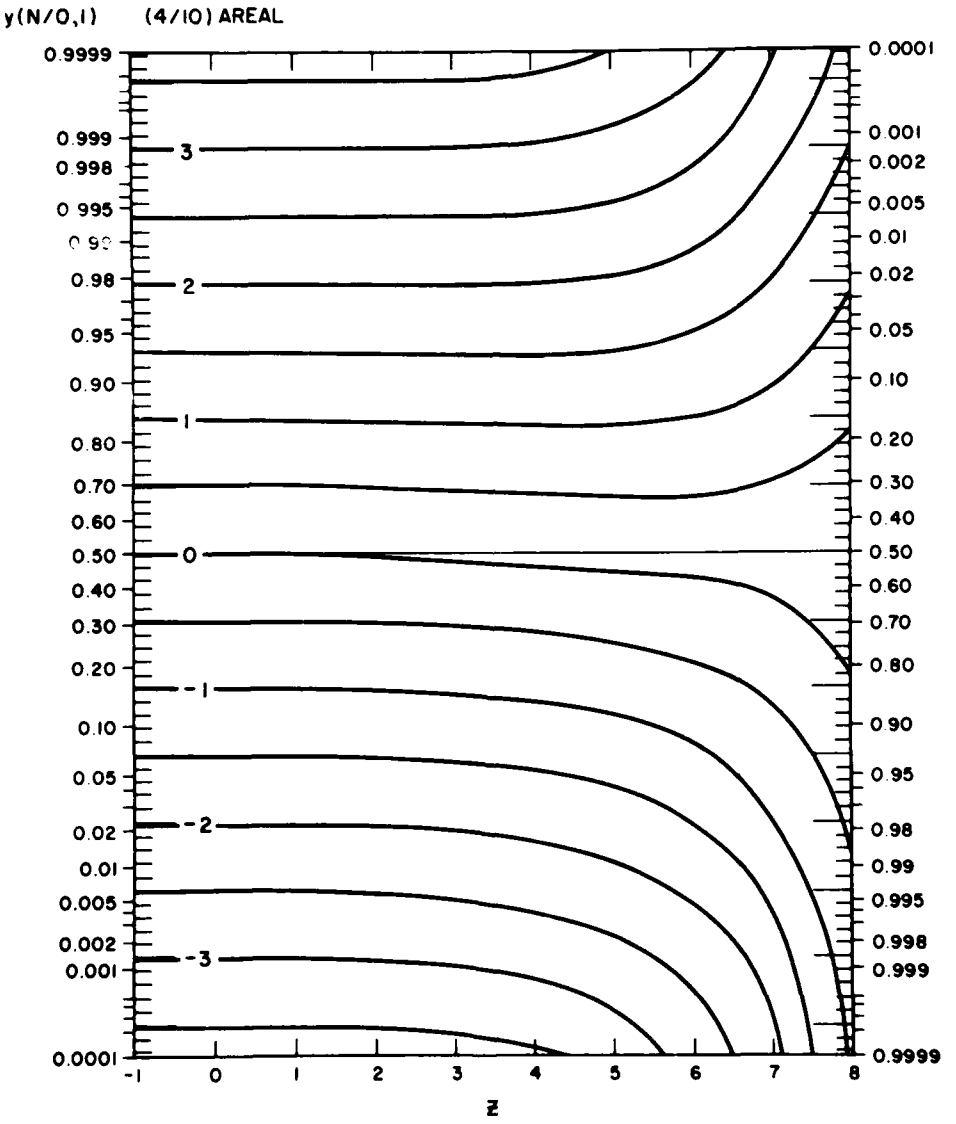

Figure 6. Graph for Estimating $P(\leq 4/10)$ and $P(\leq 6/10)$ Coverage. Each curve corresponds to a single y_o value, and $z = \ln(\sqrt{A}/r)/\ln 2$

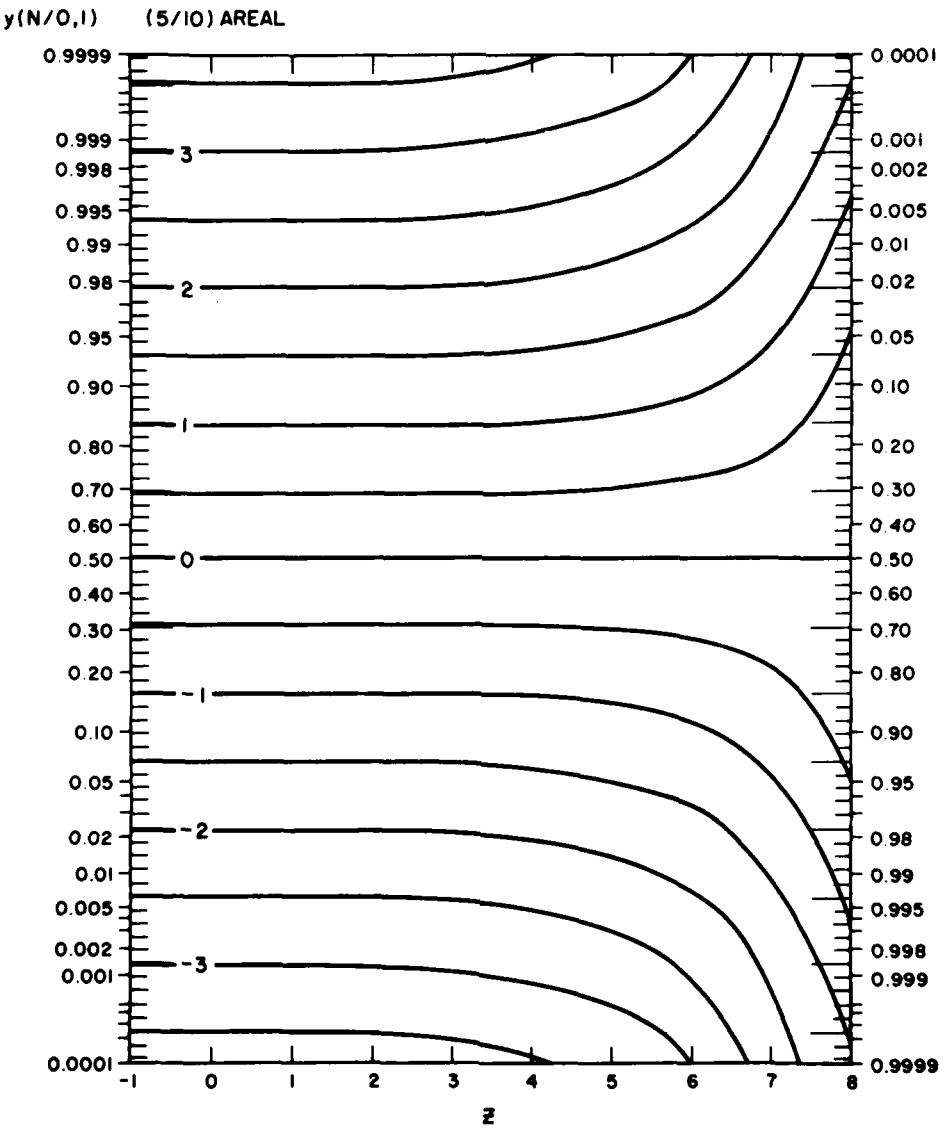

Figure 7. Graph for Estimating $P(\leq 5/10)$ Coverage. Each curve corresponds to a single y_o value, and $z = \ln(\sqrt{A}/r)/\ln 2$

Table 1. Expressions for Each Term of Eq. (9)

Term	Expression	Conditions
α	$y_o + (0.006e^{.8z} - 0.003)(F - 5)$	$-1 \le z \le 1.0$ otherwise $\alpha = 0$
β	$(0.9981 + 0.0011e^{.89z})y_o + (a_n + b_n e^{c_n z})(F + n - 6) - \sum_{i=0}^{n-1} (a_i + b_i e^{c_i z})$ $n = 5 - \mathrm{INT}(F)$	$1.0 < z \le 7$ otherwise $\beta = 0$
γ	$(0.0017e^{.95z} - 0.3129)(0.75 - 0.3y_o)(1 - 0.25F)$	$5.5 \le z \le 7$, $0 \le F \le 4$, and $y_o \ge 2.5$ otherwise $\gamma = 0$
δ	$\sum_{j=1}^{m} [d(F)_j + f(F)_j e^{g(F)_j y_o}] R_j + y'$ $(z = 7)$ $R_j = z - 7$ (when m = 1) $= 0.5$ (m = 2 and j = 1) $= z - 7.5$ (m = 2 and j = 2) $m = \mathrm{INT}(z - 5.5)$ $d(F)_j = -d(F)_j$, $f(F)_j = -f(F)_j$, $g(F)_j = -g(F)_j$ $(F = 5$ and $y_o < 0)$	$7.0 < z \le 8.0$ otherwise $\delta = 0$

Table 2. Constants for Eq. (9) (With Table 3)

n	a_n	b_n	c_n
0	0.0000	0.0000	0.00
1	-0.0071	0.0086	0.53
2	-0.0205	0.0097	0.52
3	0.0229	0.0045	0.64
4	-0.0517	0.0224	0.45
5	0.0260	0.0087	0.71

Table 3. Constants for Eq. (9) (With Table 2)

	m = 1			m = 2		
F	$d(F)_m$	$f(F)_m$	$g(F)_m$	$d(F)_m$	$f(F)_m$	$g(F)_m$
0	0.1420	-2.4090	-0.44	0.1908	-3.8406	-0.56
1	1.0686	-2.2854	-0.46	1.8710	-4.2412	-0.55
2	1.9440	-2.7842	-0.41	3.0540	-4.4752	-0.39
3	2.2560	-2.7356	-0.40	3.3960	-4.5228	-0.50
4	2.0328	-2.2910	-0.41	-2.0690	-2.5702	-0.75
5	1.2356	-1.2300	-1.30	1.6124	-1.5434	-1.51

4. PROCEDURE

We now apply the results of Section 3 to the atlas, giving a step-by-step procedure for using both the graphs and the equations. Initially, we make two important assumptions. First, we adopt the mean sky-cover as the probability of a cloud presence vertically above a single point (P_o). The no-cloud probability then becomes $P_o' = 1 - P_o$. Second, we assume that the celestial dome, as seen by the weather observer, has a radius of 27.8 km (15 nmi), giving a floor space of area $A = 2424\ km^2$. With these two assumptions, we can calculate cumulative probabilities of fractional sky-cover as seen by a ground observer (in other words, the climatology of total sky-cover) from the scale distance and mean sky-cover values in the atlas.

4.1 Graphs

The graphical procedure for obtaining the cumulative probabilities of fractional sky-cover is shown in the following steps.

1. Obtain r and P_o at the desired location and time from the atlas maps.
2. Calculate $P_o' = 1 - P_o$, and calculate z using Eq. (7) with A = 2424 km^2.
3. For F = 0- to 5-tenths coverage:
   a. Choose the graph corresponding to the appropriate coverage, 0/10 through 5/10 (Figures 2 through 7).
   b. Find P_o' on the left-hand probability scale. This defines the y_o (END) curve.
   c. Follow the y_o curve until it intersects the z value.
   d. Move left horizontally to the vertical axis and read $P(\leq F/10)$.
4. For F > 5-tenths coverage:
   a. Choose the graph corresponding to the complement of the appropriate coverage.
   b. Find the complement of P_o' on the left-hand probability scale. This defines the y_o curve.
   c. Follow the y_o curve until it intersects the z value.
   d. Move right horizontally to the vertical axis and read $P(\leq F/10)$. [In the case of 10 tenths, we have $P(< 10/10)$ and P(overcast) = 1 - $P(< 10/10)$.]

We illustrate the graphical method with a specific example. Suppose we are interested in the sky-cover climatology at a certain location for January noontime.

Step 1. We obtain r and P_o from the appropriate spot on the January 1200-1400 LST maps [Figures 15(a) and 15(b)]. Let us say r = 2.23 and P_o = 0.63.

Step 2. Next we calculate the no-cloud probability P_o' and 1 - P_o = 0.37, and z = 4.46 using Eq. (7), with A = 2424 km^2.

Step 3. To estimate the climatic probability of clear skies, use the graph for 0/10 coverage (Figure 2). On the left-hand axis, find P_o' = 0.37. Follow the appropriate y_o curve (in this case y_o = 0.33, the END of P_o', as shown by a dashed line in Figure 2) to its intersection with z = 4.46 (solid vertical line). From that point move left horizontally (solid horizontal line) to the vertical axis and read the probability of clear skies, P(0/10) = 0.165.

To estimate the probability of ≤ 1-tenth sky-cover, go to the graph for 1/10 coverage (Figure 3). Using the same procedure, Step 3, with P_o' = 0.37 and z = 4.46, we obtain $P(\leq 1/10)$ = 0.235. Similarly, the probability of ≤ 2-, ≤ 3-, ≤ 4-, and ≤ 5-tenths sky-cover is estimated from the graphs for 2/10 through 5/10 coverage (Figures 4 through 7). The values are shown in Table 4, row 1.

Step 4. Recall that the graphs for 0 through 4 tenths are the inverted mirror images of the graphs for 10 through 6 tenths, respectively. Therefore, we estimate $P(\leq 6/10)$ coverage with the graph for 1 - 6/10 = 4/10 coverage (Figure 6).

Table 4. Cumulative Probabilities for Each Tenth of Cloud Cover From the Example r = 2.23 and P_o' = 0.37 by (1) the Graphical Method and (2) by Computer

	0	≤1	≤2	≤3	≤4	≤5	≤6	≤7	≤8	≤9	< 10
1	0.165	0.235	0.270	0.310	0.330	0.370	0.410	0.430	0.460	0.510	0.620
2	0.169	0.234	0.270	0.305	0.333	0.364	0.396	0.426	0.466	0.512	0.603

The no-cloud probability becomes $P_o' = 1 - P_o' = 1 - 0.37 = 0.63$, and therefore $y_o = -y_o = 0.33$. Now follow the curve for $y_o = 0.33$ in Figure 6 to its intersection with z = 4.46. From that point, move right horizontally to the vertical axis and read the probability of ≤6-tenths coverage, P(≤6/10) = 0.410. This is the complement of the value that would be read by moving to the left-hand scale.

To estimate the probability of ≤7-tenths sky-cover, use the graph for 1 - 7/10 = 3/10 coverage (Figure 5). Using the same procedure, Step 4, with $P_o' = 0.63$ and z = 4.46, we obtain P(≤7/10) = 0.430. Similarly, the probability of ≤8-, ≤9-, and < 10-tenths sky-cover is estimated from the graphs for 2/10 through 0/10 coverage (Figures 4 through 2), and are shown in Table 4. The final value, P(< 10/10) coverage, is the probability of all fractions of coverage except overcast. In this case, P(< 10/10) = 0.620, and therefore the probability of overcast is P(overcast) = 1 - 0.620 = 0.380.

4.2 By Computer

Continuing with this example, we now solve using the empirical equations. The method is simple to program in BASIC or FORTRAN. We begin with the same values of P_o, r, and sky-dome area A, and compute $P_o' = 0.37$ and z = 4.46 as before. We then proceed as follows:

1. Calculate the END (y_o) of P_o' using the National Bureau of Standards (NBS) formula

$$y_o = k\left(t - \frac{a_o + a_1 t}{1 + b_1 t + b_2 t^2}\right) + \varepsilon \quad , \tag{10}$$

where

$$k = -1, \quad t = \sqrt{\ln \frac{1}{(P_o')^2}} \qquad \text{when } P_o' \le 0.5 \ ,$$

$$k = 1, \quad t = \sqrt{\ln \frac{1}{(1 - P_o')^2}} \qquad \text{when } P_o' > 0.5 \ ,$$

$|\varepsilon| < 0.003$,

$a_o = 2.30753$ $\quad b_1 = 0.99229$

$a_1 = 0.27061$ $\quad b_2 = 0.04481$.

2. Next, choose the fractional coverage (F/10) of interest. F can be any number in the range $0 \leq F \leq 10$.

3. Enter y_o, F, and z into Eq. (9). The expressions, conditions, and constants for the equation are shown in Tables 1 through 3, as explained in Section 3. The result is the END of $P(\leq F/10)$, y'.

4. Compute $P(\leq F/10)$ coverage from y' using the NBS formula

$$P(\leq F/10) = k + 0.5m\left(1 + c_1|y'| + c_2y'^2 + c_3|y'|^3 + c_4y'^4\right)^{-4} + \varepsilon \ ,$$

where

$k = 0, \ m = 1 \quad$ for $y' < 0$,

$k = 1, \ m = -1$ for $y' \geq 0$,

$|\varepsilon| < 0.00025$,

$c_1 = 0.196854$ $\quad c_3 = 0.000344$

$c_2 = 0.115194$ $\quad c_4 = 0.019527$.

As before, when F = 10, we have P(< 10/10) and P(overcast) = 1 - P(< 10/10). The error bars for the NBS formulas translate to a maximum computational error of $|P(\leq F/10)| \leq 0.002$. In our example we set F = 0(1)10 in step 2 and show the results in Table 4, row 2.

5. OBTAINING FREQUENCY DISTRIBUTIONS

In the example of Section 4, P_o and r were calculated from the Revised Uniform Summary of Surface Weather Observations (RUSSWO) sky-cover climatology for Minneapolis, January, 1200-1400 LST. The procedure for calculating r is described in Section 6.7. The RUSSWO provides frequencies for each tenth of sky cover from clear to overcast, as reported by the ground observer. In this case, the values represent the average of the three hourly-frequencies for 1200, 1300, and 1400 LST, and are shown in Table 5, row 1. (See Section 6 for a detailed explanation of data sources.) We assume that the categories of tenths as seen by the observer represent equal intervals, such that the 0-tenths category includes all individual observations between 0 to 0.5 tenths, the 1-tenth category all cases

Table 5. Probabilities for Each Tenth of Cloud Cover for Minneapolis, January 1200-1400 LST From (1) RUSSWO, (2) the Graphical Method, and (3) by Computer, Along With the rms Errors Between (1), (2) and (3)

	0	1	2	3	4	5	6	7	8	9	10	rms
1	0.223	0.048	0.034	0.022	0.015	0.024	0.031	0.037	0.052	0.053	0.461	-
2	0.200	0.053	0.037	0.030	0.030	0.040	0.030	0.025	0.040	0.080	0.435	0.016
3	0.200	0.052	0.035	0.031	0.030	0.032	0.031	0.035	0.043	0.069	0.442	0.012

from 0.5 to 1.5 tenths, and so on, until, lastly, the 10-tenths (overcast) category includes all cases from 9.5 to 10 tenths.

The graphical and computer models can be made to yield their results in the same format. First, we need the cumulative frequencies for F = 0.5(1)9.5-tenths sky-cover. In the graphical method, they are obtained by linear interpolation. For example, for the values in Table 4, row 1, $P(\leq 0.5/10) = 0.5\ [P(0/10) + P(\leq 1/10)] = 0.5\ (0.165 + 0.235) = 0.200$; $P(\leq 1.5/10) = 0.5\ [P(\leq 1/10) + P(\leq 2/10)] = 0.5\ (0.235 + 0.270) = 0.253$, and so on. By computer, the frequencies are calculated directly by setting F = 0.5(1)9.5 in step 2 of the procedure (Section 4.2). Since 0-tenths coverage for the observer includes all cases from 0 to 0.5 tenths, we set the model result for $P(\leq 0.5/10)$ equal to $P(0/10)$. For 1-tenth coverage, which for the observer includes all cases in the range 0.5 to 1.5 tenths, the model yields $P(1/10) = P(\leq 1.5/10) - P(\leq 0.5/10)$. We continue this process until we reach overcast, where $P(10/10) = P(> 9.5/10) = 1 - P(\leq 9.5/10)$.

We have now obtained, via the model, the frequency for each tenth of sky cover, from clear to overcast, as would be compiled from ground observations. The values for the graphical and computer methods are shown in Table 5, rows 2 and 3 respectively, for our example. Note the comparison with the RUSSWO climatological data. The root mean square (rms) error between the RUSSWO values and graphical solution is 0.016, and between the RUSSWO and computer solutions 0.012.

A visual comparison for this example is shown in the histogram of Figure 8(b). The horizontal scale is tenths of sky cover, and the vertical scale the frequency of occurrence of each tenth (in percent). The bars represent the frequency distribution of sky cover as obtained from the RUSSWO, and the lines within the bars the frequency distribution from the computer solution. Similar comparisons are made for other RUSSWO locations in Figures 8(a), 8(c), 9, and 10. The names of these locations and times of observations, as well as the RUSSWO and computer derived cumulative frequencies and rms errors between them are given in Table 6. Figures 8 through 10 give examples for different combinations of r

Table 6. Names of the Locations and Times of Observations From Figures 8 to 10. Values include P_o, r, cumulative probabilities of fractional coverage, and rms errors between the RUSSWO values and model estimates. RUSSWO values are top lines and model values bottom lines

Figure	Station	P_o	r	≤0.5	≤1.5	≤2.5	≤3.5	≤4.5	≤5.5	≤6.5	≤7.5	≤8.5	≤9.5	rms
8(a)	Fresno, CA	0.06		0.880	0.900	0.918	0.930	0.943	0.952	0.966	0.977	0.989	0.997	0.009
	Jul, 0000-0200 LST		2.46	0.879	0.908	0.924	0.935	0.944	0.952	0.959	0.966	0.973	0.981	
(b)	Minneapolis, MN	0.63		0.223	0.271	0.305	0.327	0.342	0.366	0.397	0.434	0.486	0.539	0.015
	Jan, 1200-1400 LST		2.23	0.200	0.252	0.287	0.318	0.348	0.380	0.411	0.446	0.489	0.558	
(c)	Yakutat, AK	0.89		0.041	0.055	0.067	0.078	0.092	0.109	0.123	0.150	0.192	0.253	0.014
	Jul, 0600-0800 LST		2.13	0.035	0.052	0.065	0.078	0.091	0.106	0.122	0.142	0.169	0.218	
9(a)	Fairfield, CA	0.13		0.688	0.759	0.806	0.842	0.868	0.894	0.917	0.937	0.963	0.978	0.026
	Jul, 0600-0800 LST		0.99	0.625	0.753	0.815	0.858	0.891	0.919	0.941	0.959	0.974	0.990	
(b)	Honolulu, HI	0.50		0.042	0.134	0.248	0.374	0.480	0.583	0.664	0.752	0.851	0.912	0.022
	Jul, 1800-2000 LST		0.55	0.051	0.156	0.250	0.348	0.448	0.552	0.652	0.750	0.844	0.949	
(c)	Dutch Harbor, AK	0.92		0.002	0.007	0.012	0.012	0.017	0.033	0.056	0.098	0.216	0.369	0.017
	Oct, 1200-1400 LST		0.66	0.001	0.004	0.009	0.017	0.029	0.047	0.074	0.114	0.180	0.351	
10(a)	Chunchon, Korea	0.30		0.610	0.640	0.670	0.688	0.697	0.712	0.718	0.739	0.778	0.793	0.011
	Oct, 0000-0200 LST		5.27	0.618	0.647	0.666	0.682	0.695	0.709	0.721	0.736	0.752	0.776	
(b)	Nome, AK	0.53		0.387	0.408	0.431	0.454	0.466	0.480	0.497	0.511	0.535	0.549	0.006
	Jan, 0000-0200 LST		5.63	0.383	0.411	0.430	0.447	0.460	0.475	0.489	0.506	0.525	0.554	
(c)	Finter, Germany	0.75		0.154	0.188	0.211	0.234	0.240	0.240	0.263	0.286	0.326	0.343	0.009
	Jan, 0000-0200 LST		4.13	0.165	0.190	0.208	0.224	0.238	0.254	0.269	0.287	0.310	0.345	
													$\overline{rms}$ =	0.014

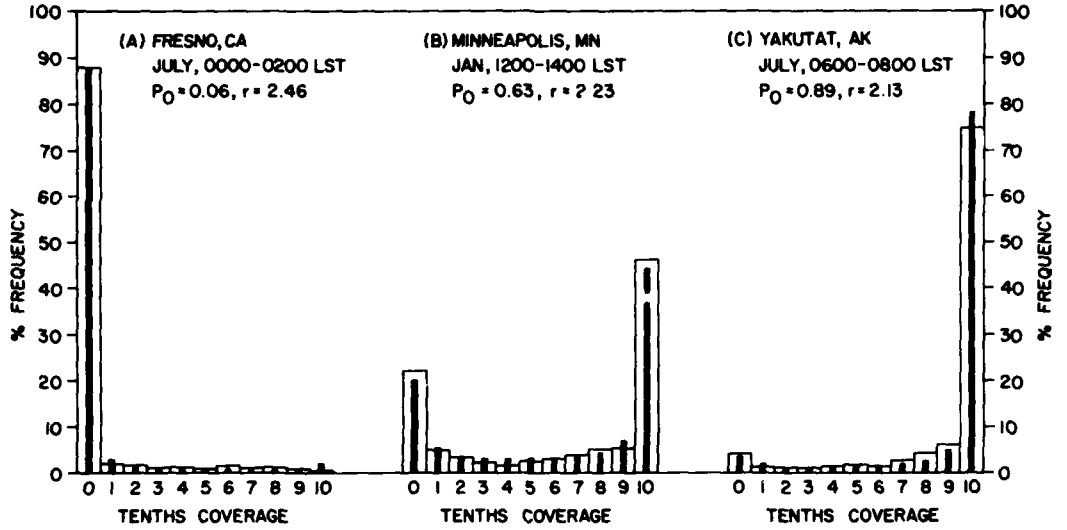

Figure 8. Histograms of the Frequency Distribution of Total Sky-Cover for Locations With Medium-Range Scale-Distances. The bars represent the RUSSWO climatologies and the lines the computerized model solutions

and P_o. In each figure, the first example (a) is a location with a low mean sky-cover ($P_o \leq 0.3$), the second (b) a location with moderate sky-cover, and the third (c) a location with considerable cloudiness ($P_o \geq 0.75$). Figure 8 contains cases with medium-range scale distances ($2.0 \leq r \leq 2.5$), Figure 9 small

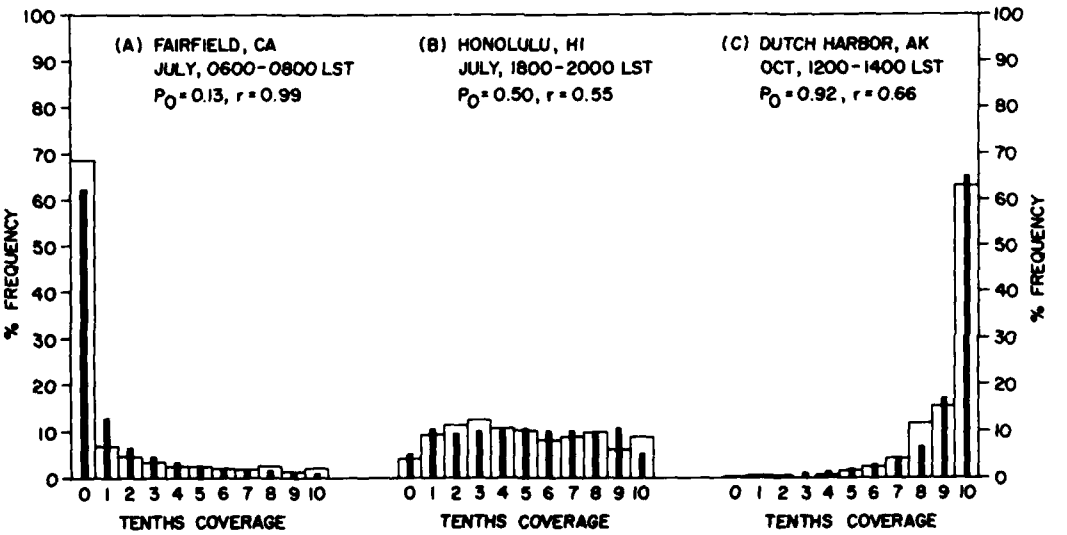

Figure 9. Histograms of the Frequency Distribution of Total Sky-Cover for Locations With Small Scale-Distances. The bars represent the RUSSWO climatologies and the lines the computerized model solutions

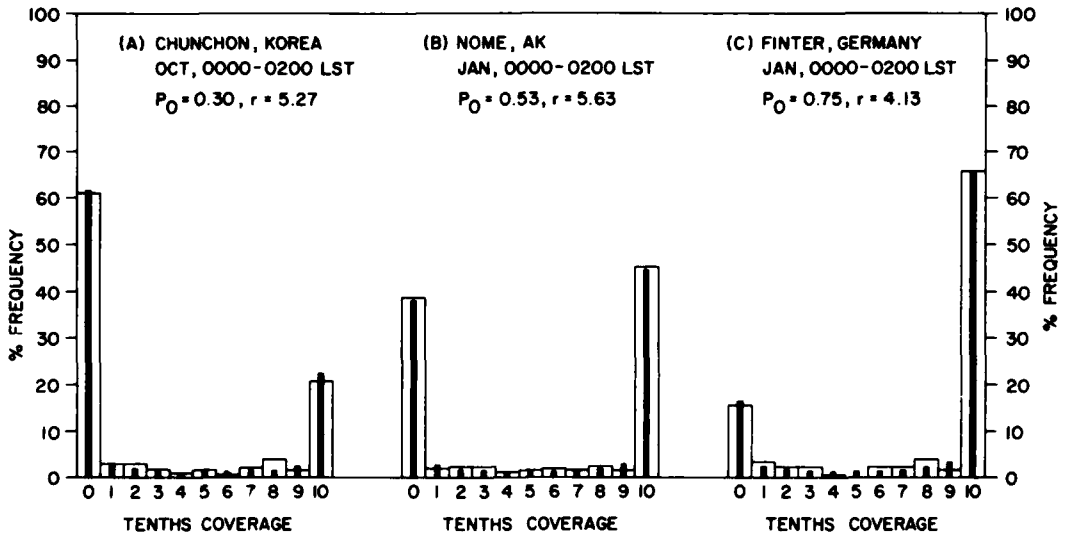

Figure 10. Histograms of the Frequency Distribution of Total Sky-Cover for Locations With Large Scale-Distances. The bars represent the RUSSWO climatologies and the lines the computerized model solutions

scale-distances ($r \leq 0.99$), and Figure 10 large scale-distances ($r \geq 4.00$). Within each category, the cases were chosen at random. The model fits well in each case. Thus, once the scale distance and mean sky-cover are known for a particular location, the probability distribution is known to within a high degree of accuracy. This becomes a very efficient means of data storage.

Notice the effect of the model parameter, r, on the distributions. As r increases (going from Figure 9 to Figure 10), the frequency of the clear and overcast categories increases while the probability of fractional coverage decreases. The most striking example is between Figures 9(b) and 10(b). Both locations have almost identical mean sky-covers ($P_o \sim 0.5$), and yet the sky-cover distribution goes from a bell shape in the case of Figure 9(b), where r = 0.55, to U-shaped in Figure 10(b), where r = 5.63. This is consistent with the definition of r, which is the distance over which $\rho(s)$ is approximately 0.99. Thus small r-values indicate relatively small-scale cloud patterns, such as summertime cumulus, in contrast to the large r-values indicative of the broad, synoptic-scale systems.

The global maps in this atlas have been analyzed on the synoptic scale, with mesoscale and local effects being smoothed out. Therefore it will not be possible, in many cases, to know the probability distribution at any location on the atlas with the same degree of accuracy as in the examples of Figures 8 through 10, but it will be possible to know the general shape of that distribution within the region in question (e.g., U-, L-, J-shaped) and see how that shape changes from region to region. Figure 11 depicts the different distributions for various mean

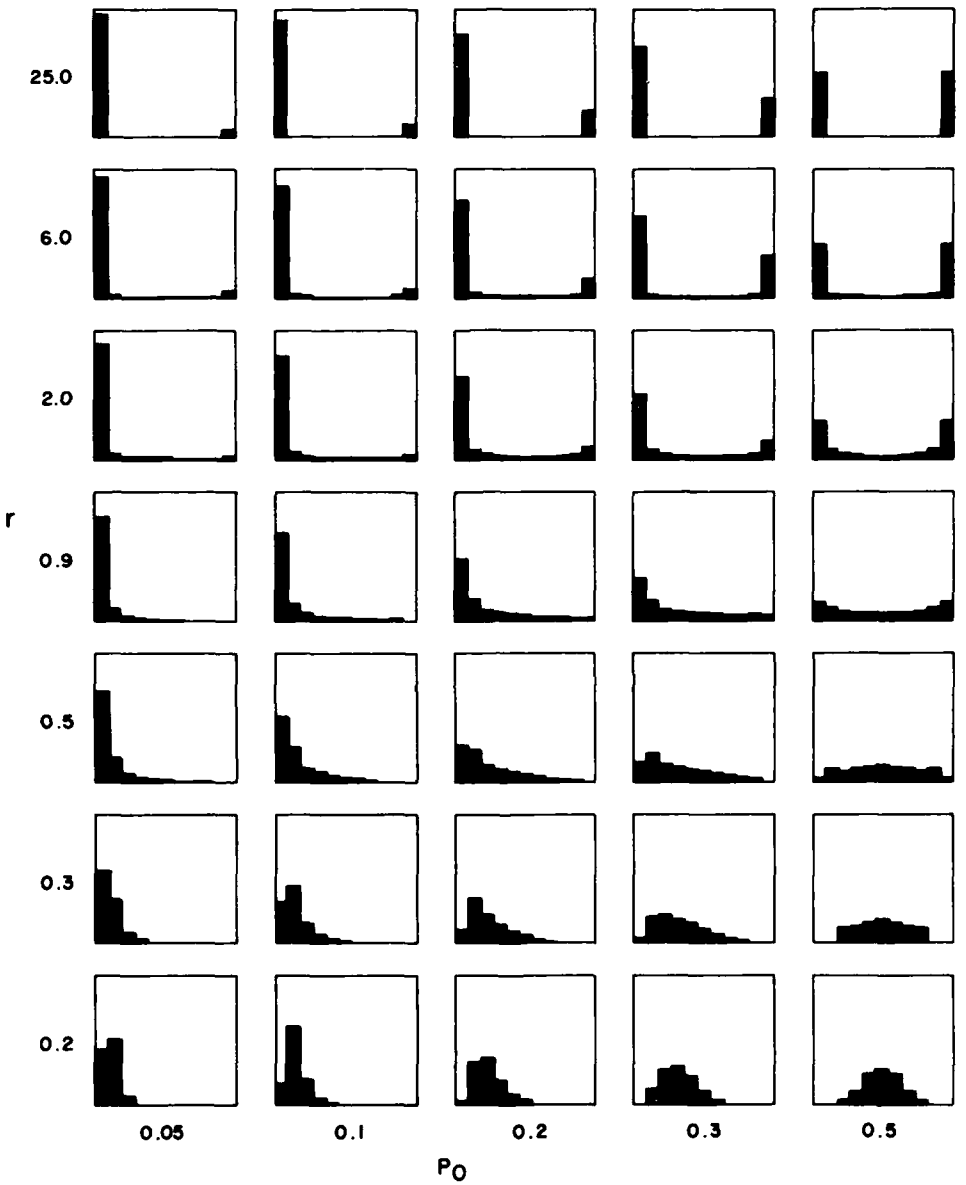

Figure 11. Frequency Distributions in Tenths of Sky-Cover, From Clear to Overcast, for Various Mean Sky-Covers (P_o) and Scale-Distances (r/km). The distributions for $P_o > 0.5$ are the mirror images of the complementary value of P_o

sky-covers and scale distances. Distributions for mean sky-covers greater than 0.5 are the mirror images of the complementary means. This figure can be used to get a good idea of the distribution in a particular region without using the graphical or computer methods (Section 4).

It is particularly significant that, in producing this atlas, it was not necessary to break the globe up into a complicated set of regions of rigid cloud climatologies with definite boundaries, as many other atlases do. Therefore, this atlas is more realistic, since changes in the sky-cover distribution take place gradually from location to location.

6. DATA SOURCES, PROCESSING, AND ANALYSIS

Data were taken from the following sources:

1. Revised Uniform Summary of Surface Weather Observations (RUSSWO)
2. National Intelligence Survey (NIS) Climatic Series
3. U. S. Navy Marine Climatic (NAV) Atlas of the World
4. Woods Hole Oceanographic Institution (WHOI) climatic data
5. Summary of Synoptic Meteorological Observations (SSMO)
6. World Survey of Climatology

6.1 RUSSWO

The RUSSWOs are weather summaries compiled by the USAF Environmental Technical Applications Center and available through the National Technical Information Service (NTIS). We obtained RUSSWO sky-cover climatologies for 273 stations, 107 in the U. S. and 166 abroad, including Canada. Figure 12 is an example of the data format. The monthly observations are grouped into eight 3-hr periods, given in Local Standard Time (LST), starting with 00-02 LST and ending with 21-23 LST. The percent frequency of total sky-cover is given in tenths, from clear to overcast; each value represents an average of the three hourly-frequencies. Also shown are the mean sky-cover (P_o in the BSW model) and number of observations for each time period, mean frequencies for the entire month, and the period of record. The same format is used for all 12 months. For the atlas, data were selected for the mid-season months for the time periods 00-02, 06-08, 12-14, and 18-20 LST. P_o was taken directly from the summaries. The scale distances were calculated using a procedure described later in this section. To use this procedure, the data had to be converted into cumulative frequencies. To do this, we assumed that the categories of tenths represent equal intervals that cover the entire spectrum from clear to overcast, as described in Section 5. Table 7 shows the cumulative frequencies calculated from Figure 12 for January, 00-02 LST, for Savannah, Ga.

DATA PROCESSING DIVISION
ETAC/USAF
AIR WEATHER SERVICE/MAC

SKY COVER

13824	SAVANNAH GEORGIA/HUNTER AAF	48-70	JAN
STATION	STATION NAME	PERIOD	MONTH

PERCENTAGE FREQUENCY OF OCCURRENCE
(FROM HOURLY OBSERVATIONS)

MONTH	HOURS (L.S.T.)	PERCENTAGE FREQUENCY OF TENTHS OF TOTAL SKY COVER											MEAN TENTHS OF SKY COVER	TOTAL NO. OF OBS.
		0	1	2	3	4	5	6	7	8	9	10		
JAN	00-02	34.9	4.3	4.5	3.9	3.3	1.7	2.6	3.1	4.5	3.2	34.0	4.9	2137
	03-05	33.8	2.6	4.4	3.9	3.0	1.4	3.5	3.8	5.2	2.9	35.4	5.1	2138
	06-08	24.0	3.7	5.1	4.3	3.2	2.6	3.1	4.5	5.2	5.5	38.7	5.8	2136
	09-11	21.4	4.7	5.4	4.7	3.6	2.2	2.1	3.8	5.0	5.9	41.2	6.0	2139
	12-14	18.1	5.5	5.1	4.9	3.7	2.9	3.8	3.9	6.3	5.4	40.3	6.1	2139
	15-17	17.6	6.3	5.9	5.1	3.6	3.4	3.1	4.5	5.8	5.5	39.4	6.0	2138
	18-20	24.6	5.8	5.7	5.3	3.6	3.4	2.9	4.3	5.6	3.5	35.3	5.4	2139
	21-23	32.4	3.1	5.2	4.2	4.0	2.7	3.2	3.6	4.5	3.5	33.5	5.0	2137
TOTALS		25.9	4.5	5.2	4.5	3.5	2.5	3.0	3.9	5.3	4.4	37.2	5.5	17103

Figure 12. RUSSWO Data for Savannah, Georgia; January

Table 7. Cumulative Frequency of Total Sky-Cover for Savannah, Georgia, in January, for 00-02 LST (From Figure 12)

X (tenths)	0.5	1.5	2.5	3.5	4.5	5.5	6.5	7.5	8.5	9.5
P(≤ x)	0.349	0.392	0.437	0.476	0.509	0.526	0.552	0.583	0.628	0.660

6.2 NIS

Section 23 of the NIS, Weather and Climate, was our largest data source, with 1846 stations world-wide. The intelligence community updated some of these data until the early 70's, although for many stations the updates ended even earlier. The station data consist of: a mean sky-cover; the probability of being less than or equal to a certain fractional coverage, such as 2/8 or 3/10; and the probability of exceeding a certain coverage, such as 6/8 or 7/10. These values generally appear for several times daily for each of the twelve months, although some countries only report daily averages. Since the observing time varies from country to country, the data had to be fit into the atlas time periods that correspond most closely to the time of the observation. The only change that needed to be made in these data for estimating the scale distances was to convert the second probability value to a cumulative frequency by taking the complement.

6.3 NAV Atlas

The NAV atlas (NAVAIR 50-1C-528) provided cloud climatologies for 222 ocean locations around the world. Most of the data are from ship observations. Since ships are always moving, point statistics were obtained by collecting a sufficient number of observations in an area small enough to permit an approximation. The data are given in the form of cumulative percent frequency curves from 0- to 8-eights coverage. The values are daily averages, and are given for each month. The cumulative frequency of each eighth of sky cover was simply obtained from the curves. The mean sky-cover was then estimated from the frequency distribution. Since ships tend to avoid bad weather when possible, these data may be biased toward good weather samples.[20]

---

20. Quayle, R. G. (1974) A climatic comparison of ocean weather station and transient ship records, Mariners Weather Log 18 (No. 5), NOAA Environmental Data Service.

6.4 WHOI

WHOI compiled their mean sky-cover summaries from a collection of surface marine observations held by the National Climatic Center, Asheville, N. C. The data were taken primarily by ships and within the established shipping lanes of the Atlantic Ocean during the period 1942-1972. The values are daily and spatial averages, calculated over all valid observations in a month within a Marsden Square, and plotted at the center point of a square. (A Marsden Square covers an area 10° latitude by 10° longitude.) There are 116 squares partially or totally within the North and South Atlantic Ocean, and each of the midseason months had mean sky-covers calculated for most of these squares. Within any single 10° square, the spatial coverage of observations may vary considerably depending on the location and number of shipping lanes and the fraction of the square covered by land areas. As with the NAV atlas data, there may be a bias toward good weather samples.

6.5 SSMO

The SSMO is produced by the Naval Oceanography Command Detachment at Asheville, N. C. It is a series of coastal marine summaries developed from ship observations at or near ports world-wide. The mean sky-cover is given once per day for each month of the year. Since the data are based upon observations made by ships in passage, the geographic location of each value is the central position of the observations within an area. Values were available from 443 locations.

6.6 World Survey of Climatology

The World Survey of Climatology[21] contains an appendix with climatic tables for 125 stations in the Soviet Union. The sources of these data are also provided. Mean sky-cover is given three times daily (0700, 1300, and 1900 LST) for each month at each station, and were fit into the atlas time periods 0600-0800, 1200-1400, and 1800-2000 LST, respectively.

6.7 Calculation of Scale Distances

We estimated the scale distances for the RUSSWO, NAV atlas, and NIS data sets. The other data do not contain probabilities of fractional coverage, which are necessary in determining r. Our procedure was to use Eq. (8) to calculate

---

21. Lydolph, Paul E. (1977) Climates of the Soviet Union, World Survey of Climatology 7:363-427, Elsevier Scientific Publishing Co., Amsterdam, The Netherlands.

r by setting A = 2424 km^2, and z equal to the value obtained from Eq. (9). The latter equation cannot be solved to yield z directly, and therefore z was estimated using an iterative process that converges on z.[19] At each location where an estimate of z was made, the value was based on the geometric average of several solutions. For example, in the case of the RUSSWO data, the climatologies consist of 10 cumulative frequency values, $P(\leq F)$, where F = 0.5(1)9.5 tenths of coverage, and a mean sky-cover, P_o. The probabilities were converted into END values, $P(\leq F) \rightarrow y'$ and $P_o \rightarrow 1 - y_o$. Ten estimates of z were then made from the 10 pairs of y' and F values, and their geometric mean ($\bar{z}$) taken. Outliers were then eliminated by omitting z when $|z - \bar{z}| > 1$, and recalculating $\bar{z}$ if necessary. We then plugged $\bar{z}$ into Eq. (8) to obtain r. The same procedure was used to estimate r from the NAV atlas and NIS data. In the case of the former, there were eight pairs of y' and F since the sky cover is given in octas, and in the case of the latter, two pairs of y' and F.

The validity of calculating r using just two pairs of y' and F was tested by recalculating r for selected RUSSWO stations using only the two pairs. The new r values compared favorably with those calculated using the 10 pairs of y' and F; differences were within the noise level. The conclusion is that our method for calculating r is as valid for the NIS data as for the RUSSWO and NAV atlas data.

6.8 Plotting and Analysis

The atlas contains a set of 20 global maps for each parameter, P_o and r, 16 of which are for the time periods 0000-0200, 0600-0800, 1200-1400, and 1800-2000 LST for the midseason months, and 4 of which are monthly means, also for the midseason months. Data for the maps depicting diurnal variations in P_o [Figures 13(a) to 28(a)] came from the RUSSWO, World Survey of Climatology, and most of the NIS. The rest of the NIS, along with the NAV, WHOI, and SSMO data sets, were used for the seasonal P_o maps [Figures 29(a) to 32(a)]. Only the RUSSWO, NAV, and NIS data could be used to calculate r, since they were the only data sets containing the fractional as well as the mean sky-covers. The RUSSWO and most of the NIS were used for the diurnal depictions of r [Figures 13(b) to 28(b)], while the remainder of the NIS along with the NAV data were used for the seasonal maps [Figures 29(b) to 32(b)].

Due to the split between diurnal and seasonal map sets, missing data, and regions with no data, each map contains gaps where no analyses could be performed, as outlined by the heavy lines in the analyses. In general, the diurnal climatologies are found mostly over the landmasses, with the seasonal climatologies mostly over the oceans.

The data were plotted by computer on Gringorten polar equal area maps,[22] and analyses were done by hand. The contours for P_o are whole tenths of sky cover, beginning at 1 tenth and going through 9 tenths. The contours for r are as follows: 0.25, 0.30, 0.40, 0.60, 0.80, 1.1, 1.5, 2.0, 3.0, 6.0, 12.0, and 25.0 km. The reason for the gradual change in contour interval from 0.05 to 13 km is that small r-values are more sensitive to changes in the sky-cover frequency than large values. To illustrate this fact, we look at the graphs (Figures 2 to 7). The y_o curves have greater slopes, in general, for large z-values (small r-values) than for small z-values (large r-values). In addition, an interval on the z scale at the high end corresponds to a smaller change in the values of r than an identical interval on the low end of the z scale [see Eq. (8)]. For instance, from $z = 8$ to $z = 7$, r goes from 0.2 to 0.4 km, whereas from $z = 3$ to $z = 2$, r goes from 6 to 12 km. In both instances $\Delta z = 1$, but $\Delta r = 0.2$ km in the first case and 6 km in the second. Thus, with a horizontal axis uniform in r instead of z, the change in the slopes of the y_o curves would be greatly accentuated. In order to compensate for this effect, the contour intervals for r were designed to permit more precise map readings for small values than for large values.

---

22. Gringorten, I. I. (1981) Mapping the Climate, AFGL-TR-81-0015, AD A102904.

Figure 13a. Analysis of Mean Sky-Cover (P_o) for January, 0000 to 0200 LST

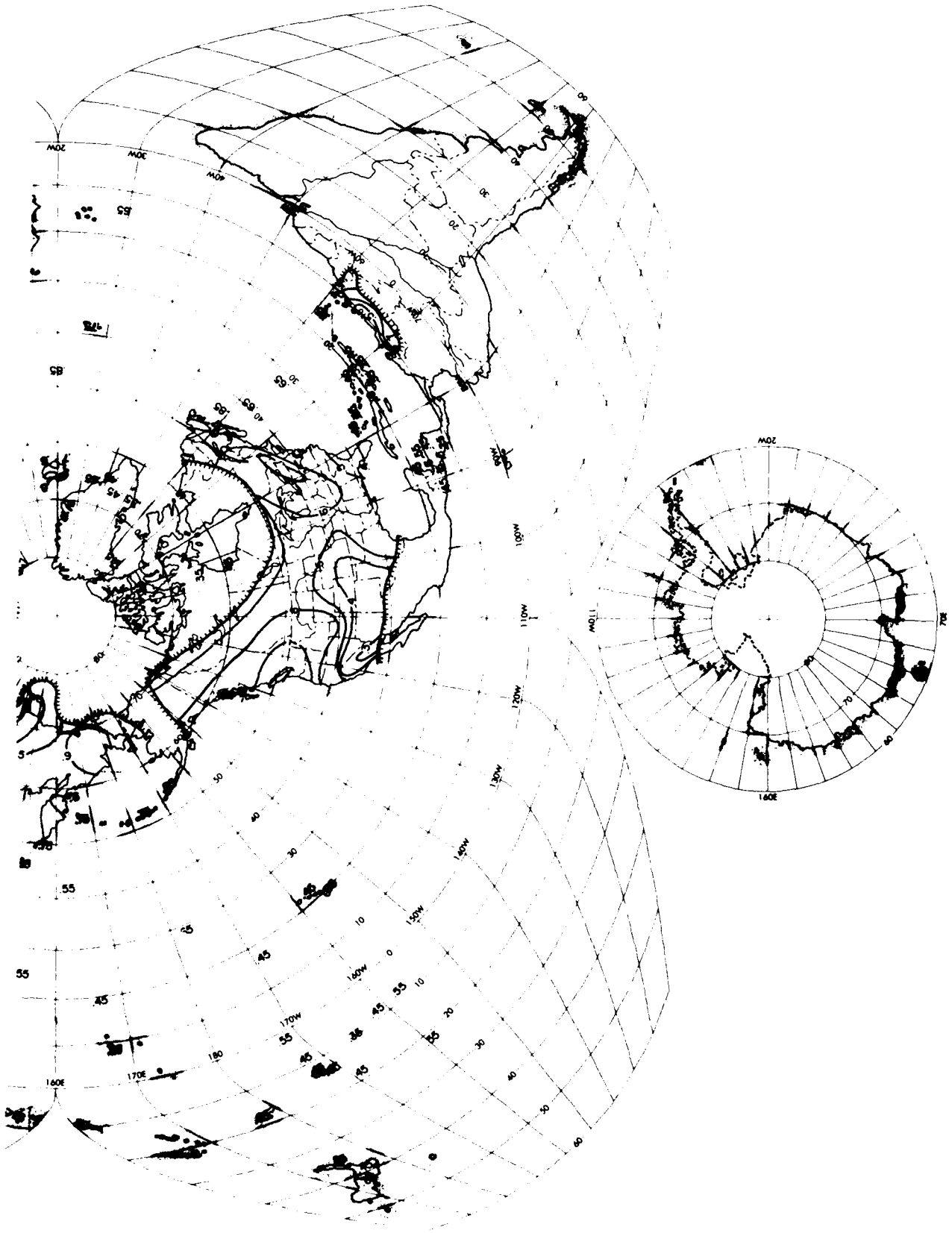

Figure 13a. Analysis of Mean Sky-Cover (P_o) for January, 0000 to 0200 LST (Contd)

Figure 13b. Analysis of Scale Distance (r) for January, 0000 to 0200 LST

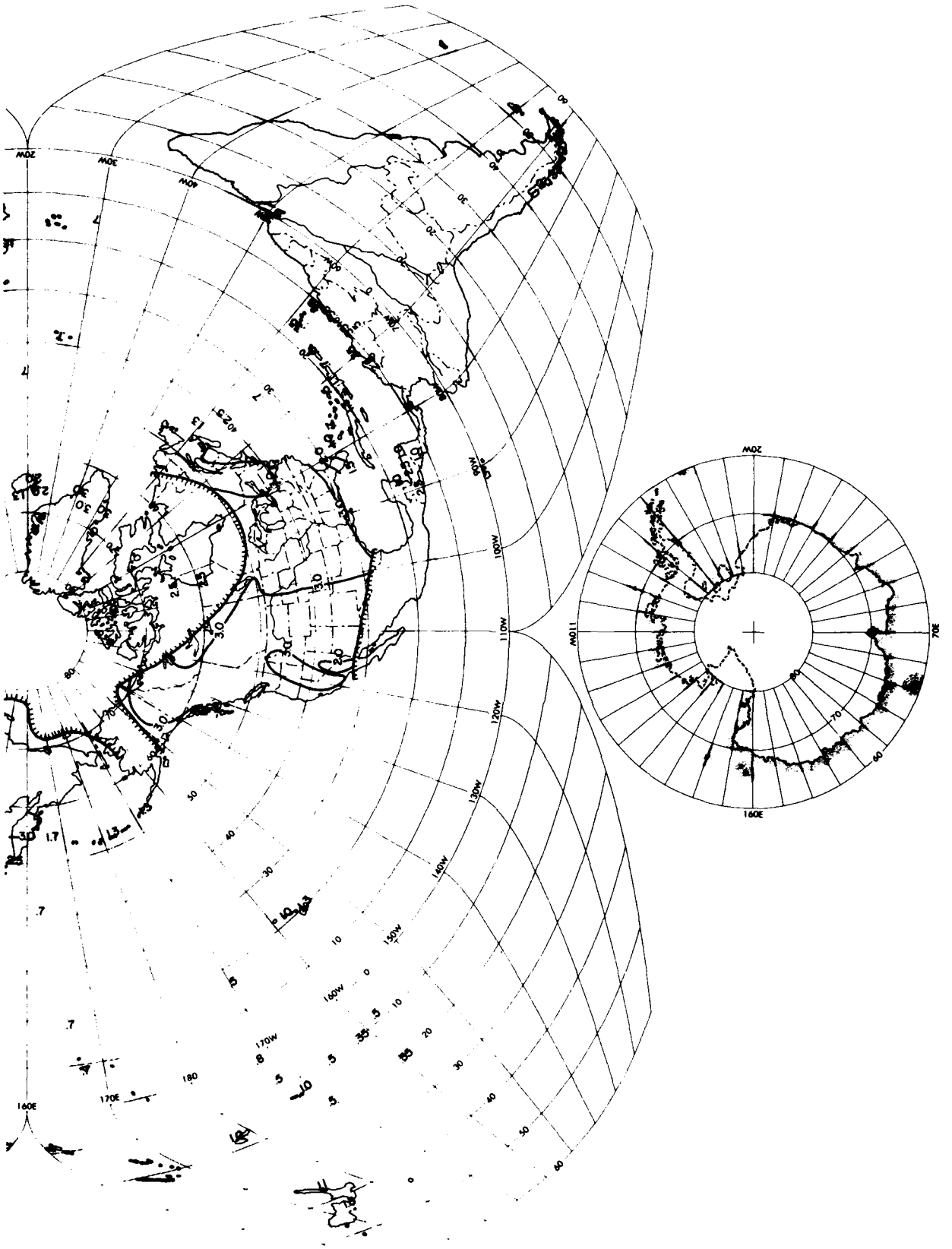

Figure 13b. Analysis of Scale Distance (r) for January, 0000 to 0200 LST (Contd)

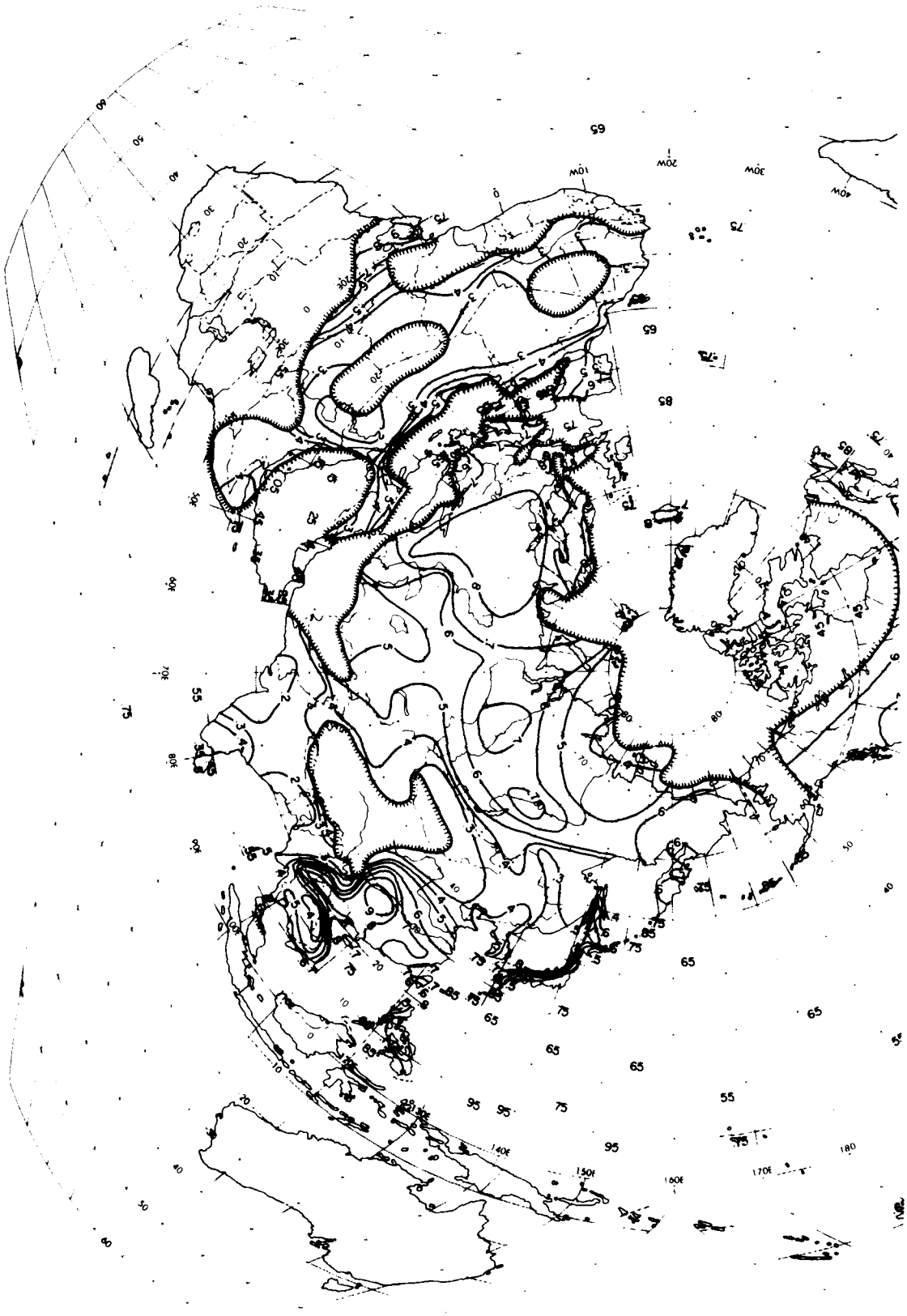

Figure 14a. Analysis of Mean Sky-Cover (P_o) for January, 0600 to 0800 LST

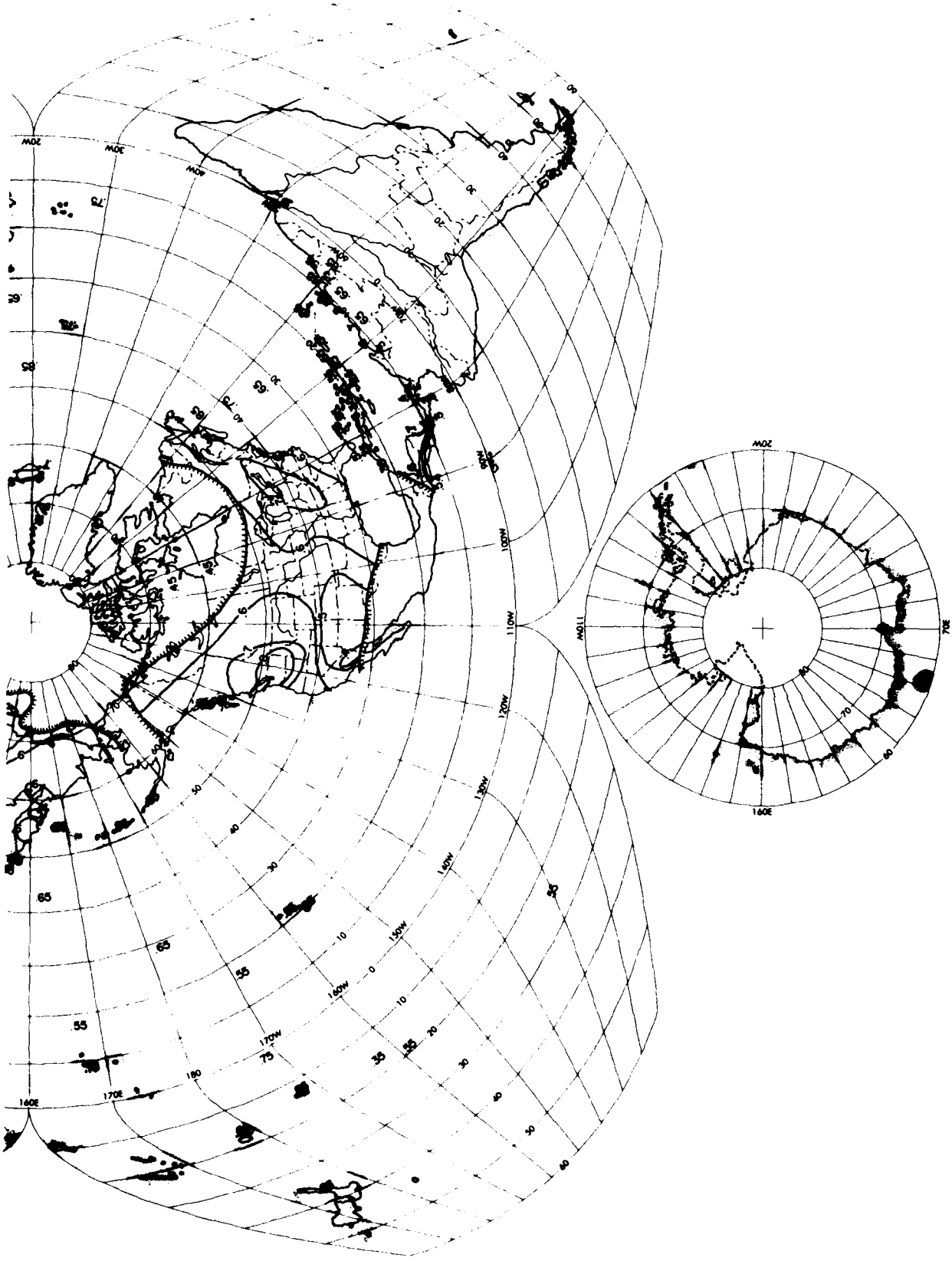

Figure 14a. Analysis of Mean Sky-Cover (P_o) for January, 0600 to 0800 LST (Contd)

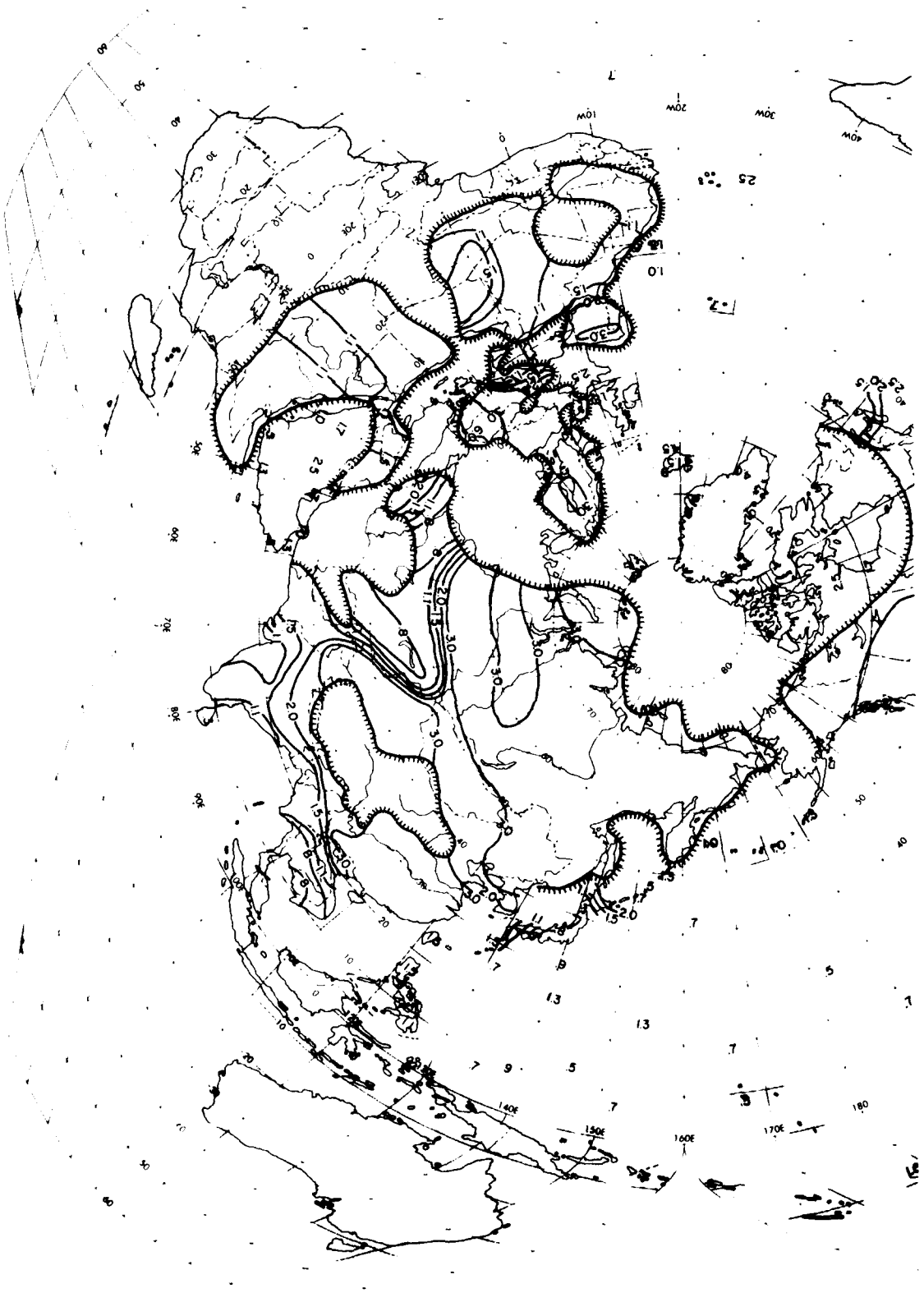

Figure 14b. Analysis of Scale Distance (r) for January, 0600 to 0800 LST

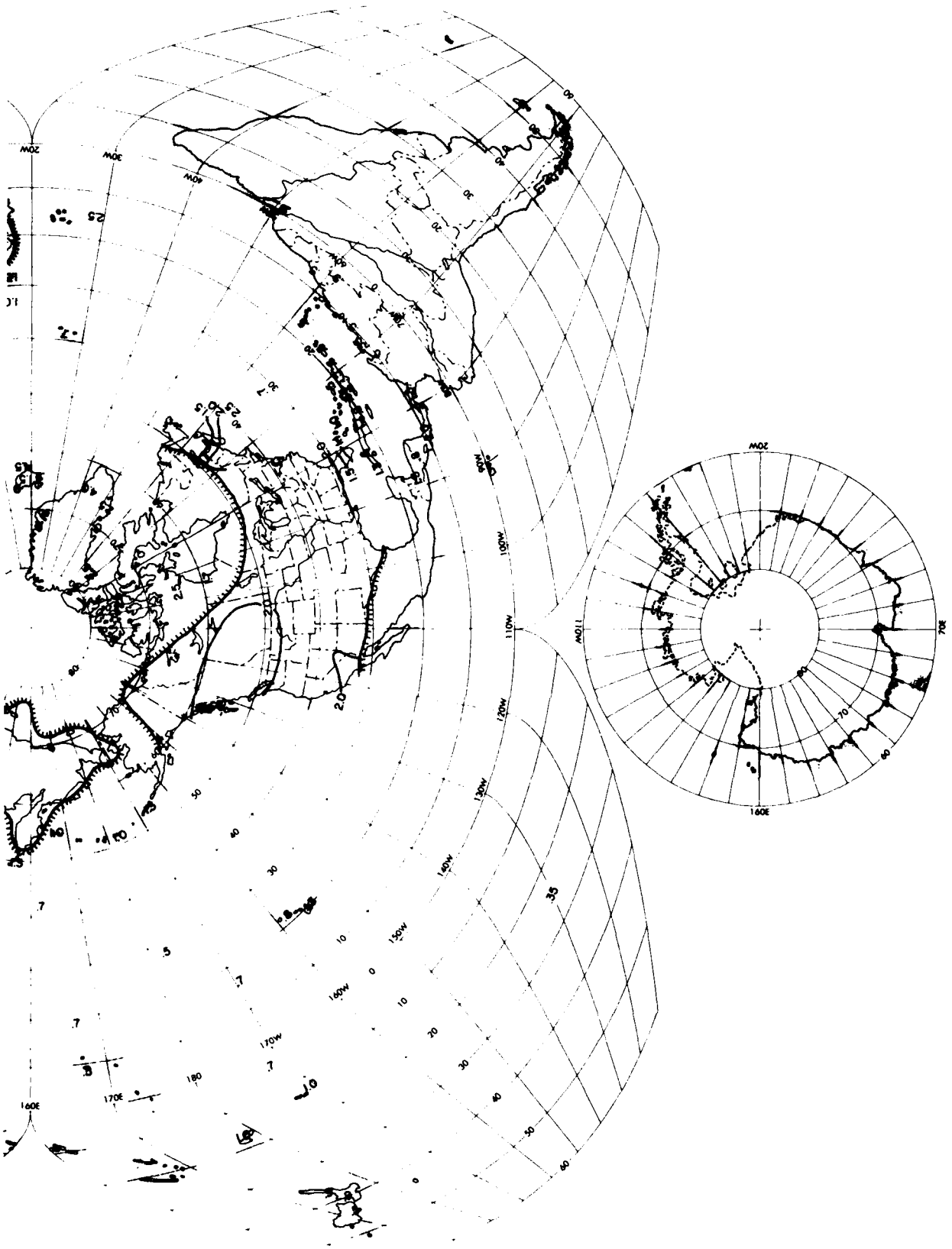

Figure 14b. Analysis of Scale Distance (r) for January, 0600 to 0800 LST (Contd)

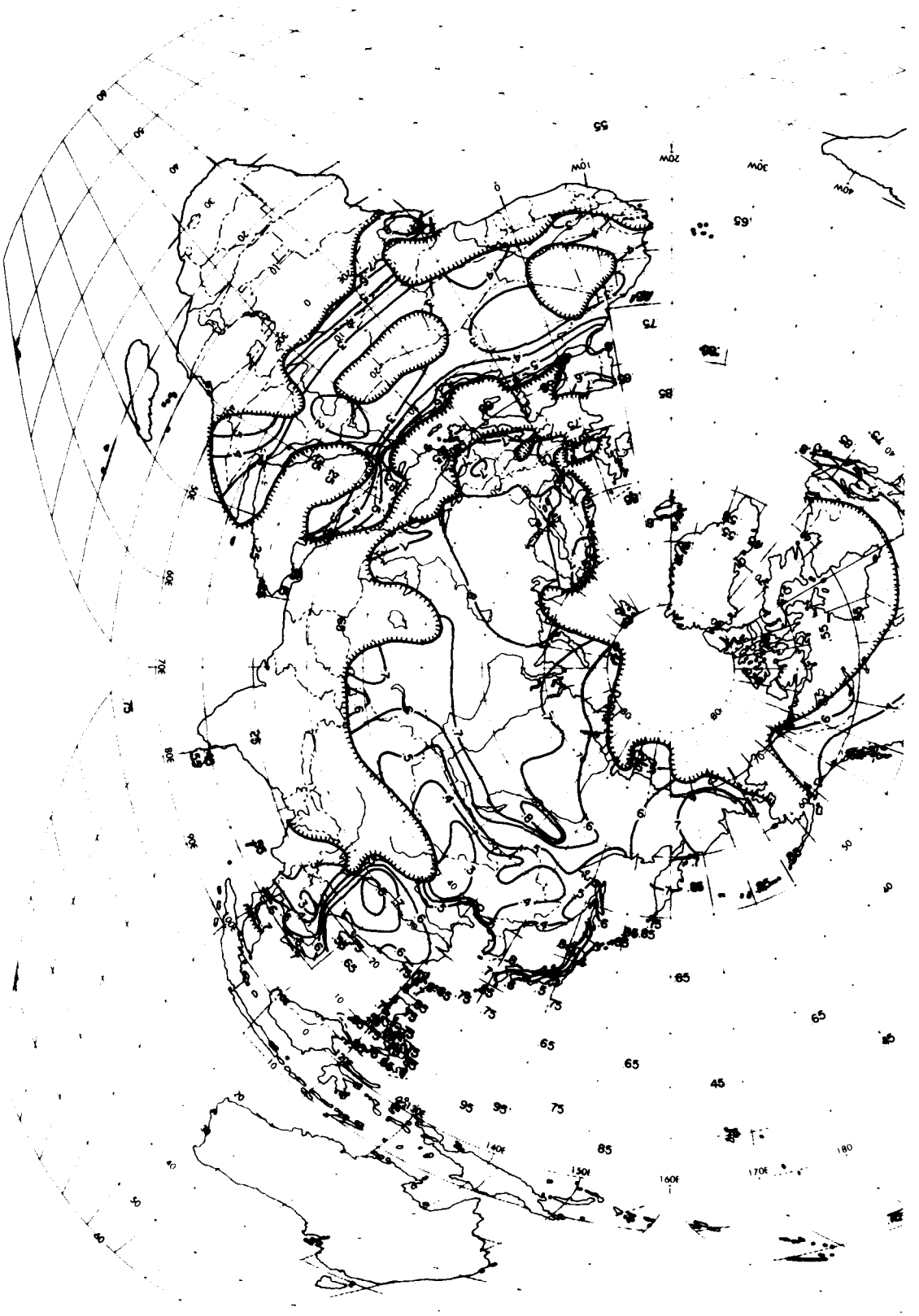

Figure 15a. Analysis of Mean Sky-Cover (P_o) for January, 1200 to 1400 LST

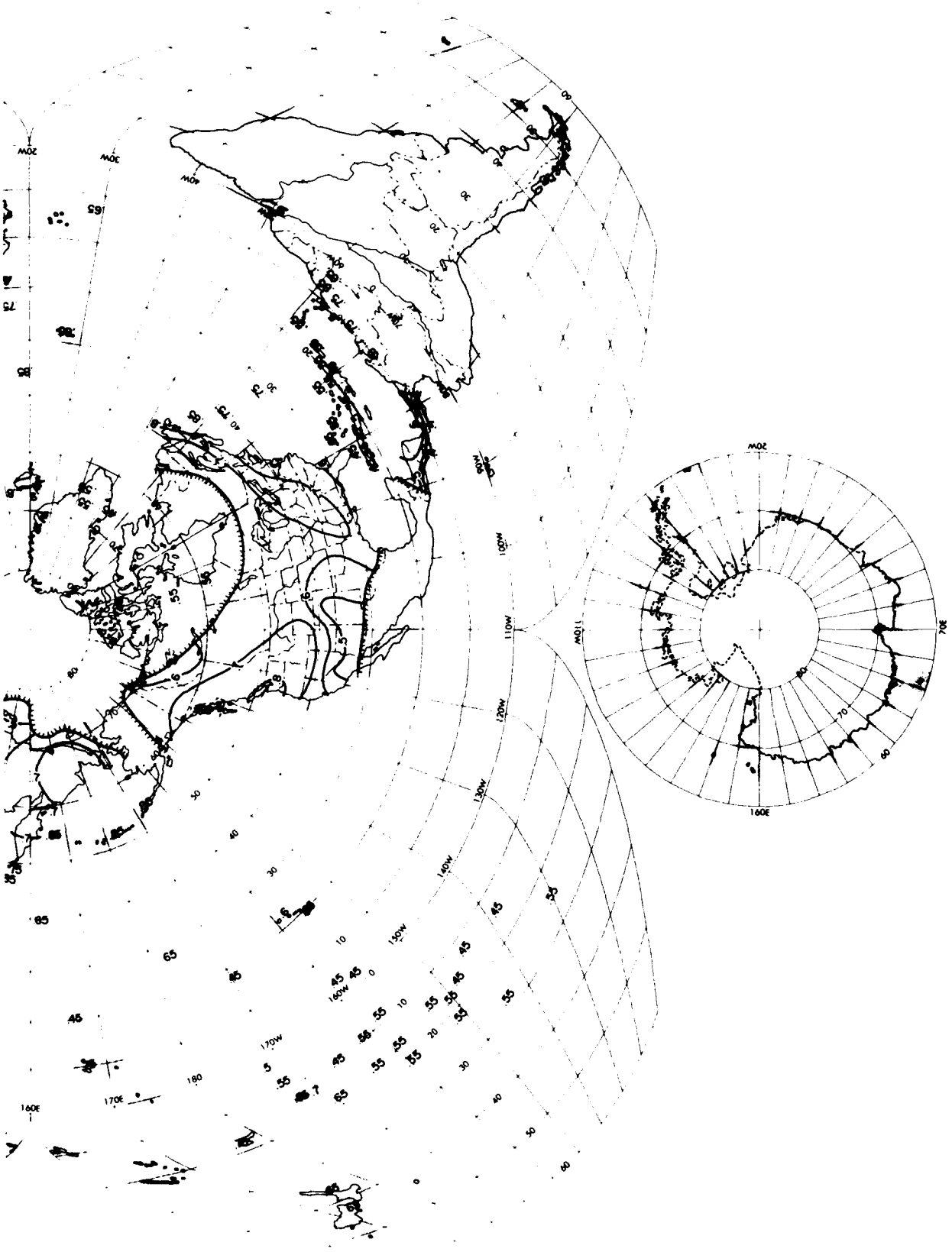

Figure 15a. Analysis of Mean Sky-Cover (P_o) for January, 1200 to 1400 LST (Contd)

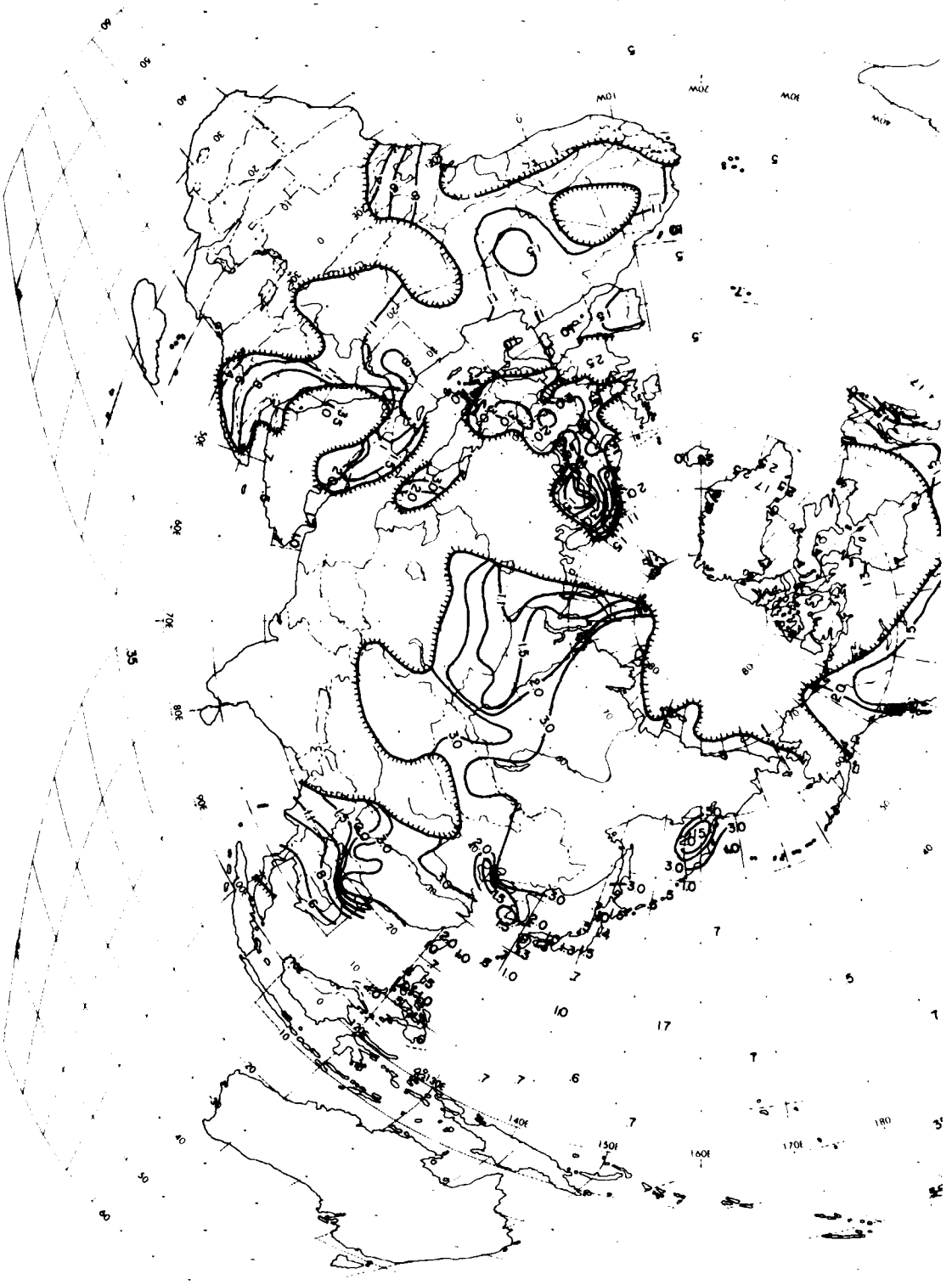

Figure 15b. Analysis of Scale Distance (r) for January, 1200 to 1400 LST

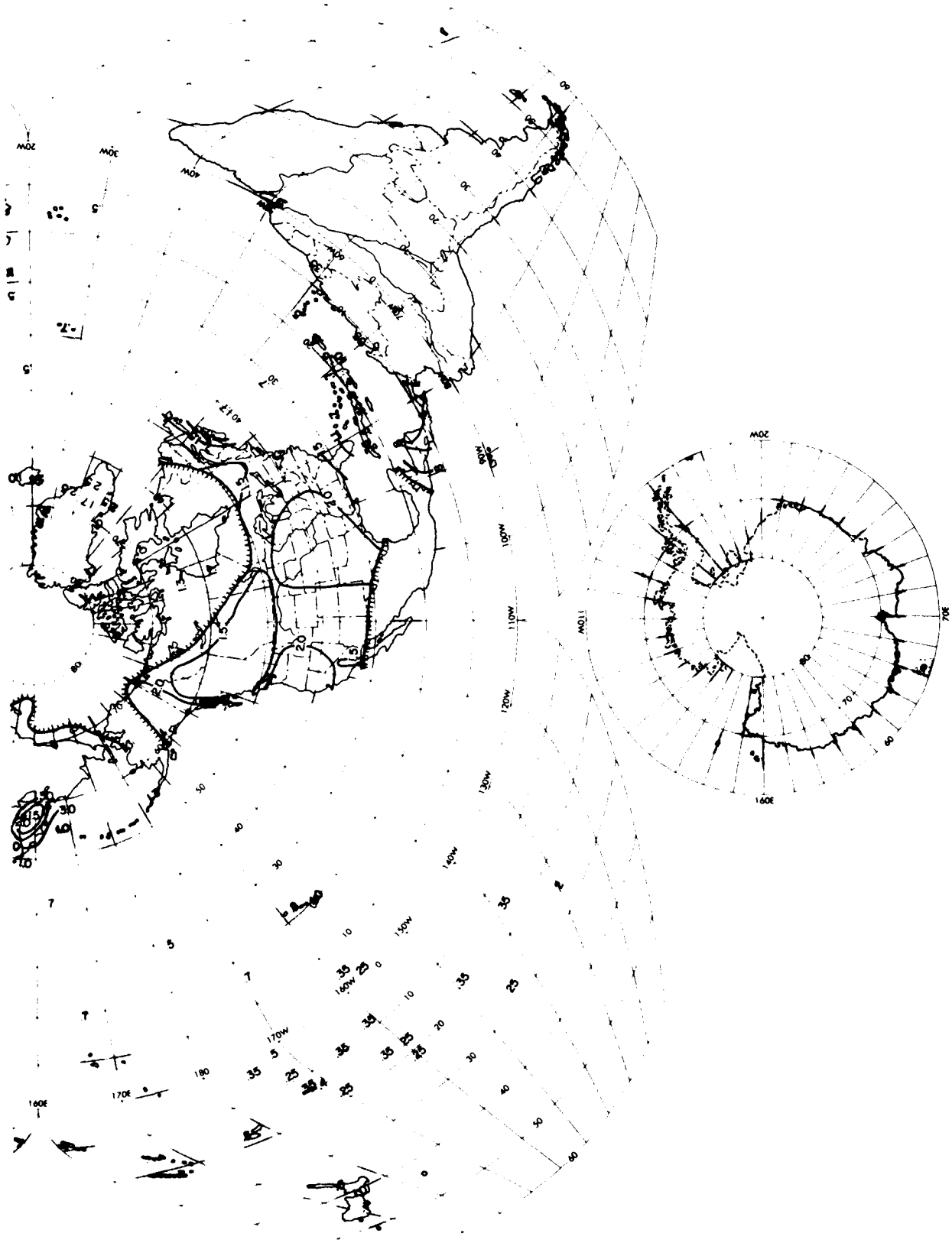

Figure 15b. Analysis of Scale Distance (r) for January, 1200 to 1400 LST (Contd)

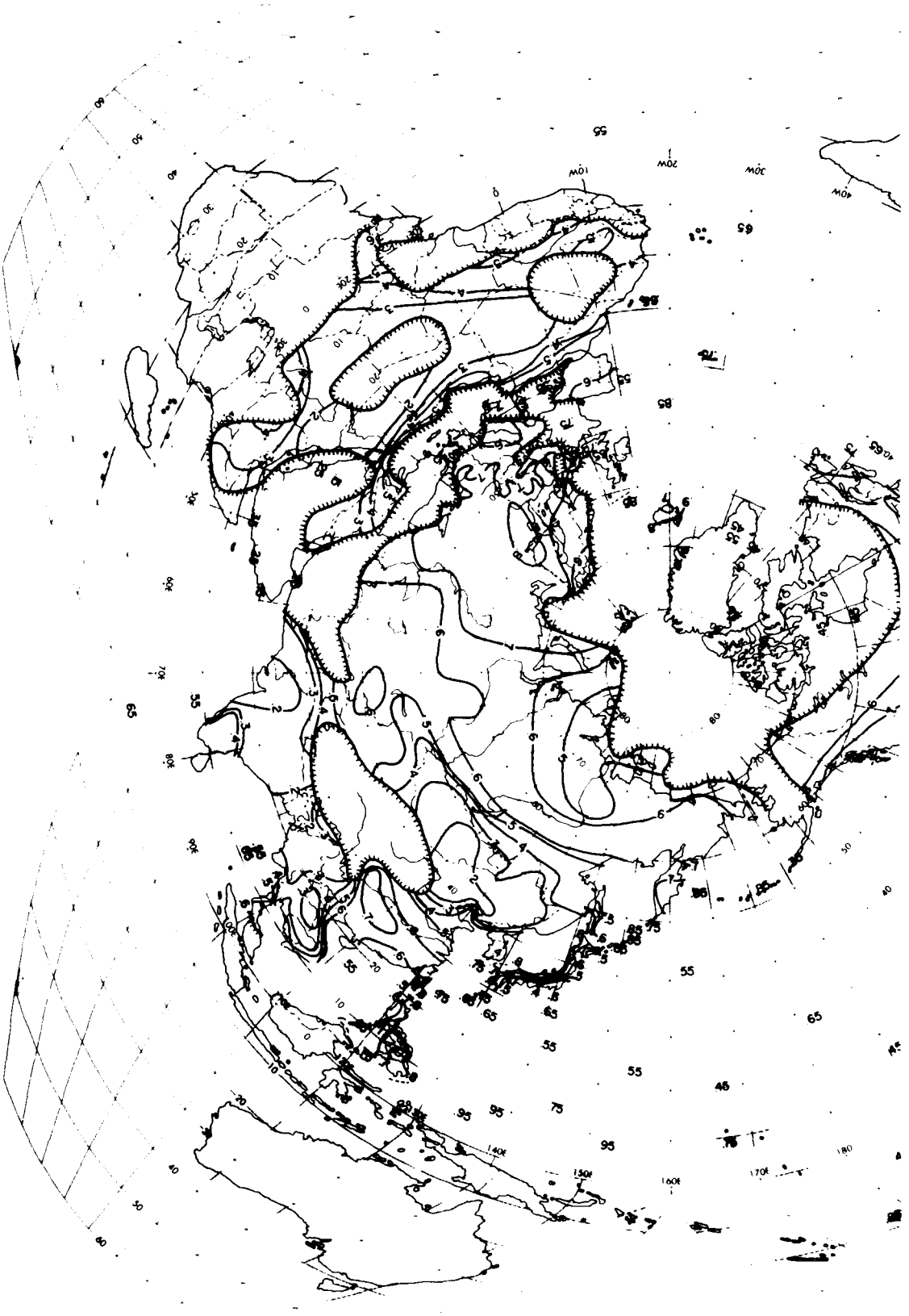

Figure 16a. Analysis of Mean Sky-Cover (P_o) for January, 1800 to 2000 LST

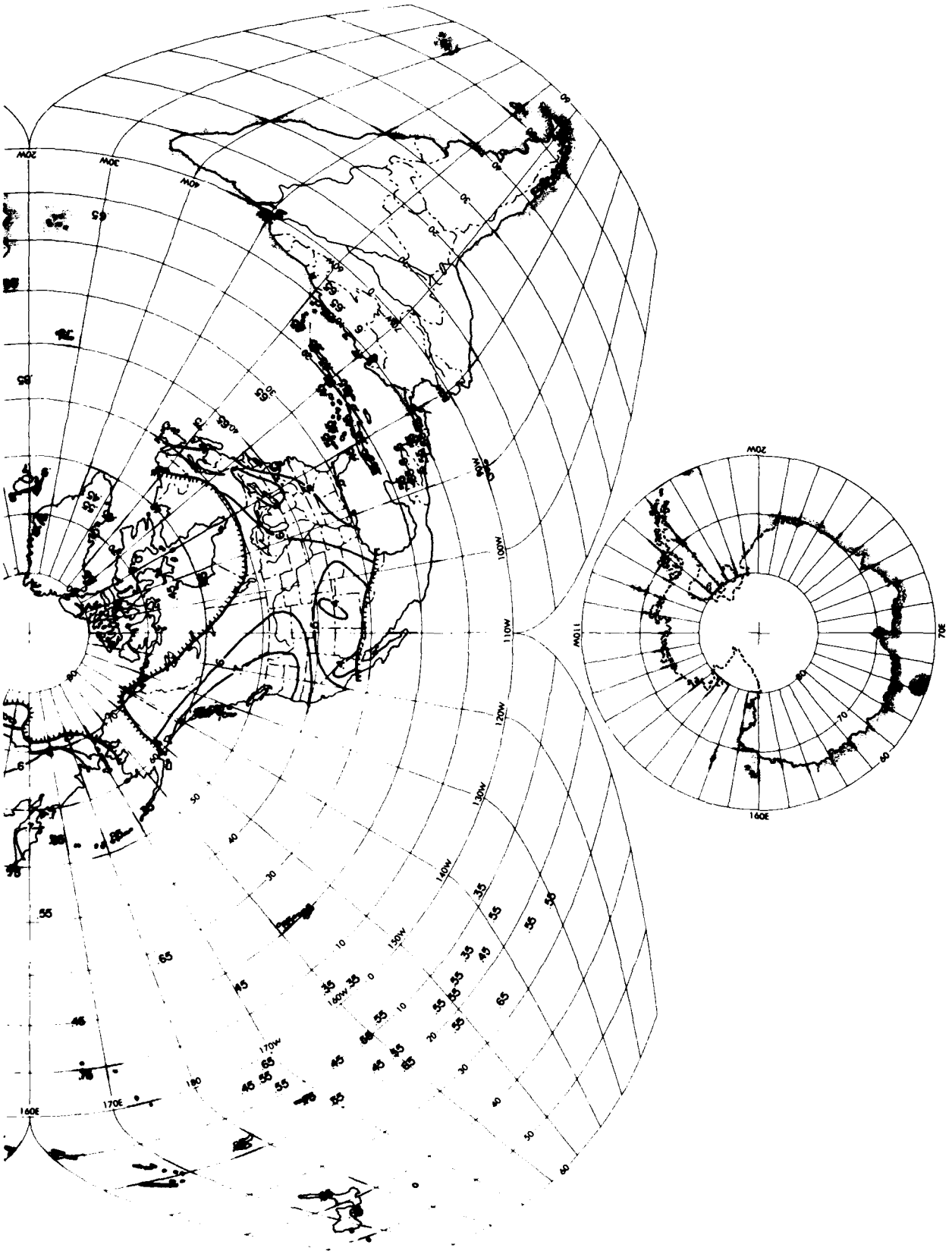

Figure 16a. Analysis of Mean Sky-Cover (P_o) for January, 1800 to 2000 LST (Contd)

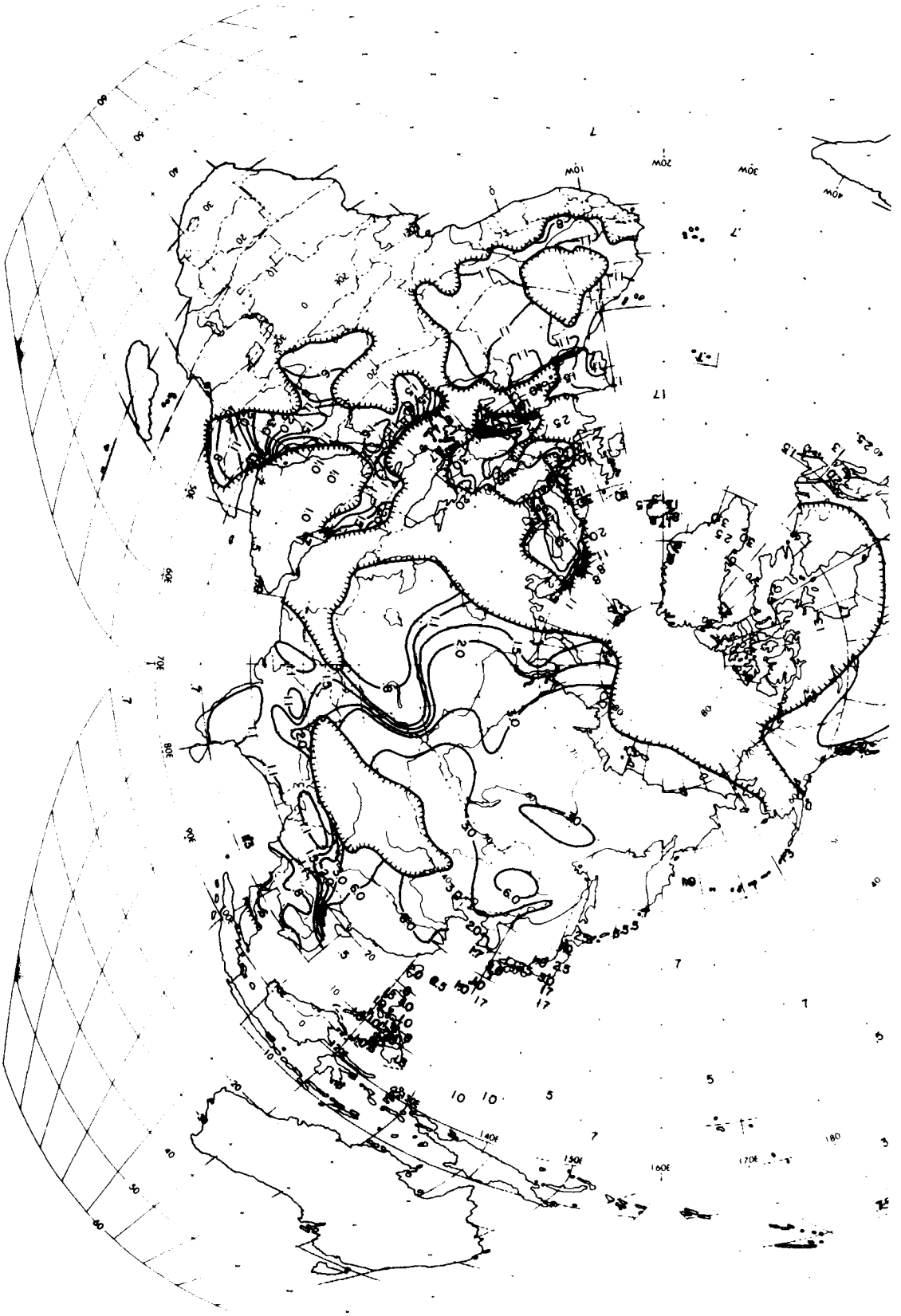

Figure 16b. Analysis of Scale Distance (r) for January, 1800 to 2000 LST

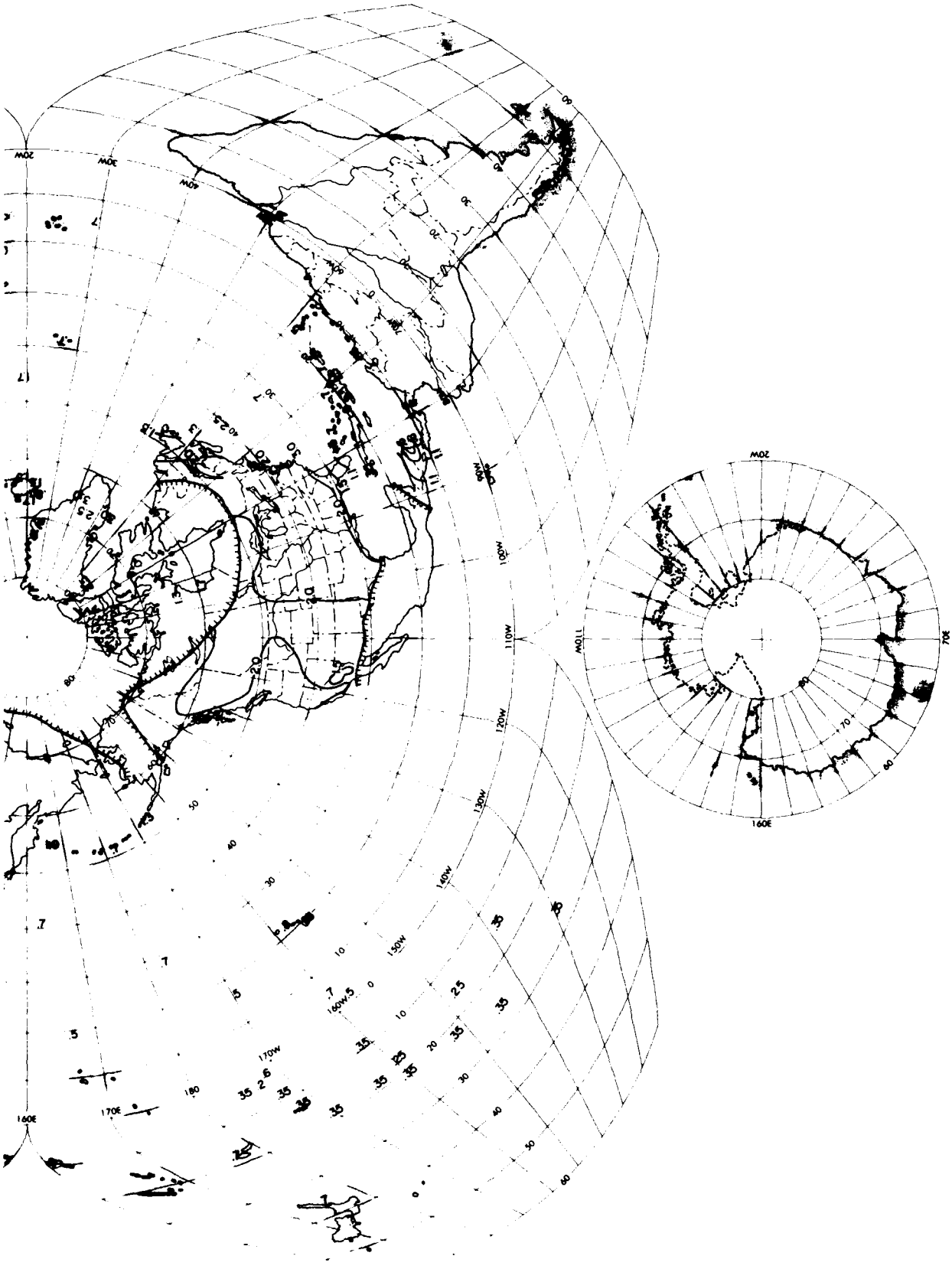

Figure 16b. Analysis of Scale Distance (r) for January, 1800 to 2000 LST (Contd)

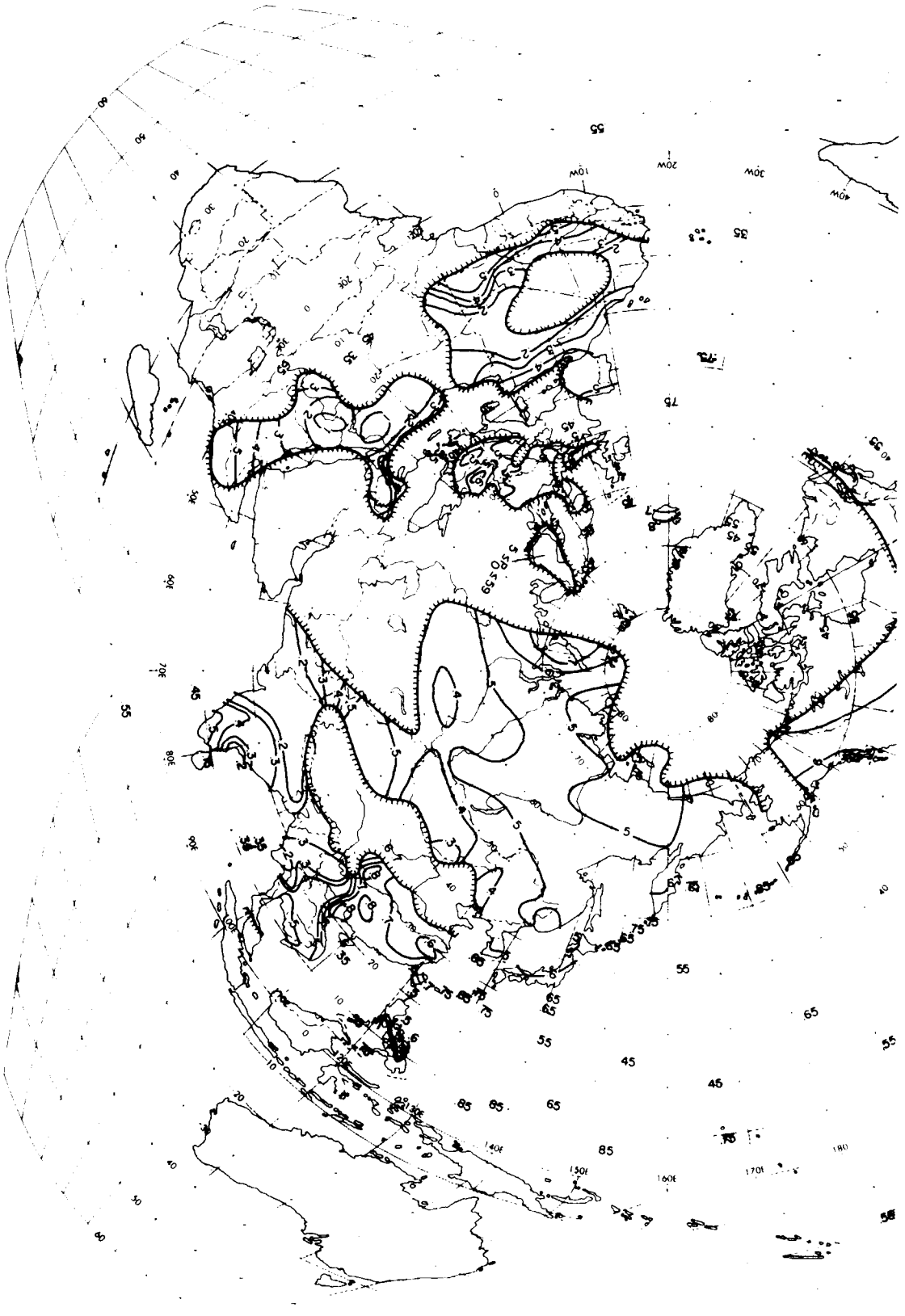

Figure 17a. Analysis of Mean Sky-Cover (P_o) for April, 0000 to 0200 LST

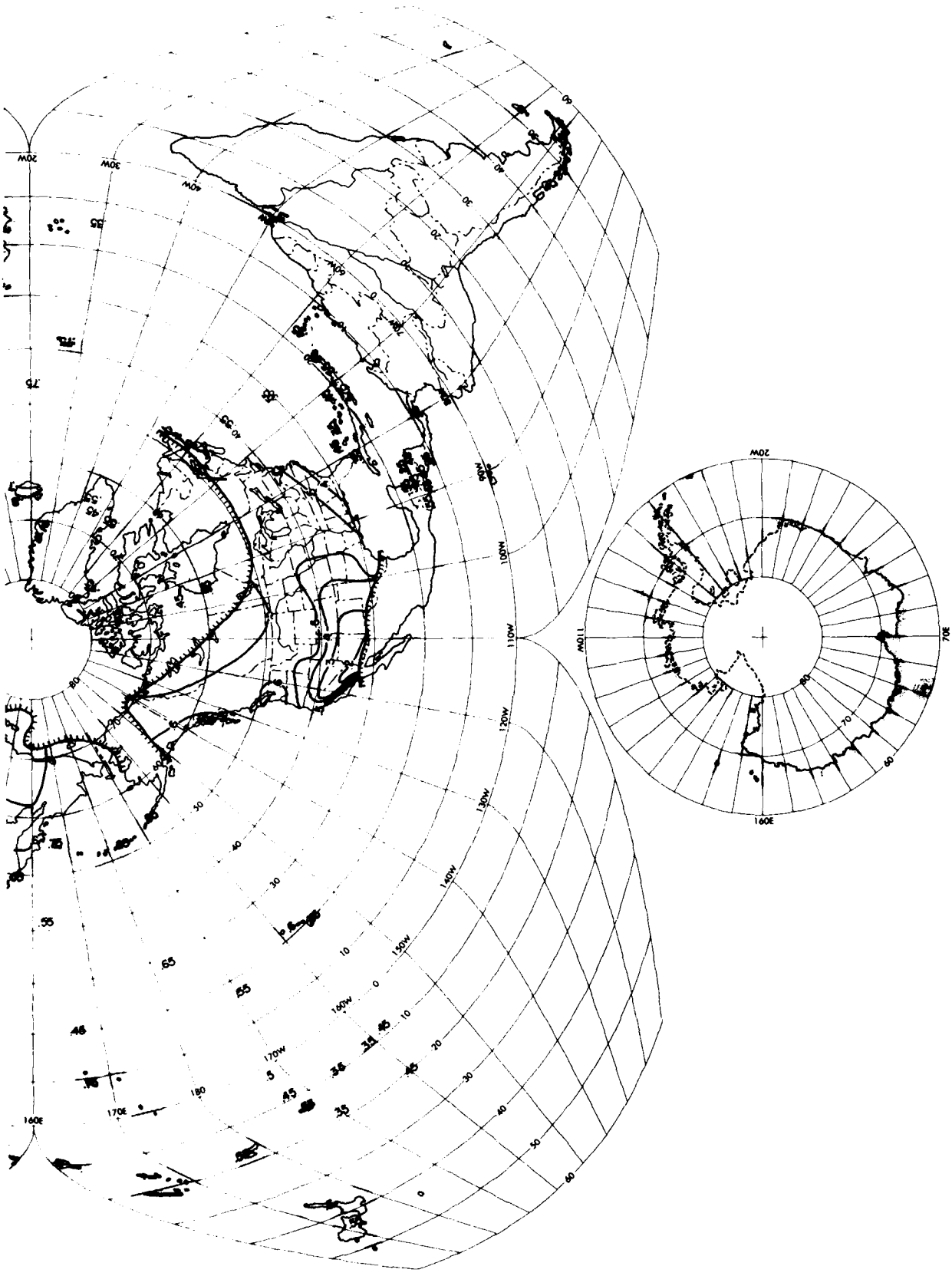

Figure 17a. Analysis of Mean Sky-Cover (P_o) for April, 0000 to 0200 LST (Contd)

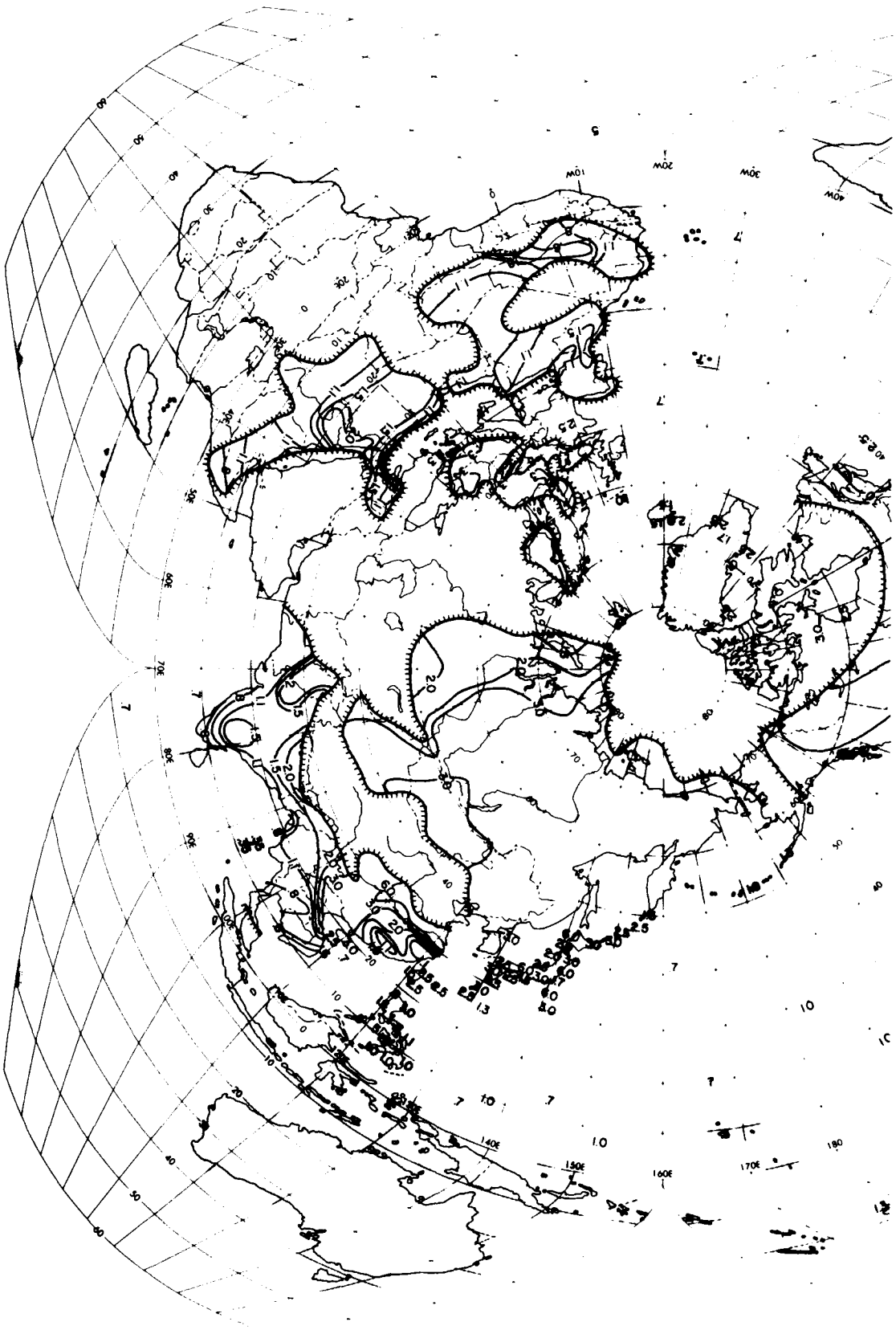

Figure 17b. Analysis of Scale Distance (r) for April, 0000 to 0200 LST

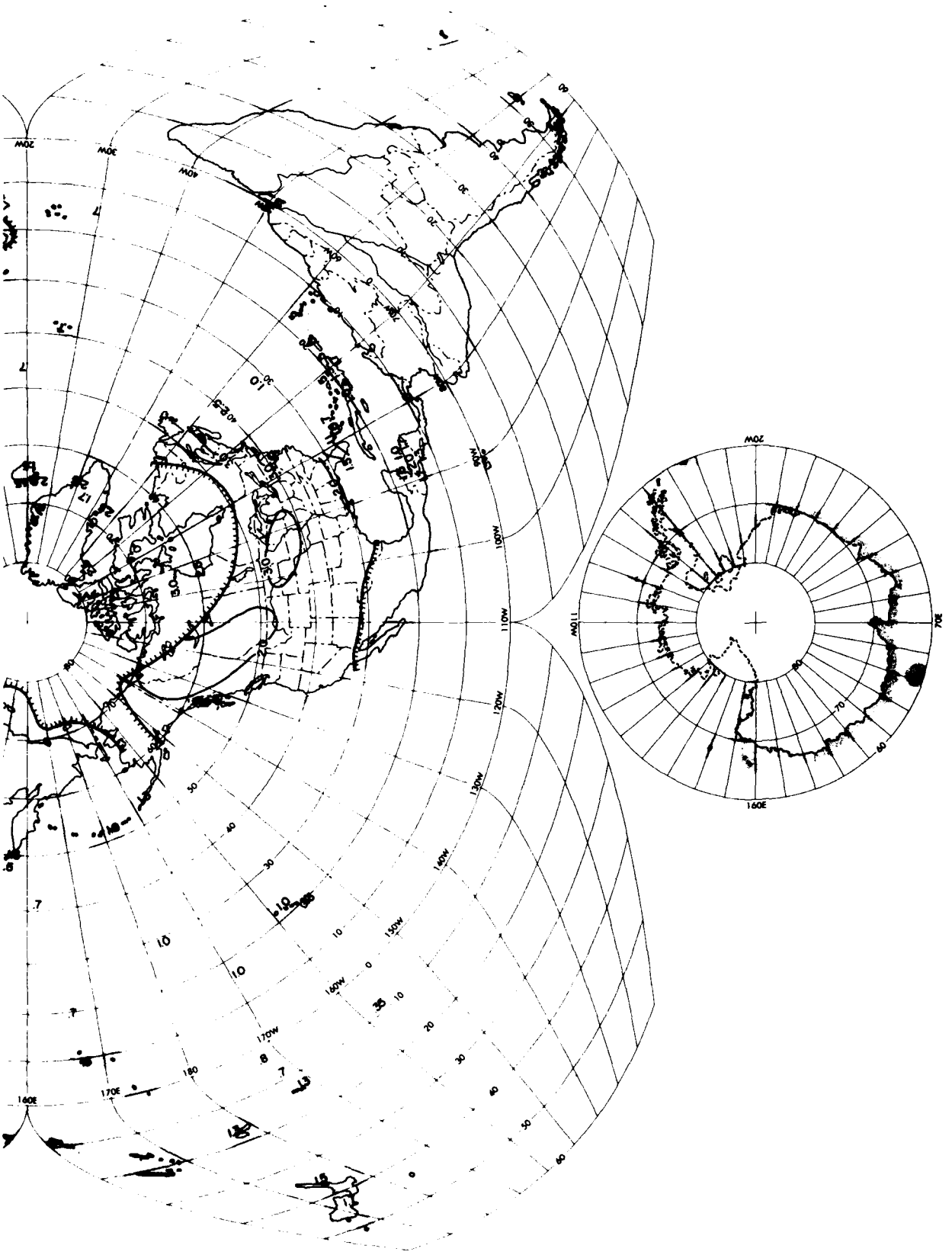

Figure 17b. Analysis of Scale Distance (r) for April, 0000 to 0200 LST (Contd)

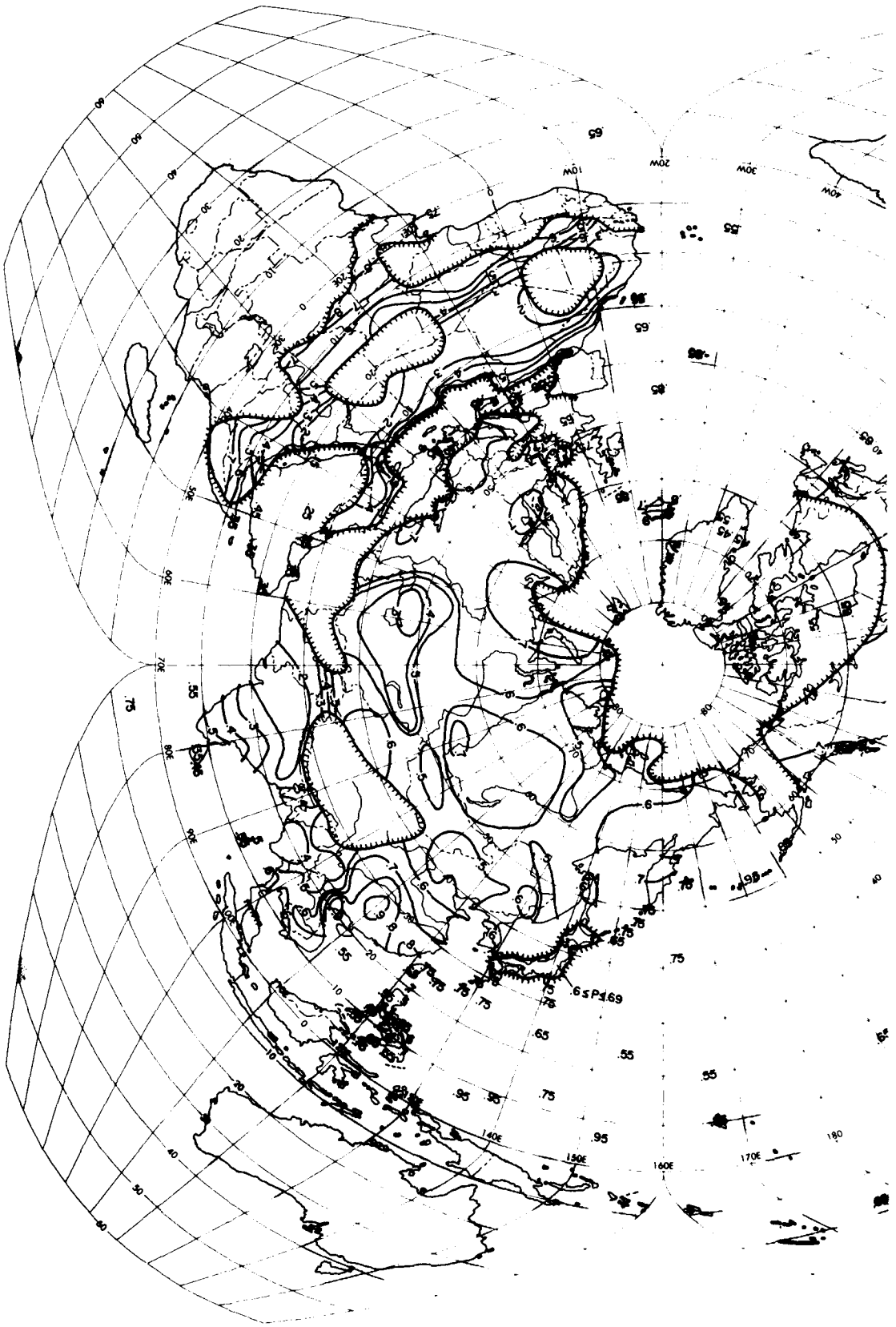

Figure 18a. Analysis of Mean Sky-Cover (P_o) for April, 0600 to 0800 LST

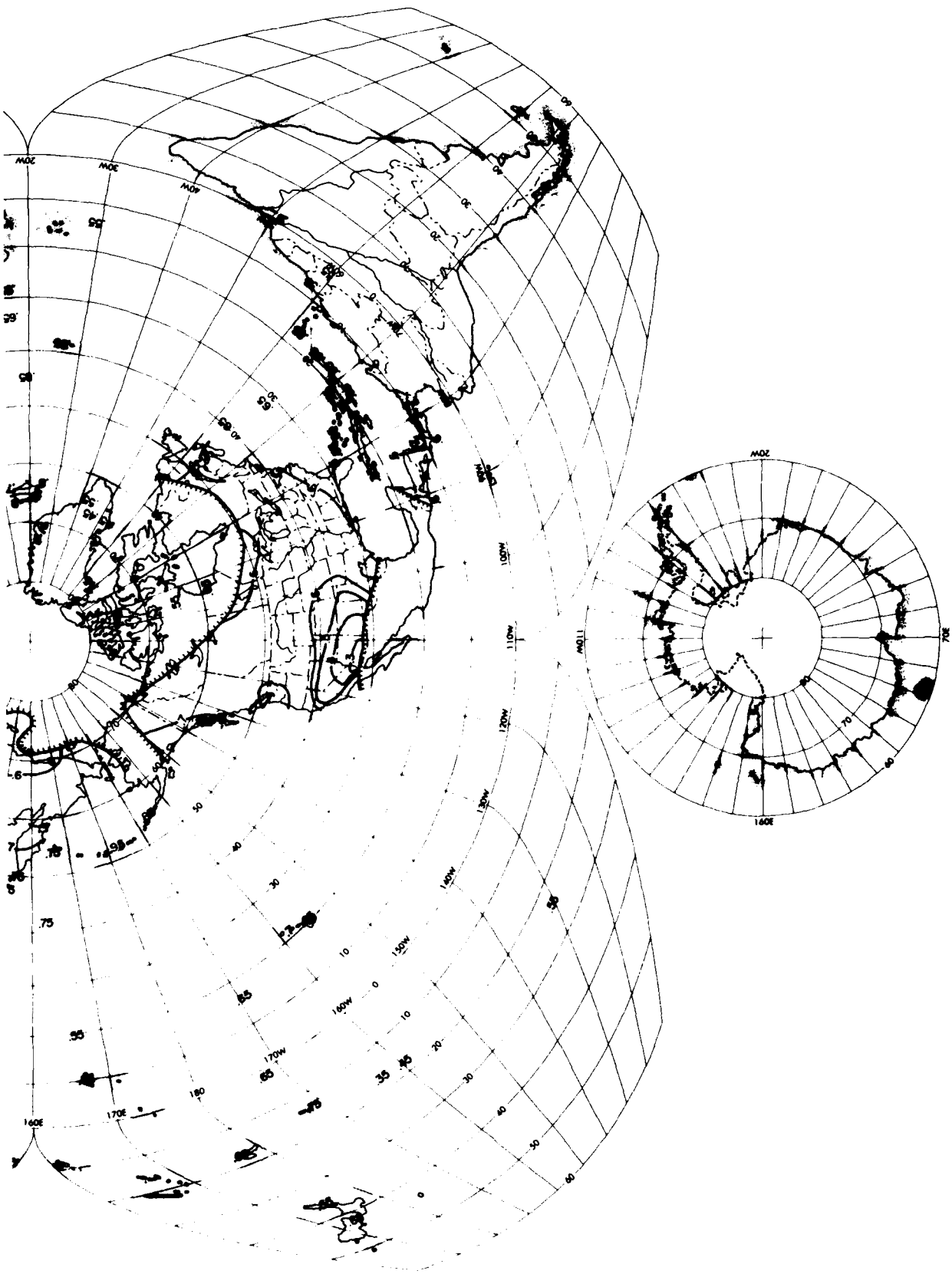

Figure 18a. Analysis of Mean Sky-Cover (P_o) for April, 0600 to 0800 LST (Contd)

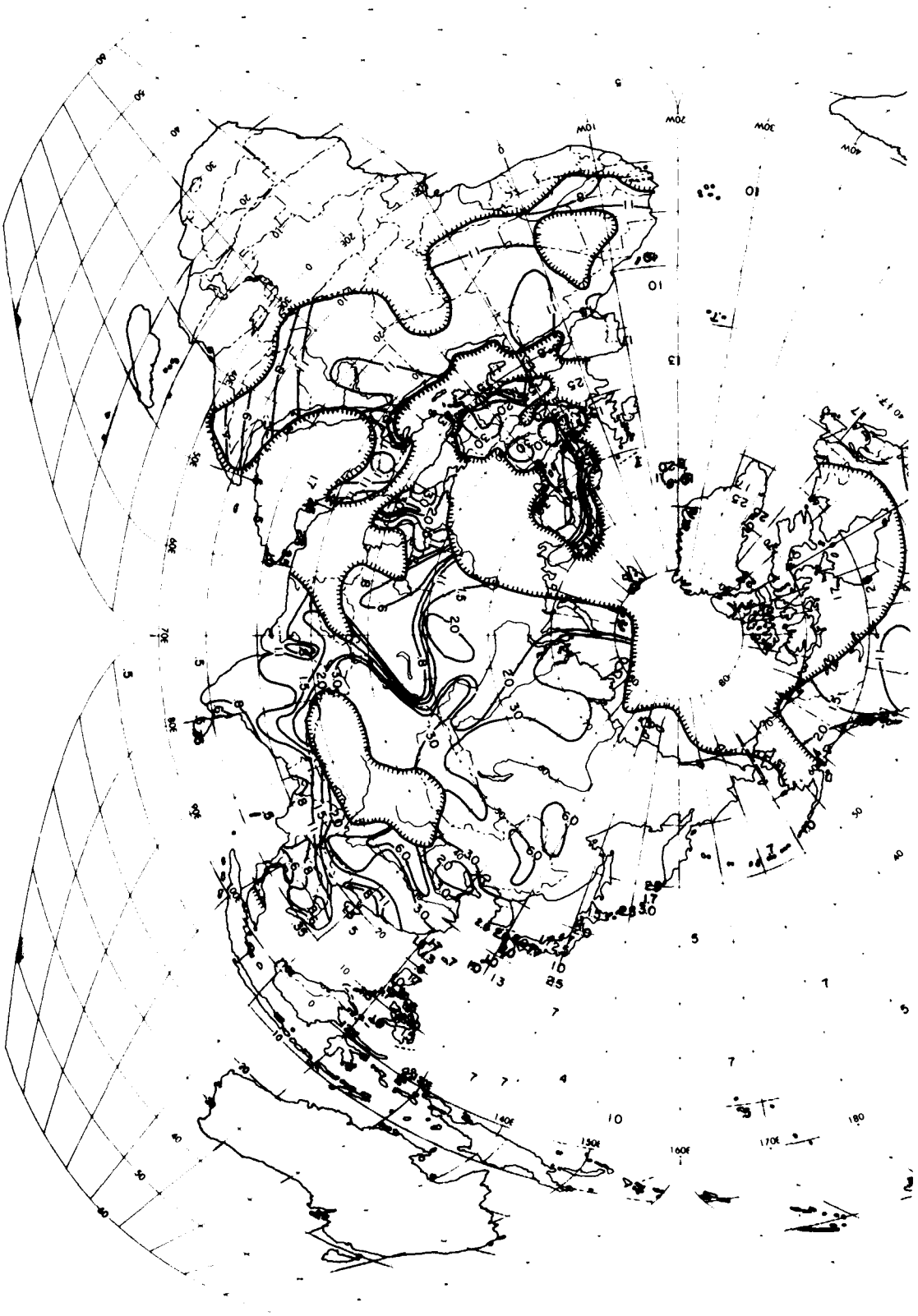

Figure 18b. Analysis of Scale Distance (r) for April, 0600 to 0800 LST

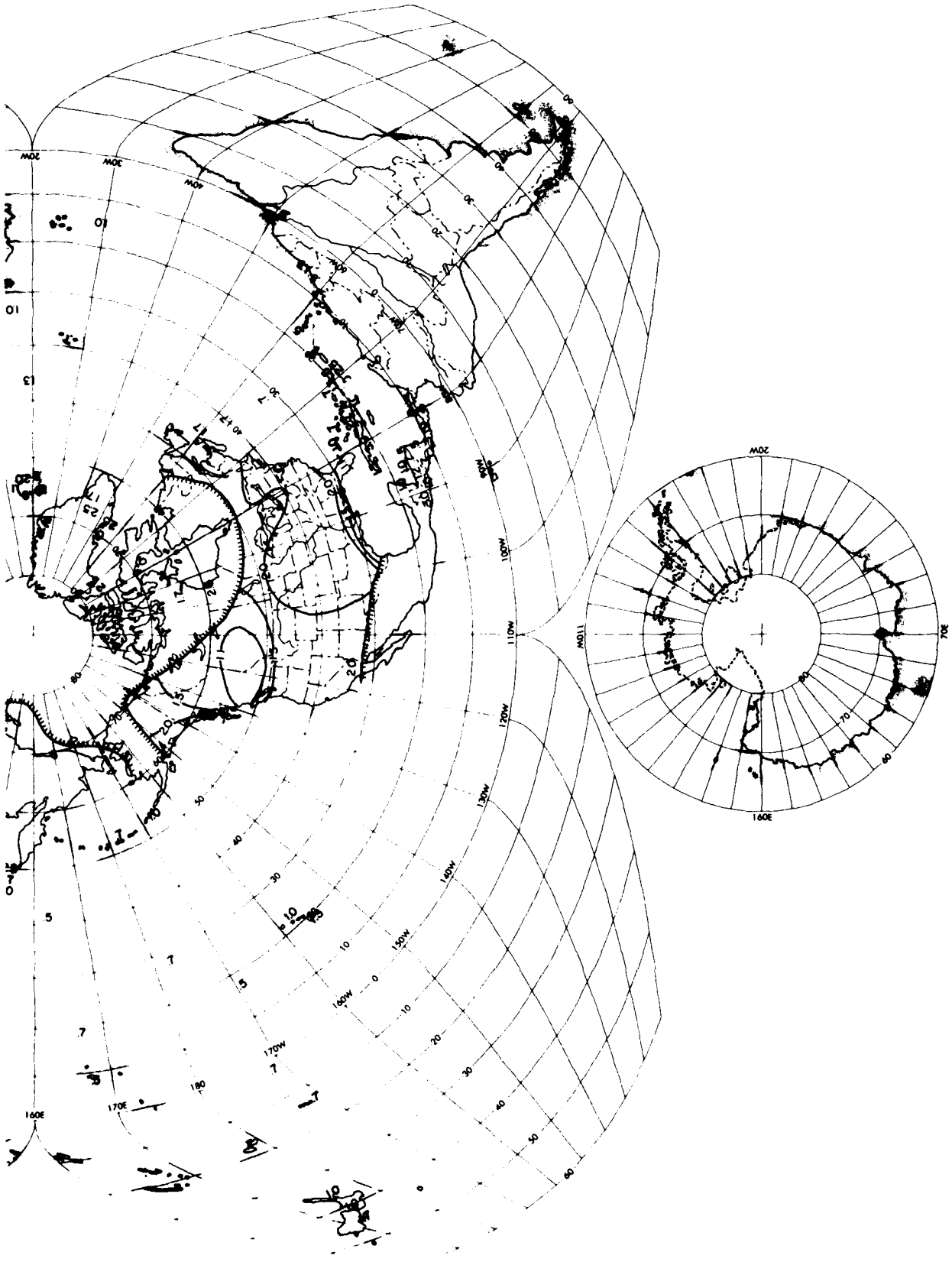

Figure 18b. Analysis of Scale Distance (r) for April, 0600 to 0800 LST (Contd)

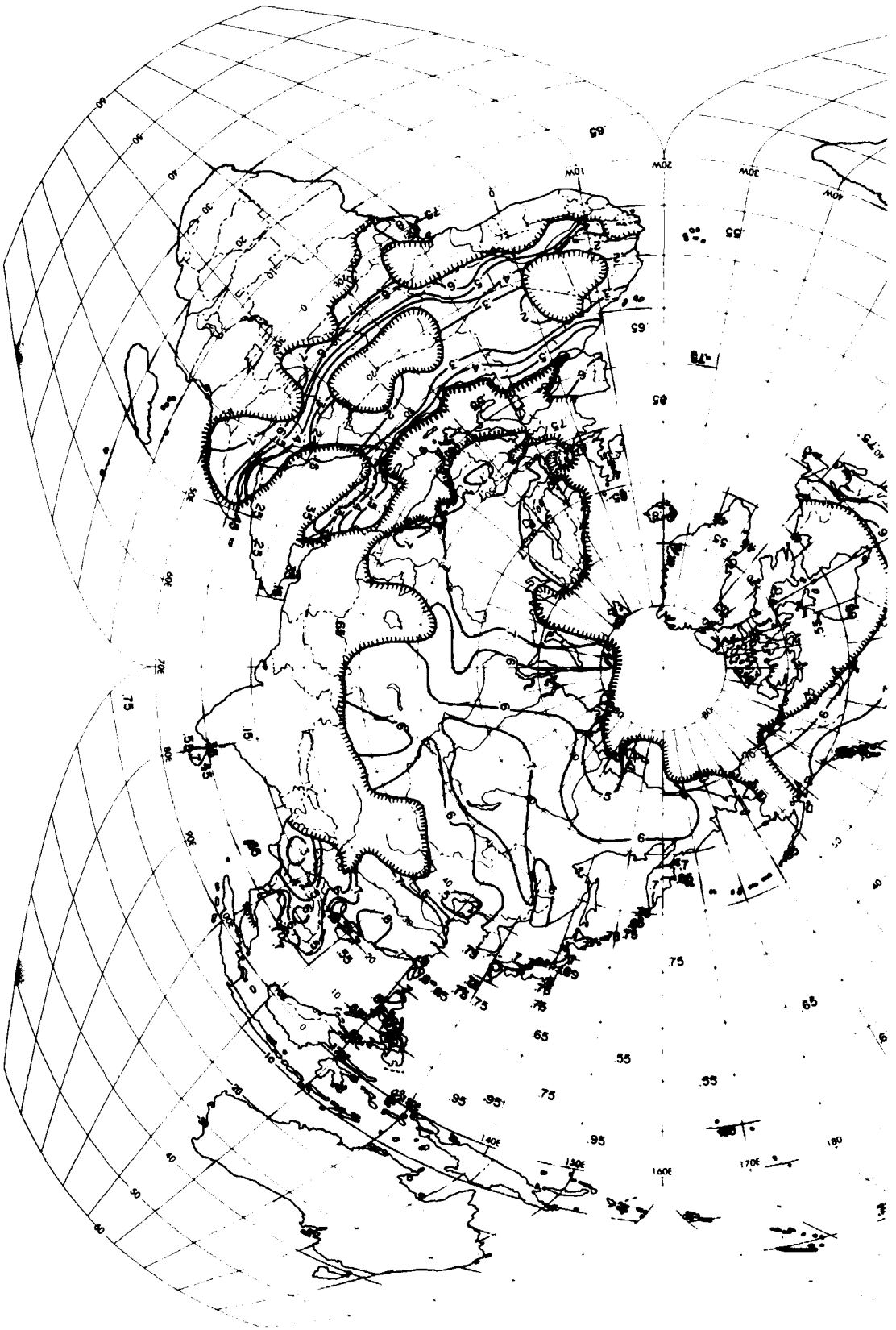

Figure 19a. Analysis of Mean Sky-Cover (P_o) for April, 1200 to 1400 LST

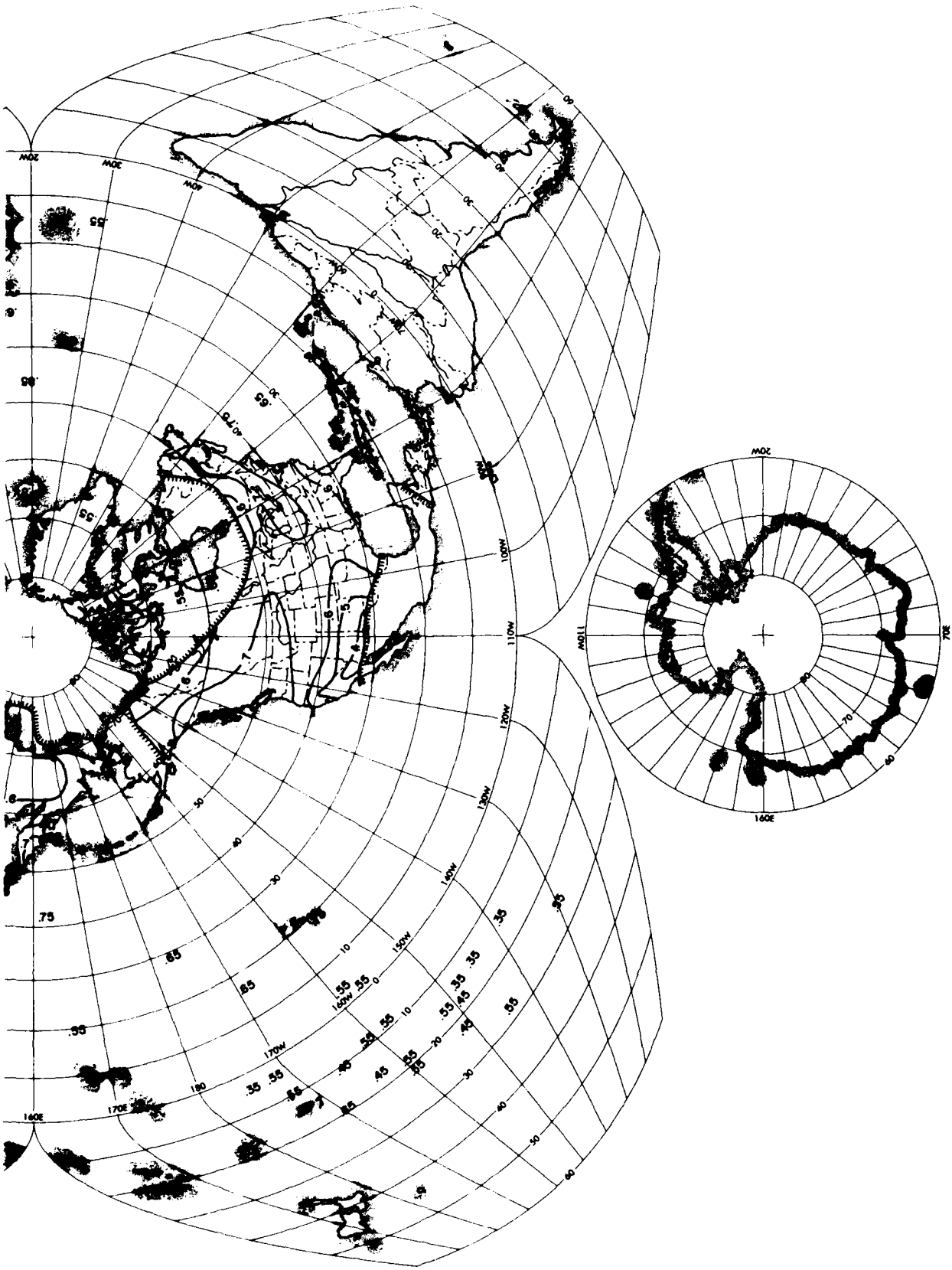

Figure 19a. Analysis of Mean Sky-Cover (P_o) for April, 1200 to 1400 LST (Contd)

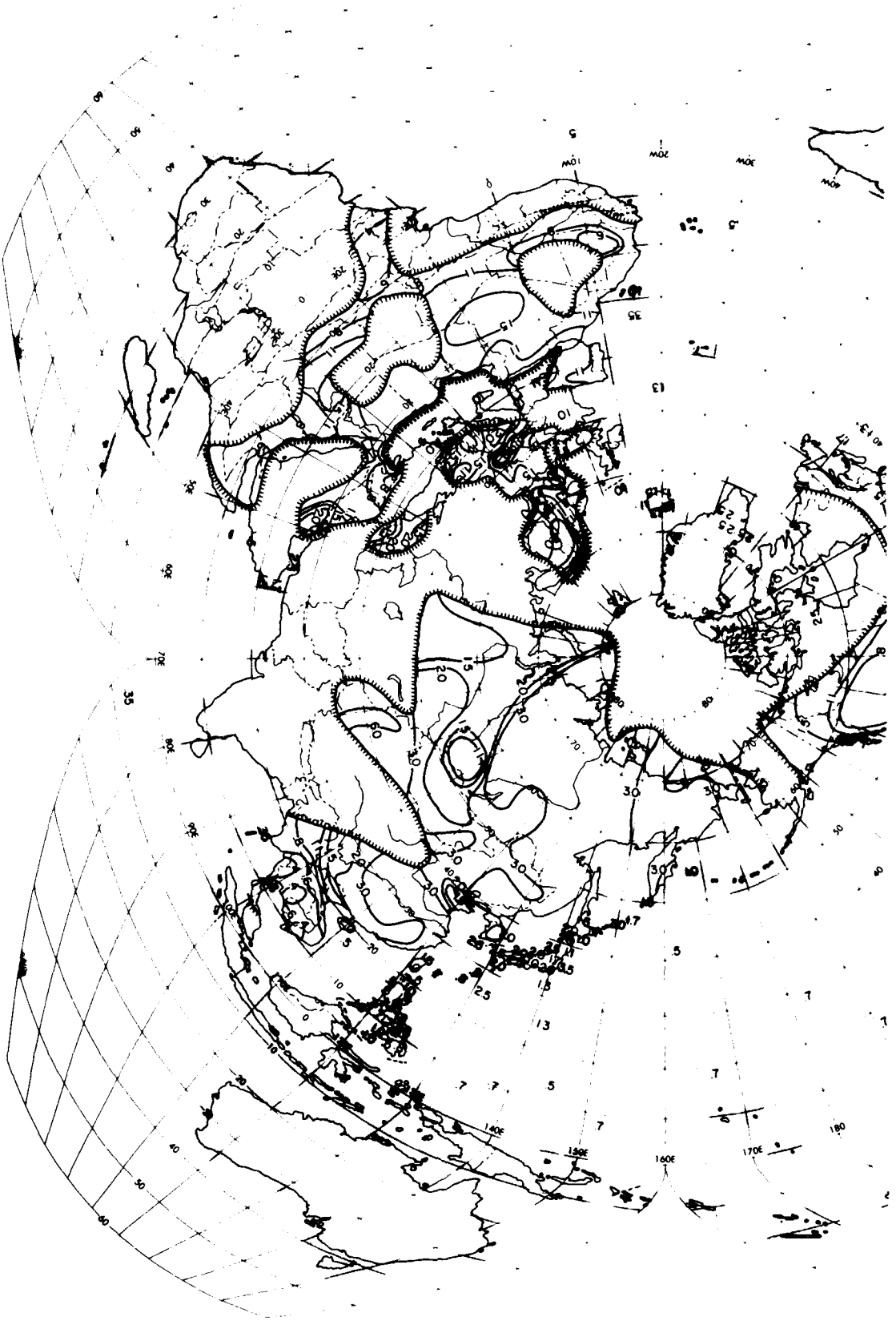

Figure 19b. Analysis of Scale Distance (r) for April, 1200 to 1400 LST

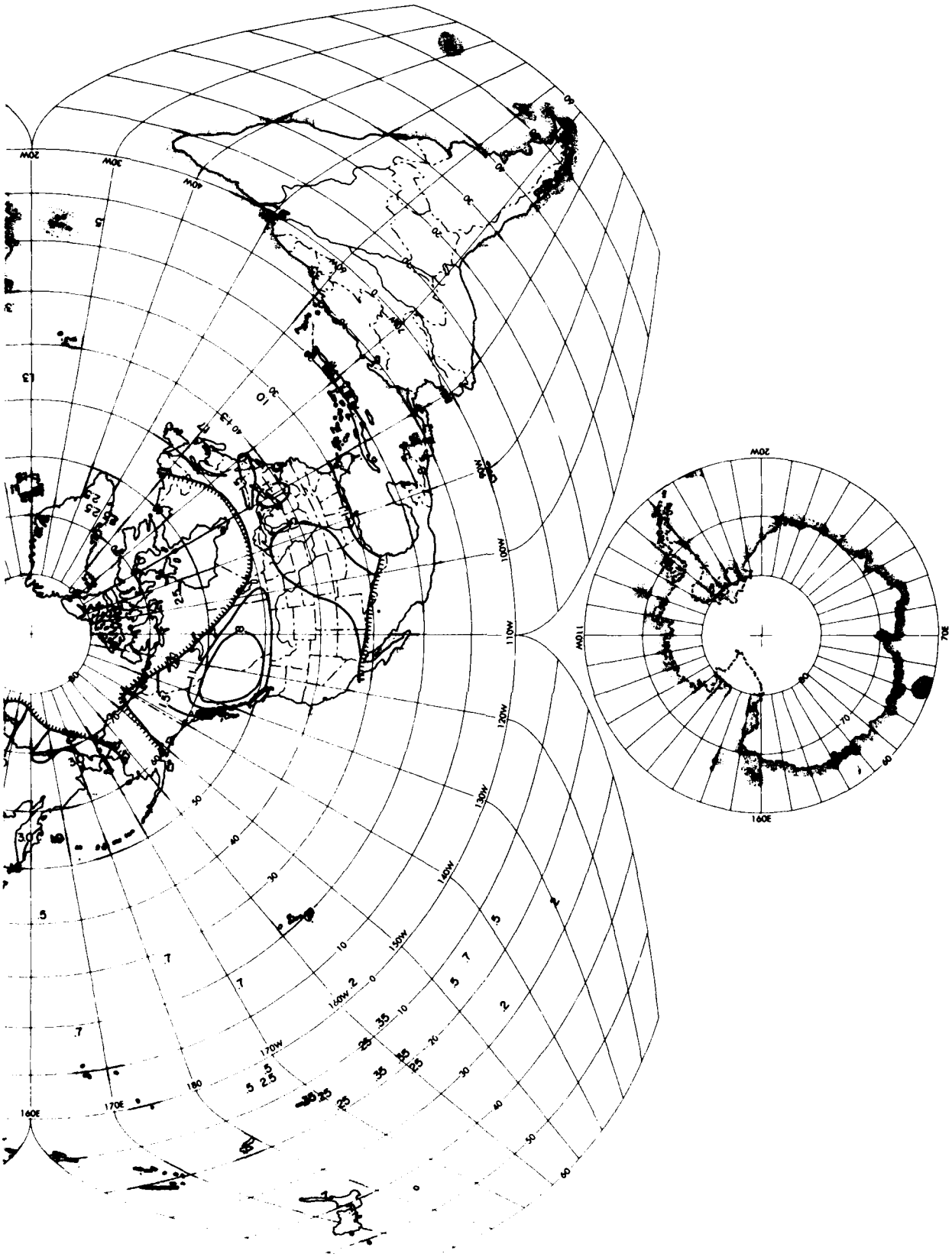

Figure 19b. Analysis of Scale Distance (r) for April, 1200 to 1400 LST (Contd)

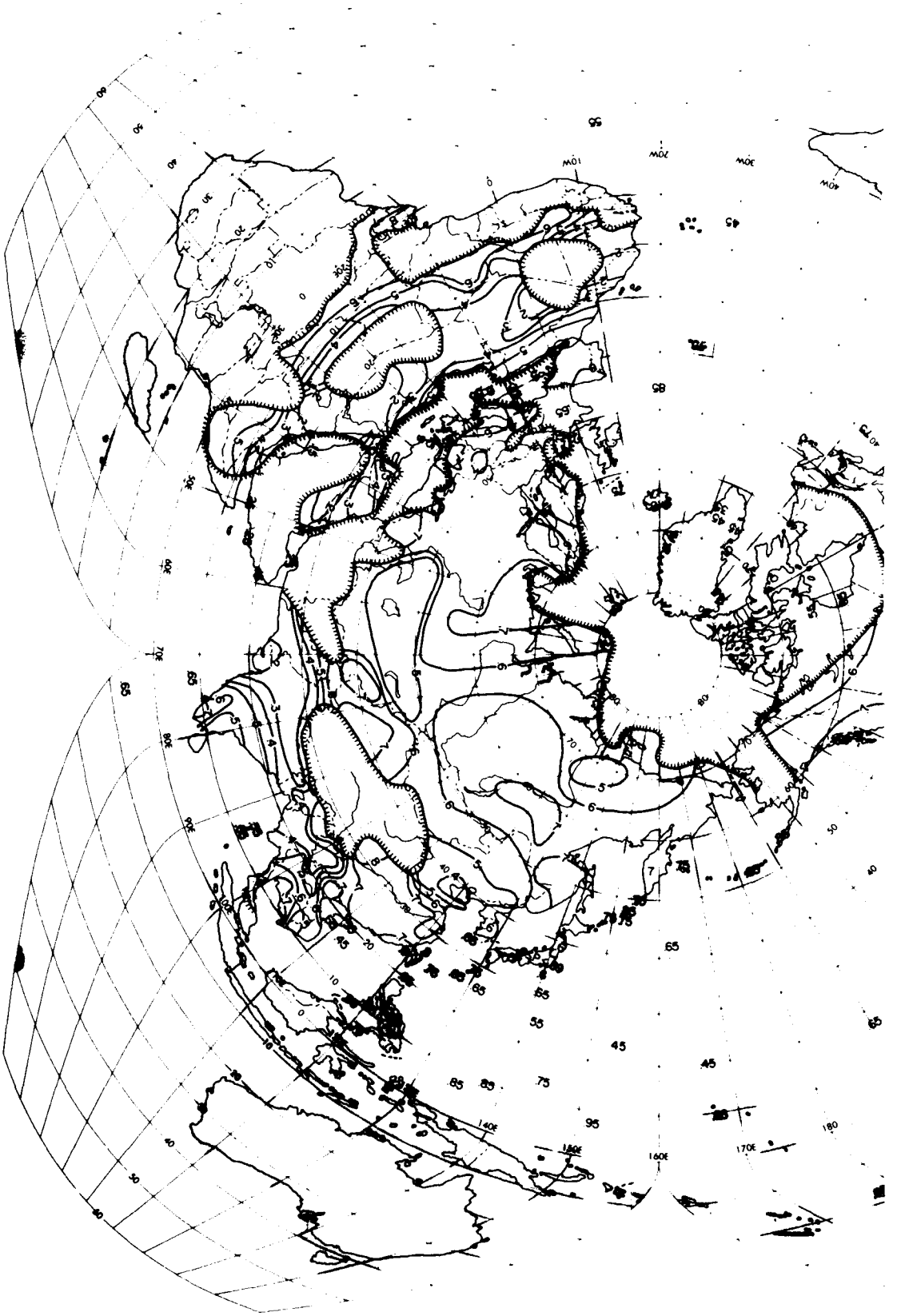

Figure 20a. Analysis of Mean Sky-Cover (P_o) for April, 1800 to 2000 LST

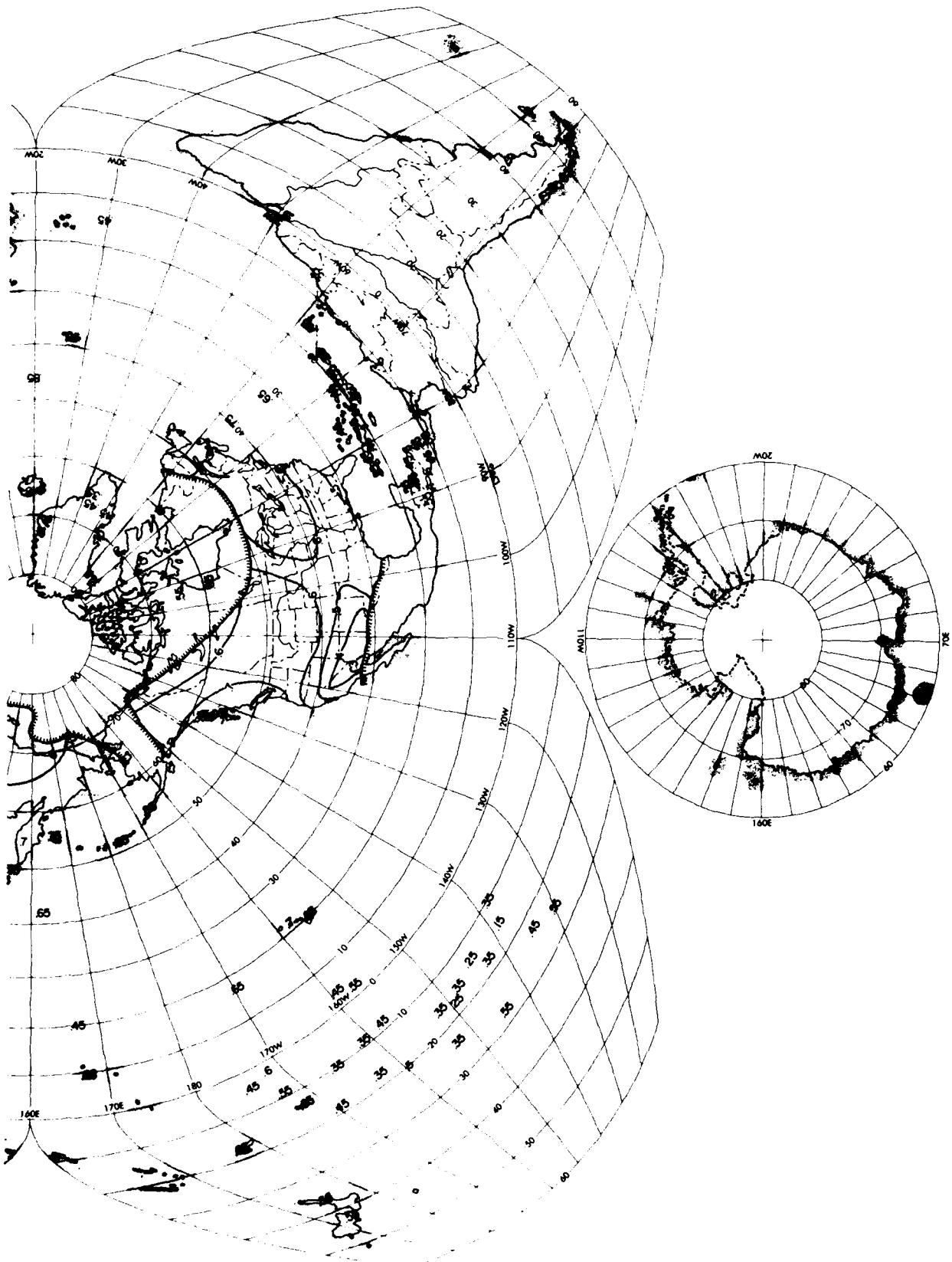

Figure 20a. Analysis of Mean Sky-Cover (P_o) for April, 1800 to 2000 LST (Contd)

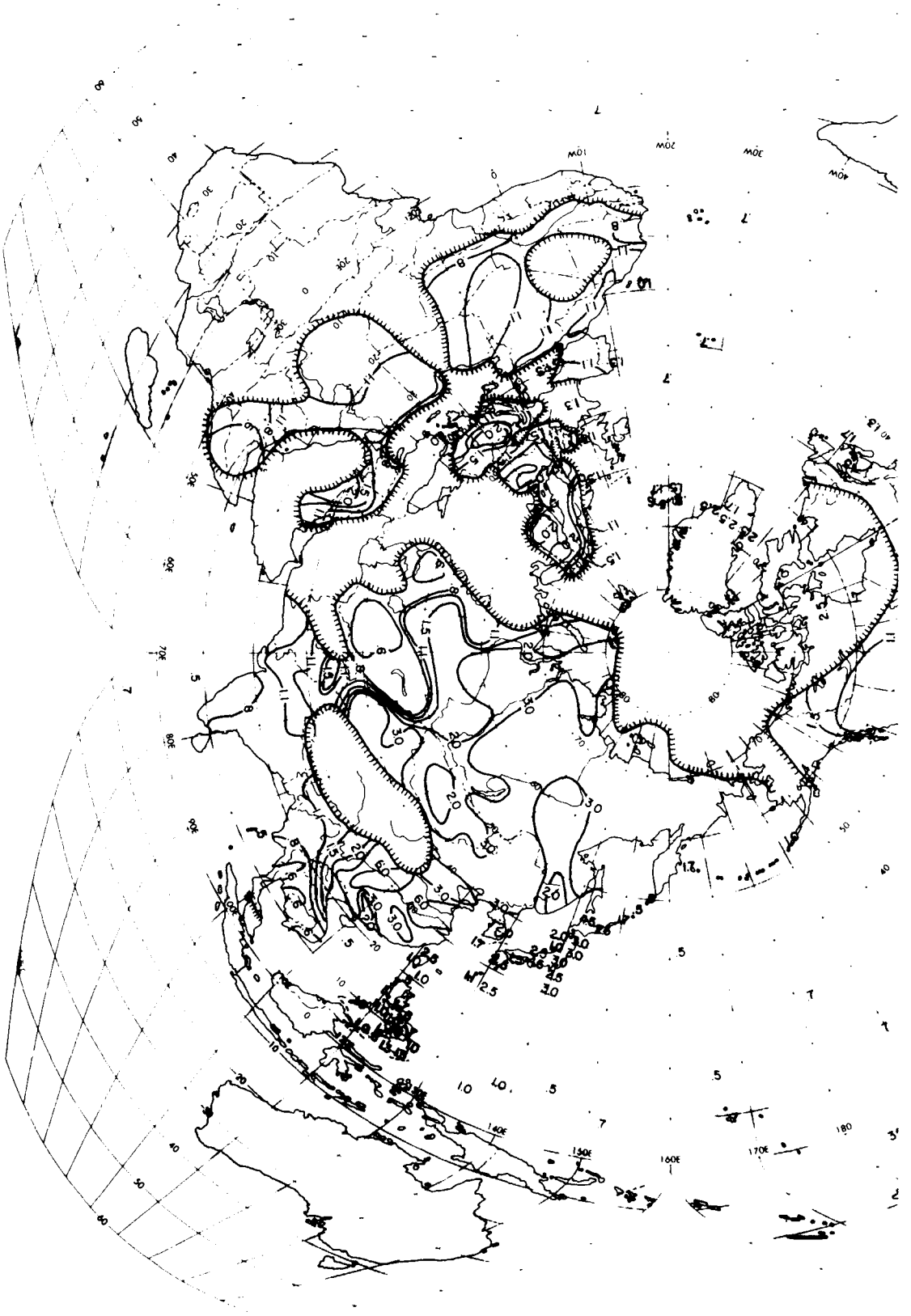

Figure 20b. Analysis of Scale Distance (r) for April, 1800 to 2000 LST

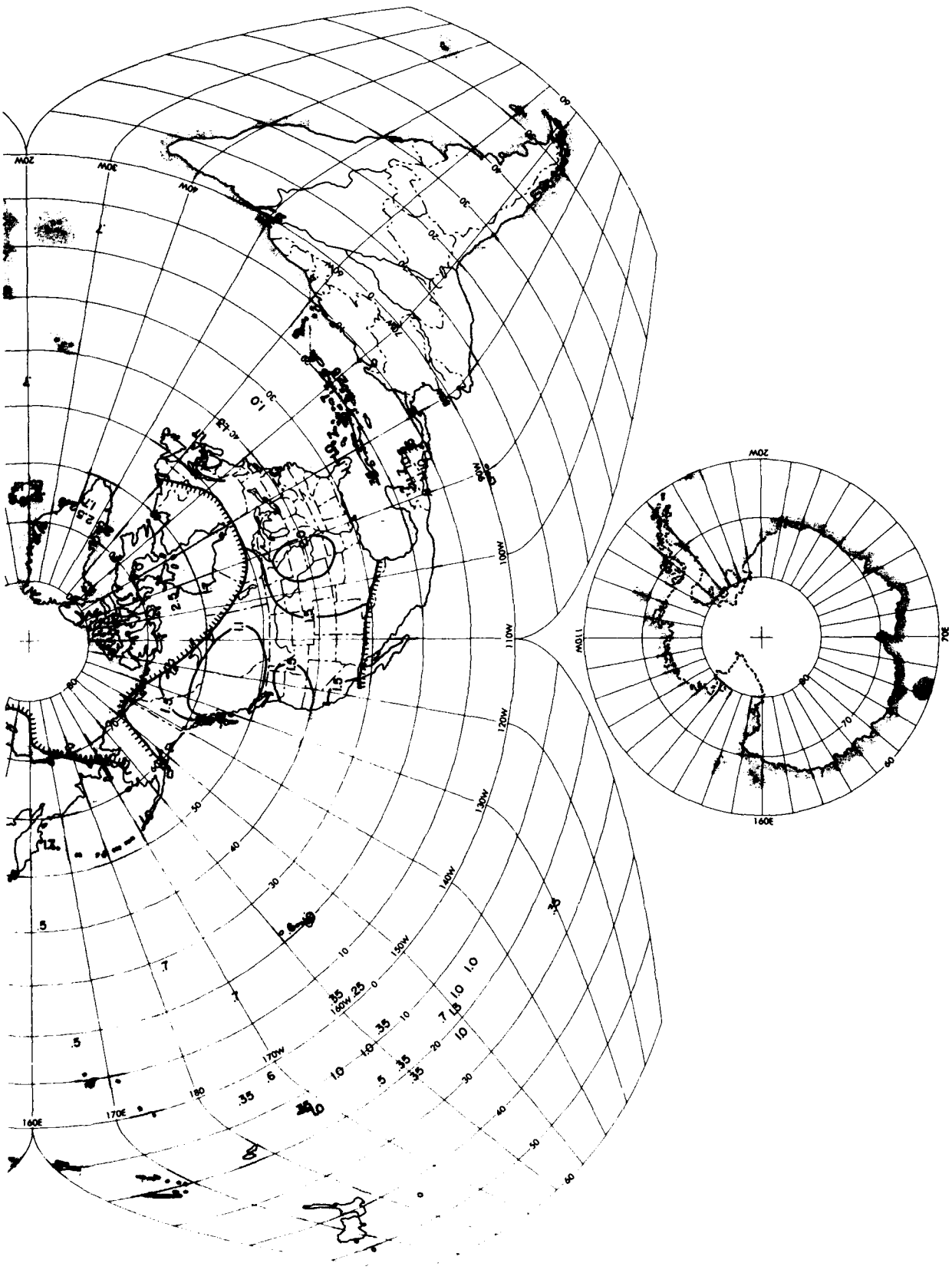

Figure 20b. Analysis of Scale Distance (r) for April, 1800 to 2000 LST (Contd)

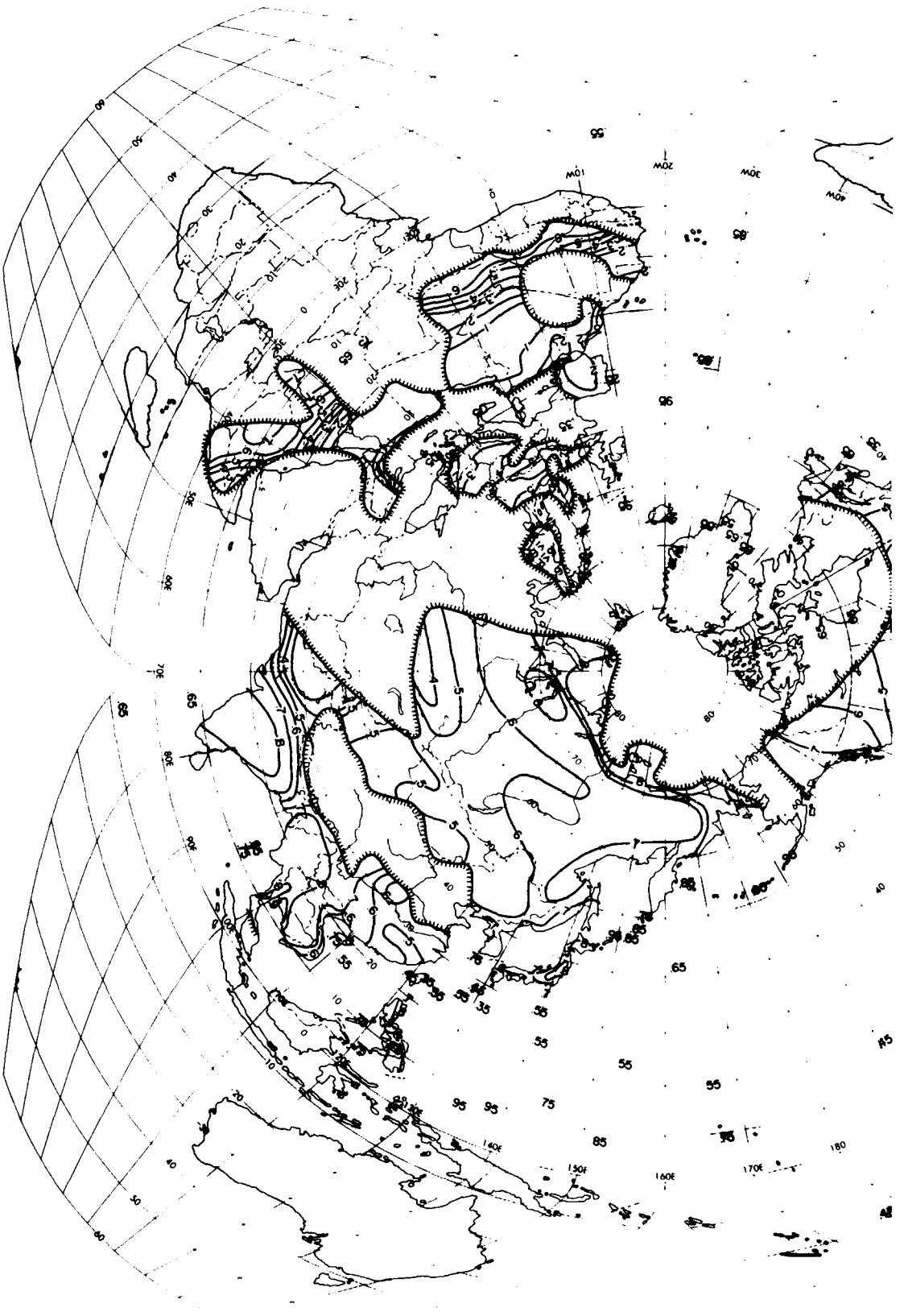

Figure 21a. Analysis of Mean Sky-Cover (P_o) for July, 0000 to 0200 LST

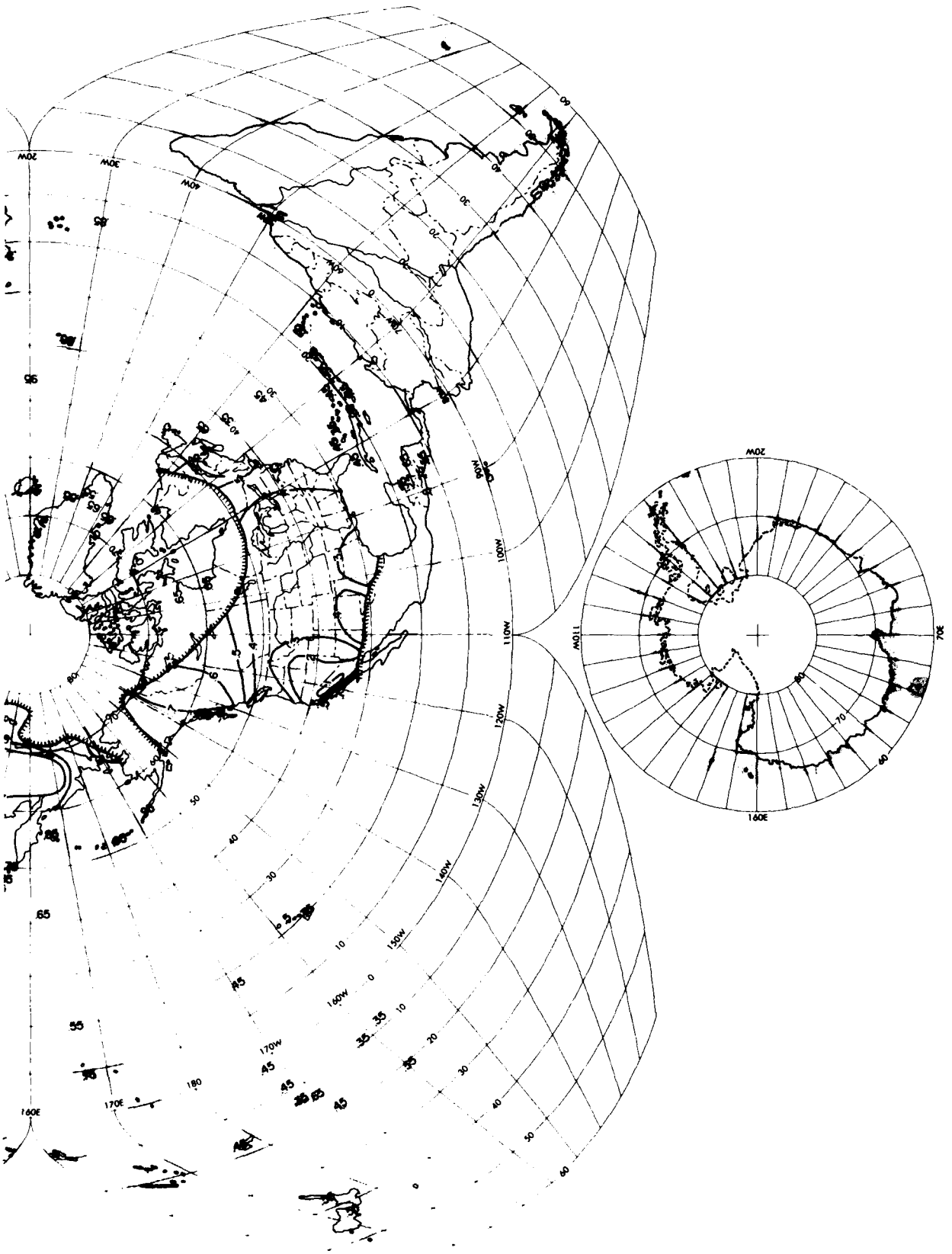

Figure 21a. Analysis of Mean Sky-Cover (P_o) for July, 0000 to 0200 LST (Contd)

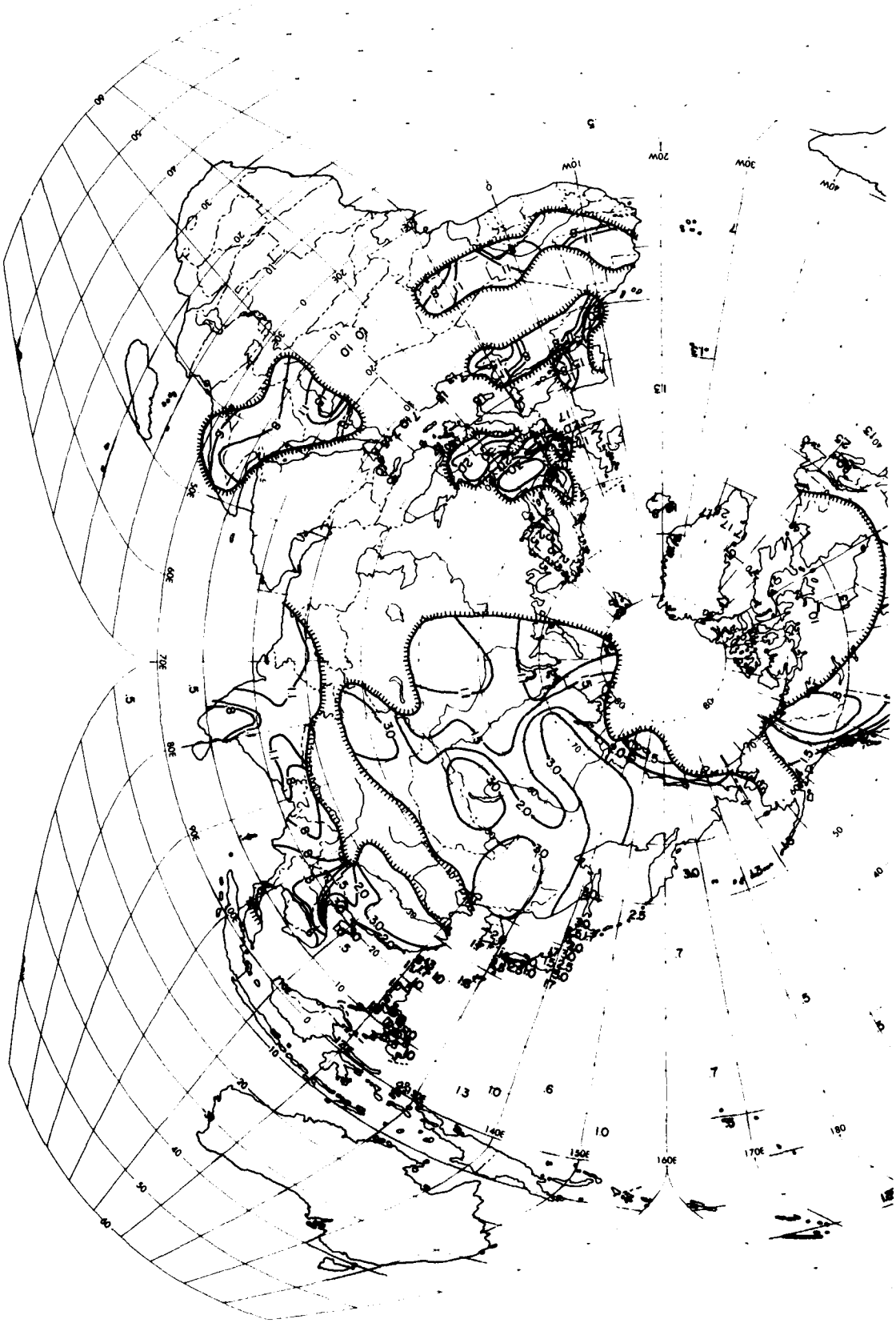

Figure 21b. Analysis of Scale Distance (r) for July, 0000 to 0200 LST

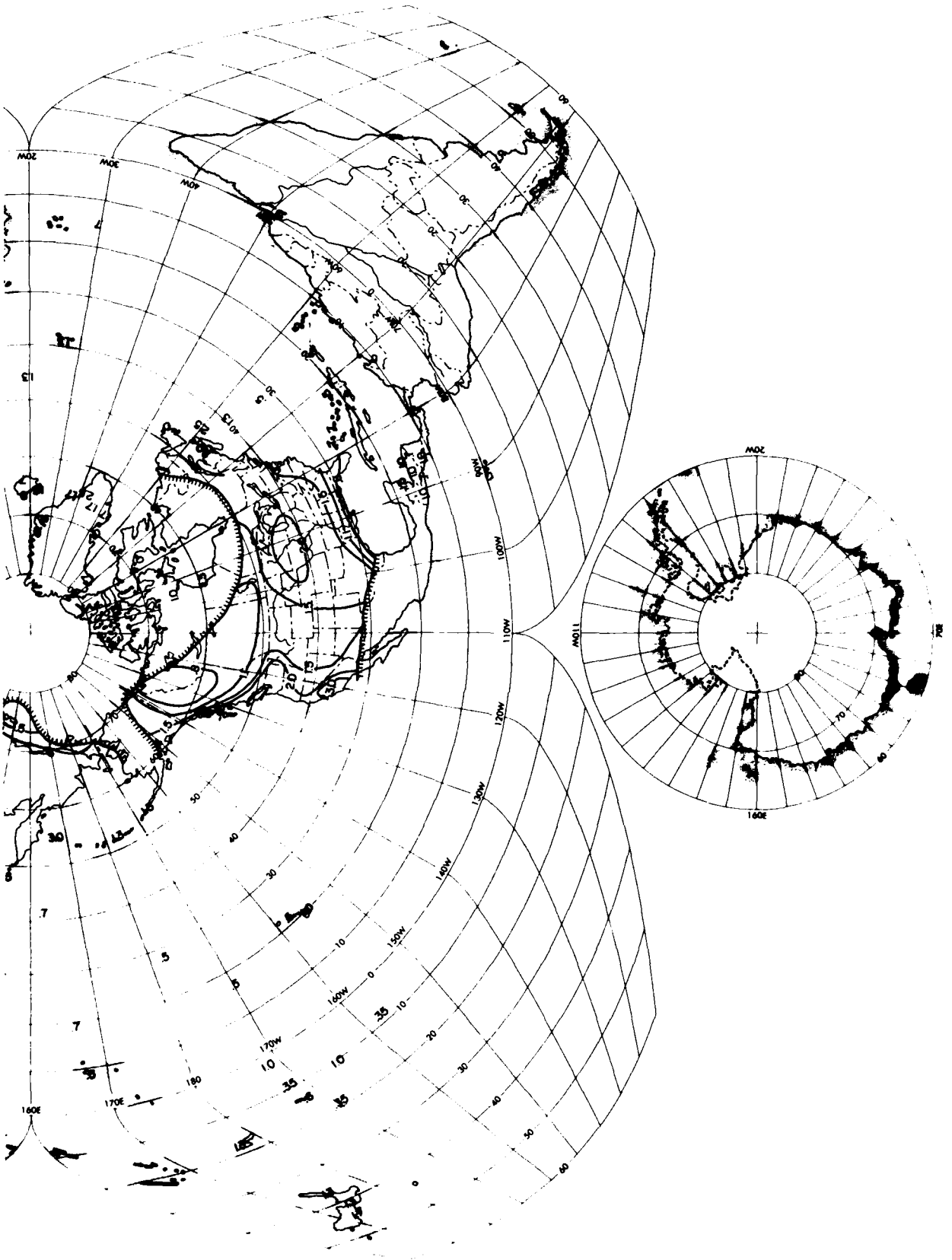

Figure 21b. Analysis of Scale Distance (r) for July, 0000 to 0200 LST (Contd)

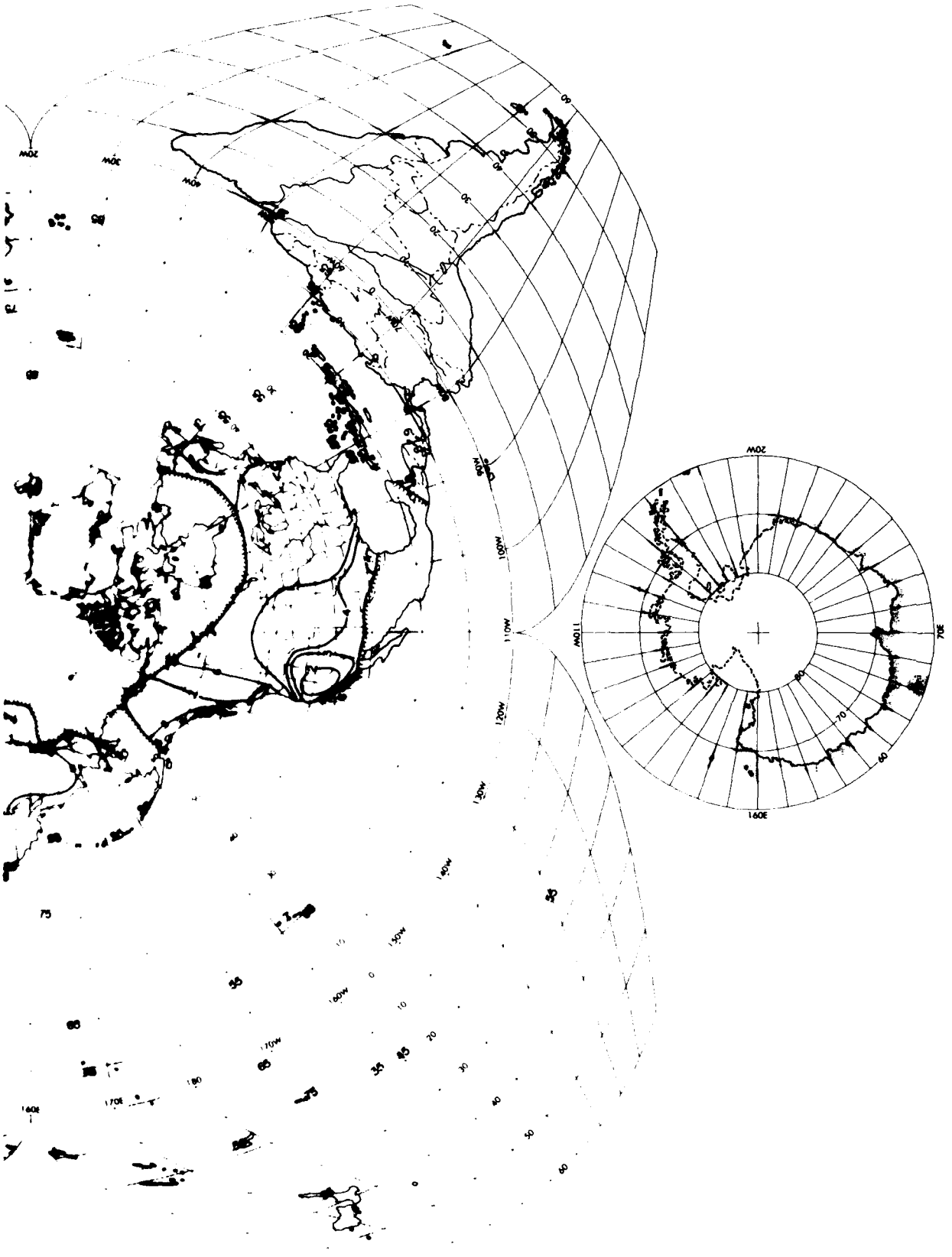

Figure 22a. Analysis of Mean Sky-Cover (P_o) for July, 0600 to 0800 LST

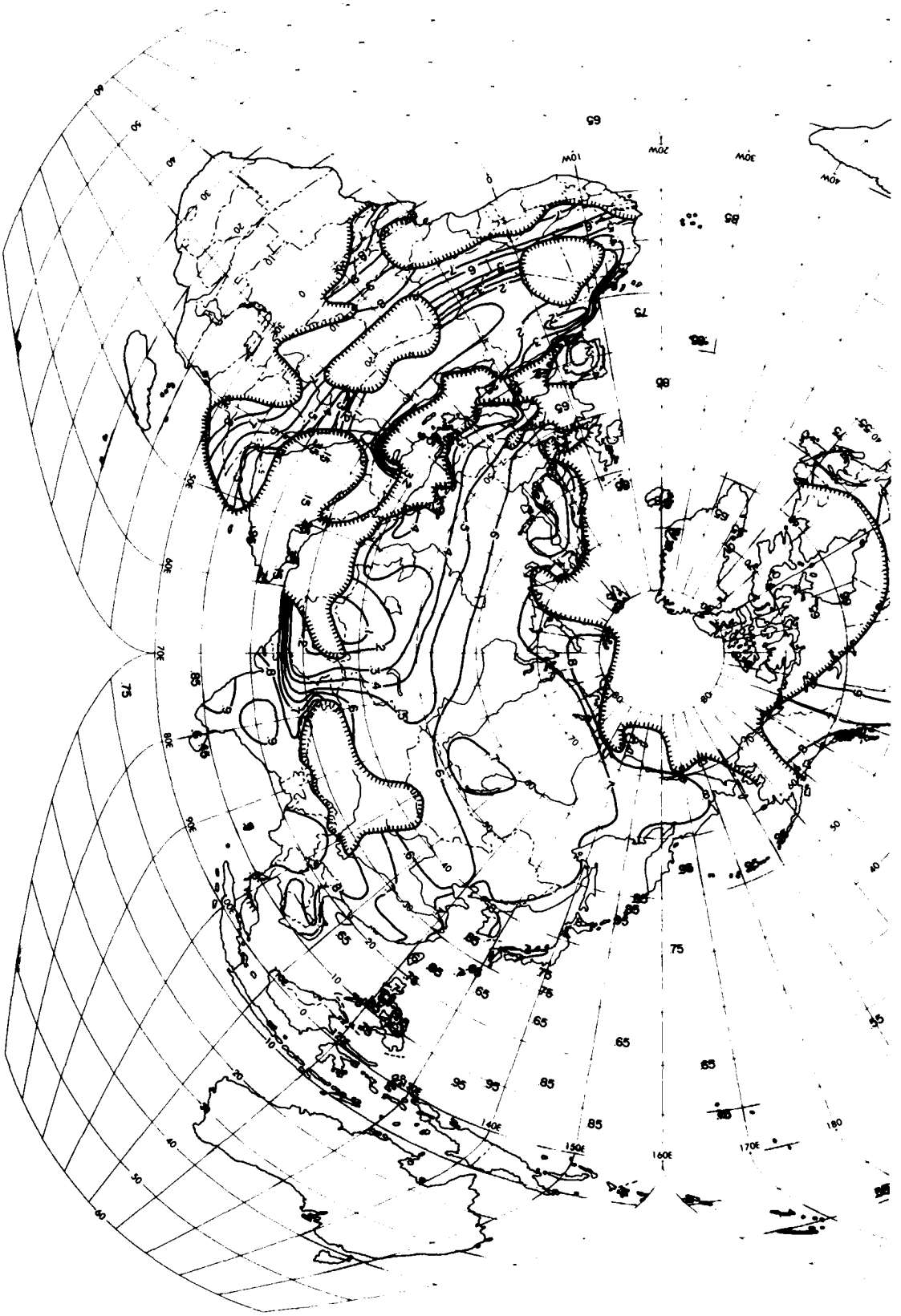

Figure 22a. Analysis of Mean Sky-Cover (P_o) for July, 0600 to 0800 LST (Contd)

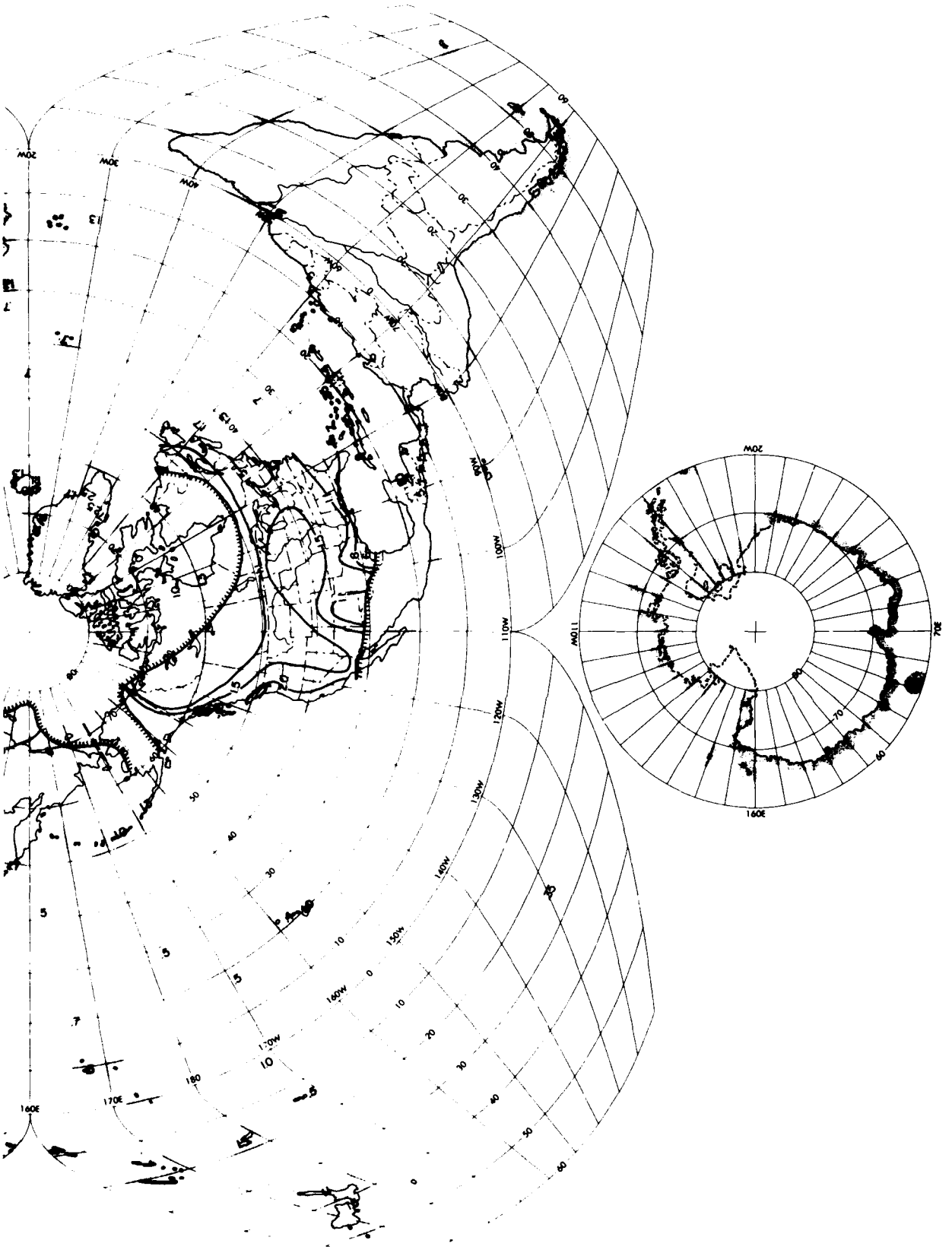

Figure 22b. Analysis of Scale Distance (r) for July, 0600 to 0800 LST

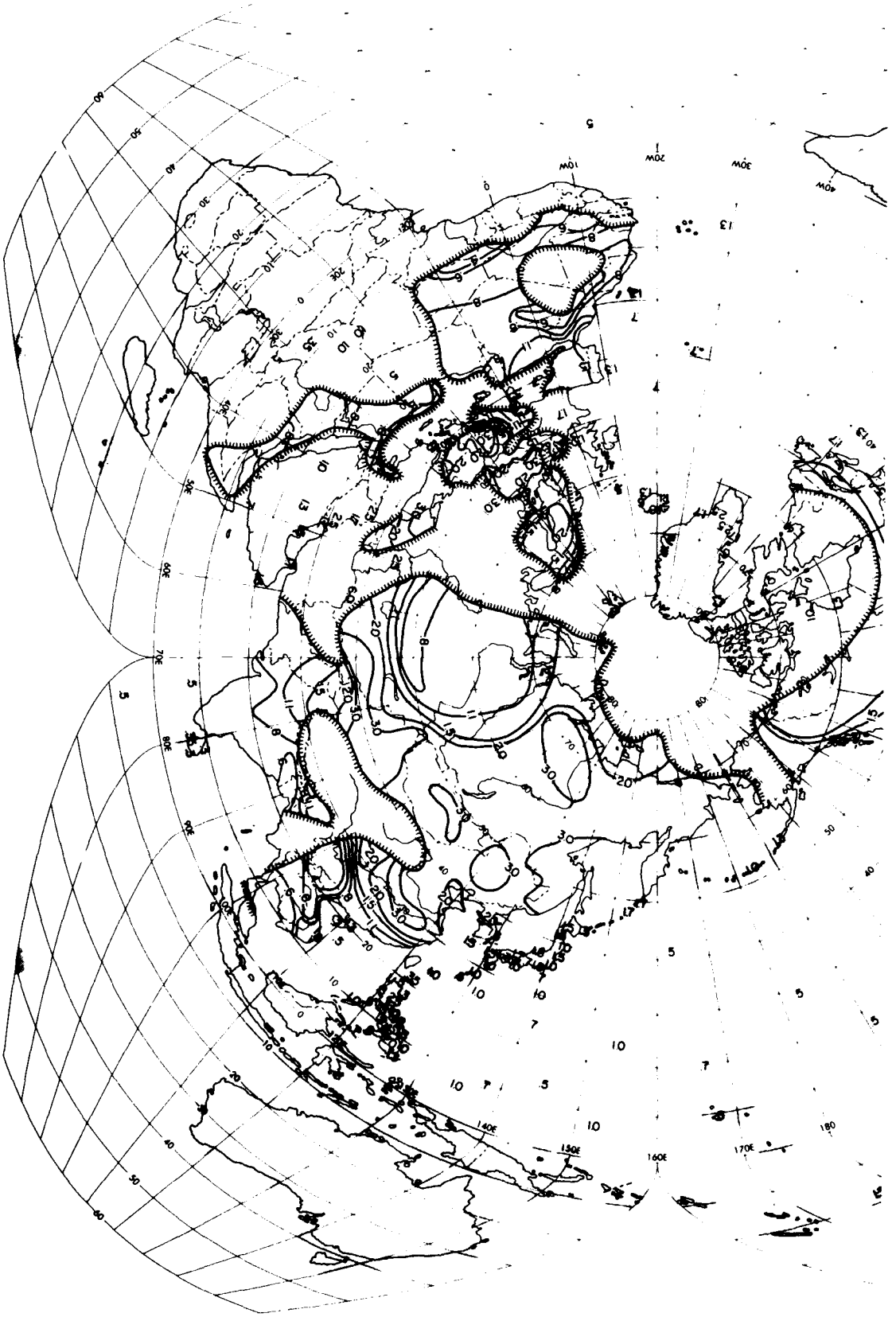

Figure 22b. Analysis of Scale Distance (r) for July, 0600 to 0800 LST (Contd)

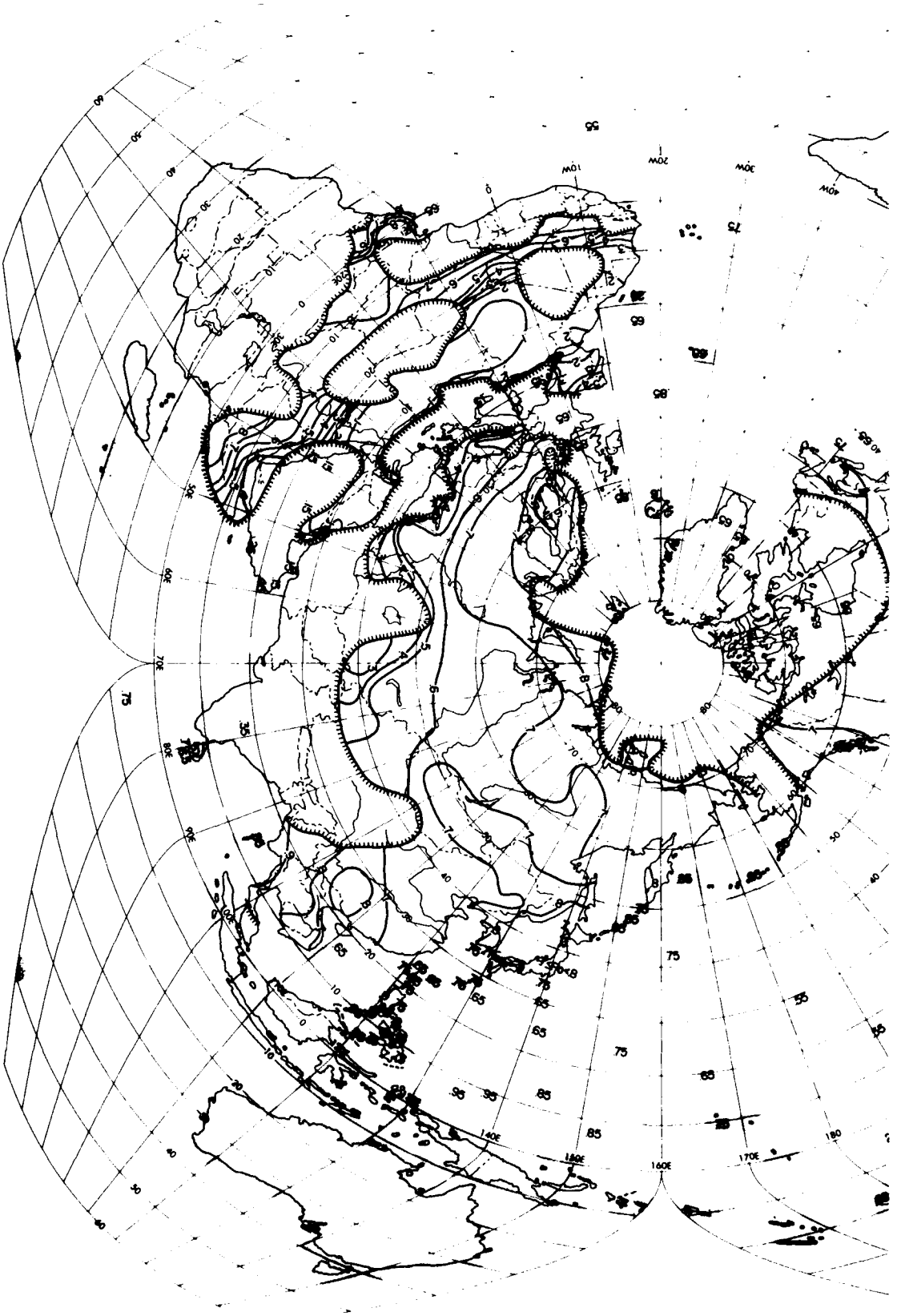

Figure 23a. Analysis of Mean Sky-Cover (P_o) for July, 1200 to 1400 LST

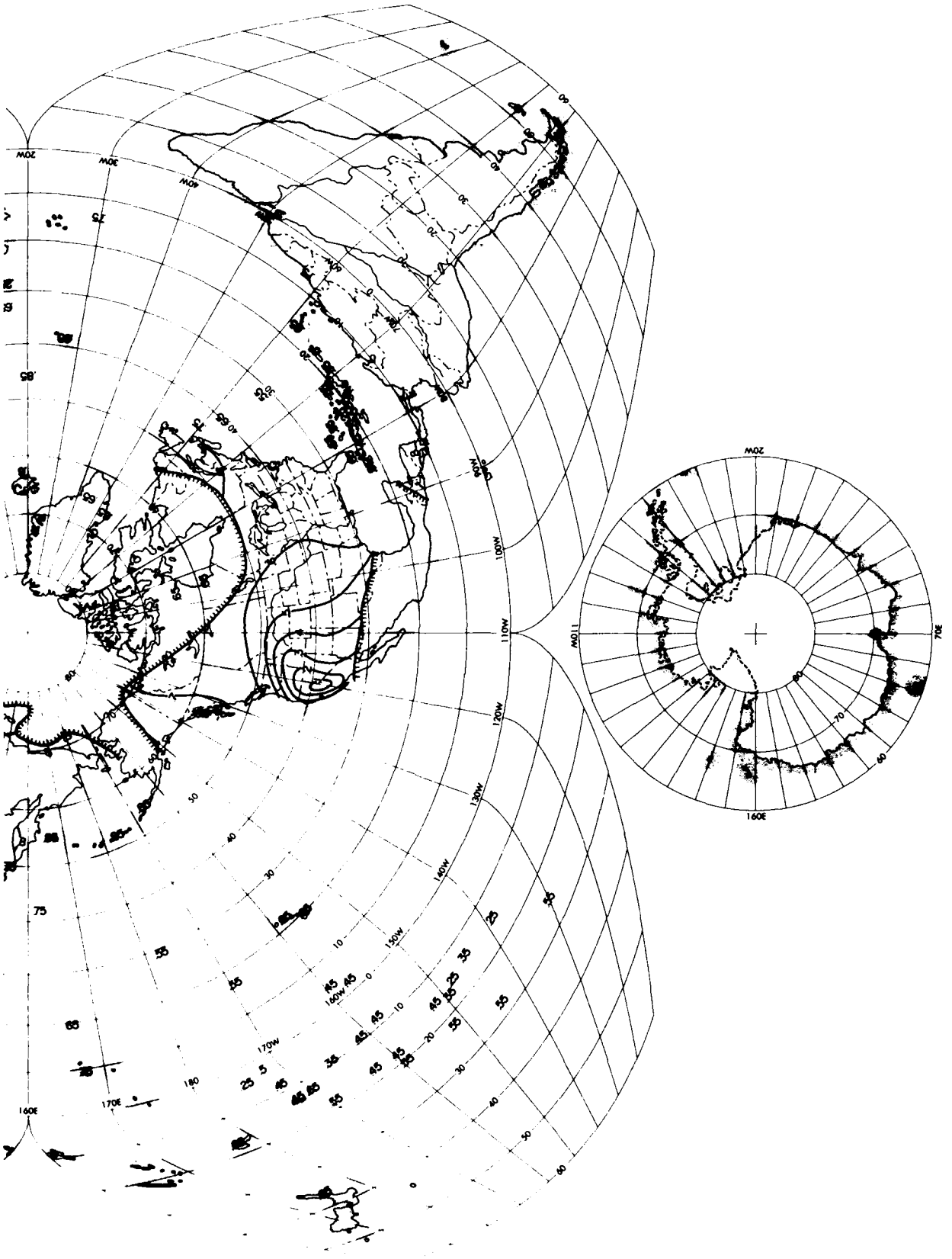

Figure 23a. Analysis of Mean Sky-Cover (P_o) for July, 1200 to 1400 LST (Contd)

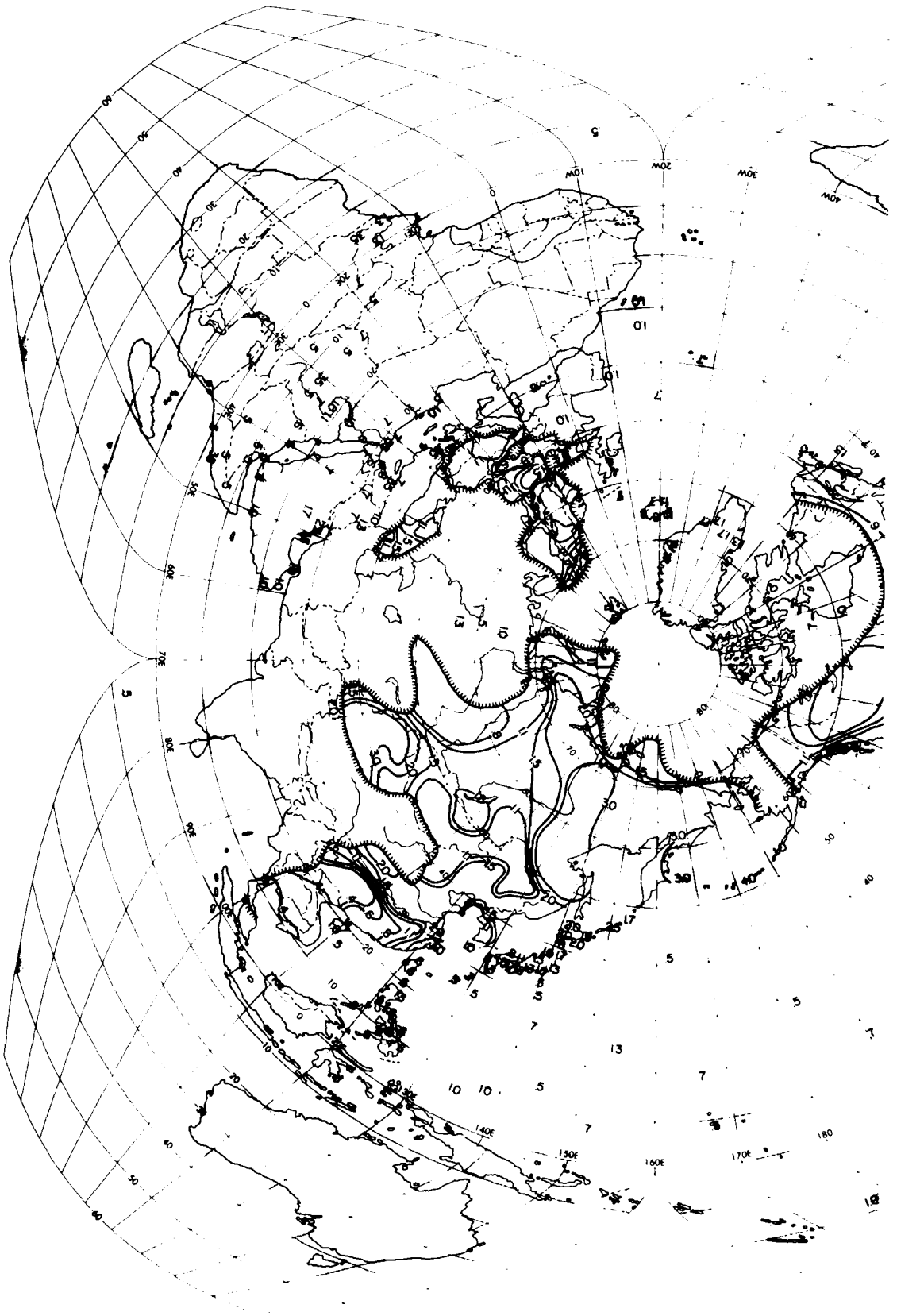

Figure 23b. Analysis of Scale Distance (r) for July, 1200 to 1400 LST

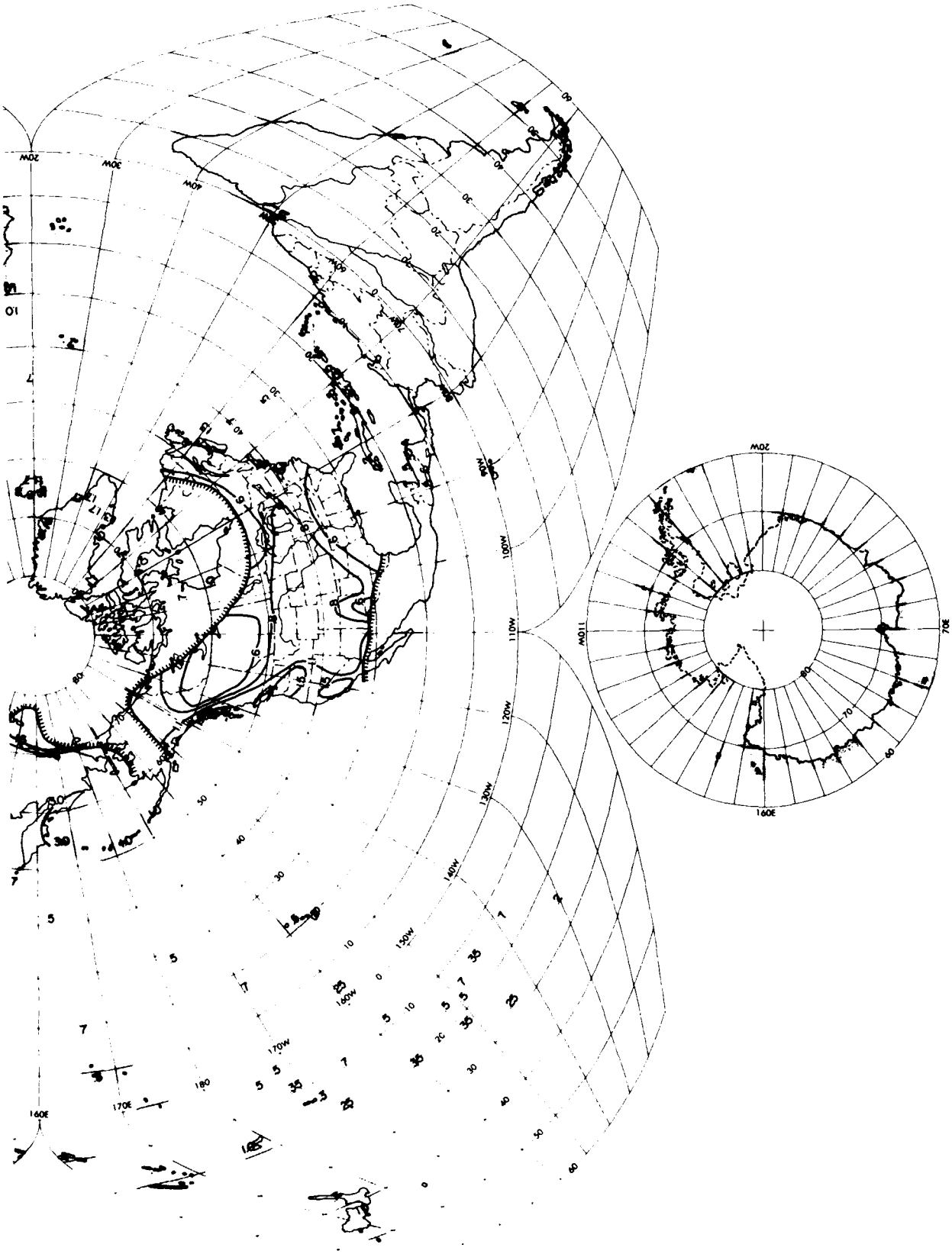

Figure 23b. Analysis of Scale Distance (r) for July, 1200 to 1400 LST (Contd)

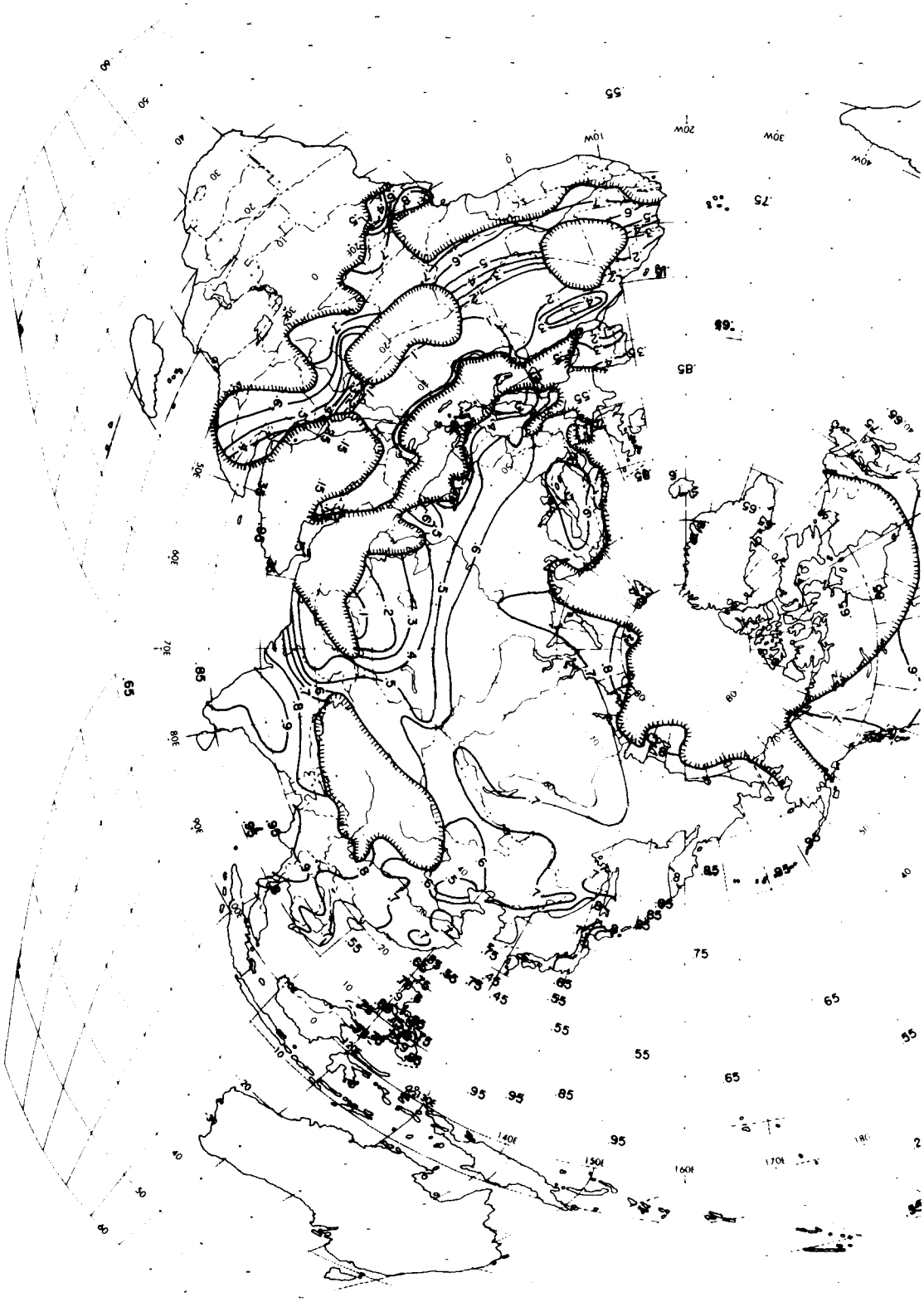

Figure 24a. Analysis of Mean Sky-Cover (P_o) for July, 1800 to 2000 LST

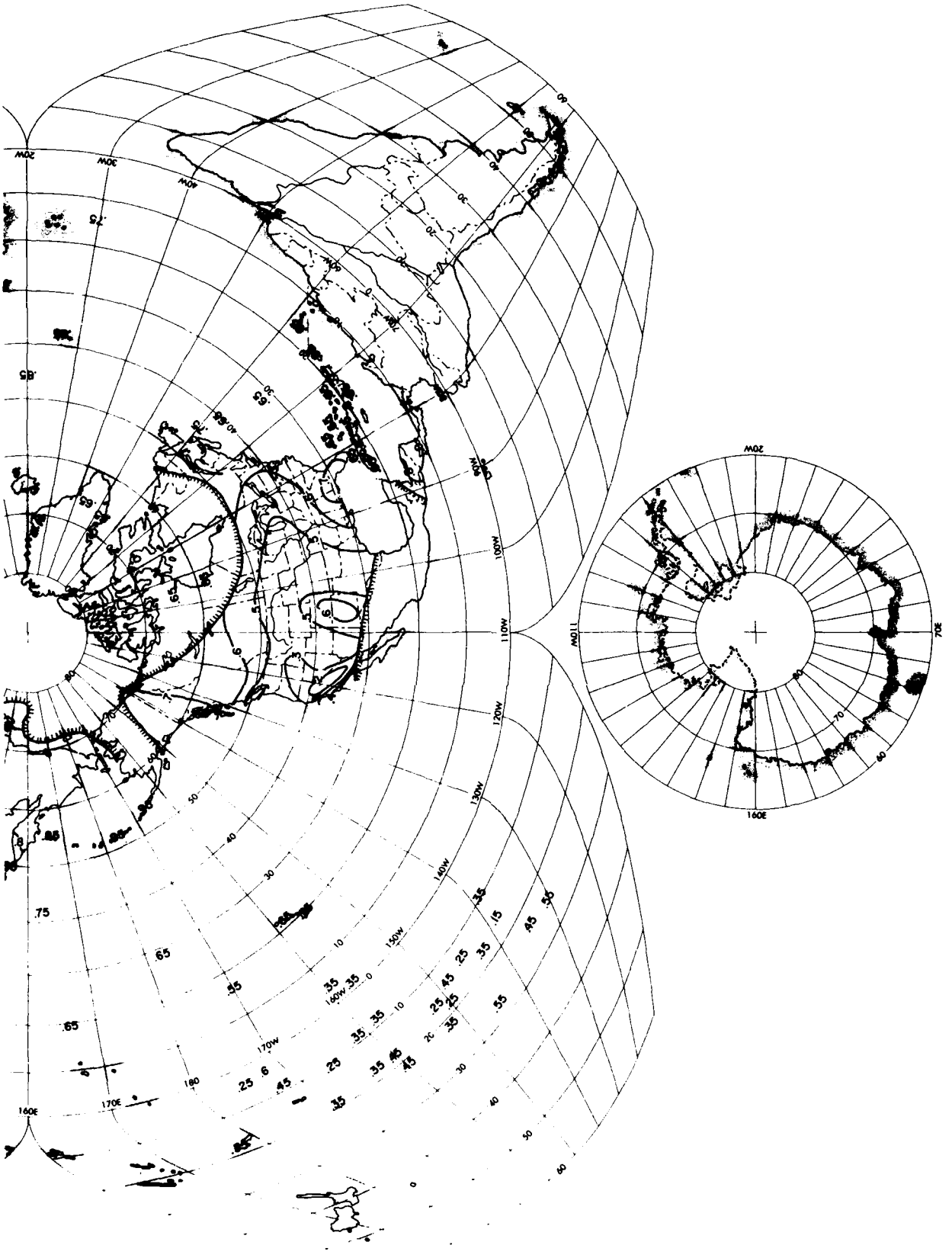

Figure 24a. Analysis of Mean Sky-Cover (P_o) for July, 1800 to 2000 LST (*Contd*)

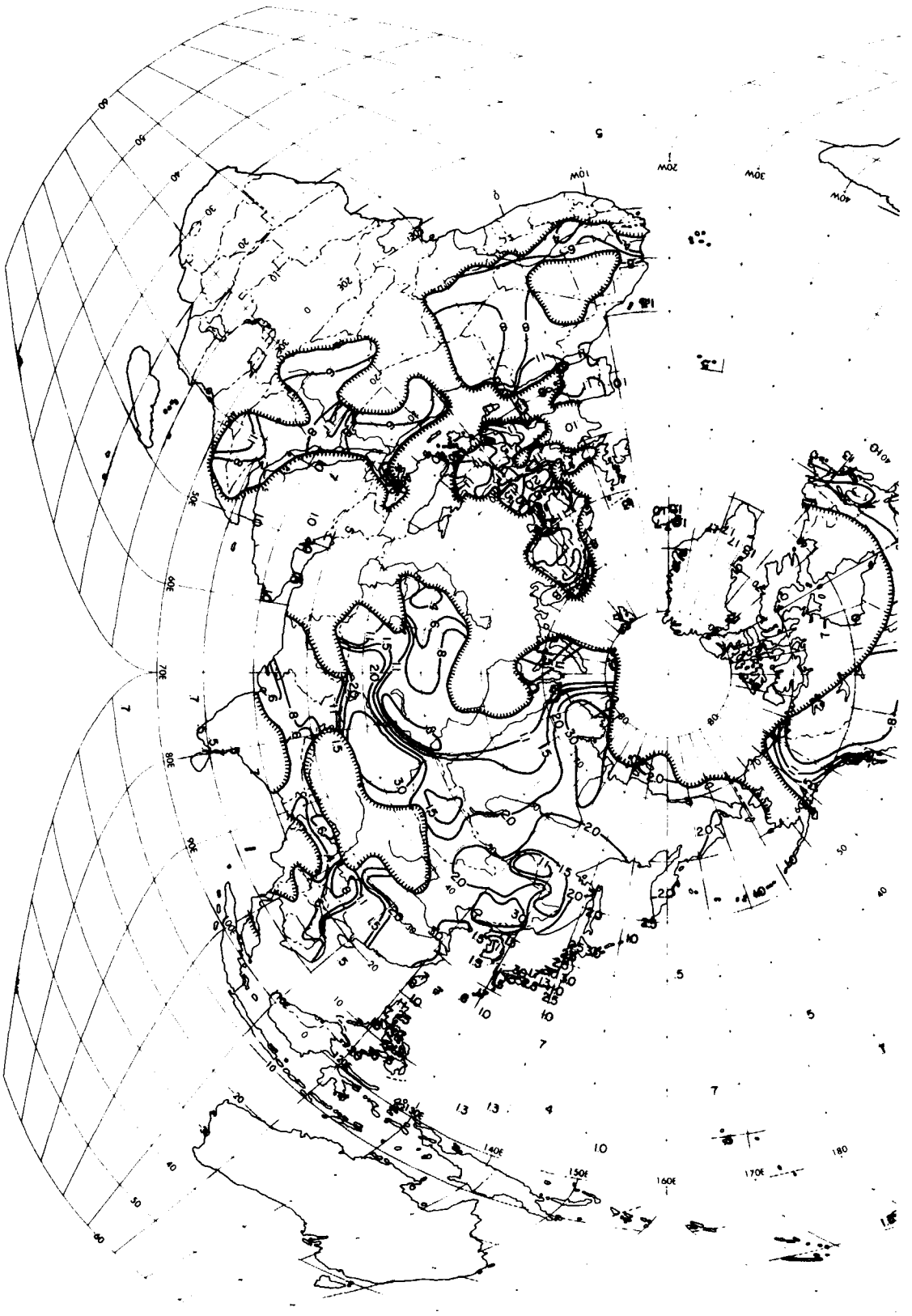

Figure 24b. Analysis of Scale Distance (r) for July, 1800 to 2000 LST

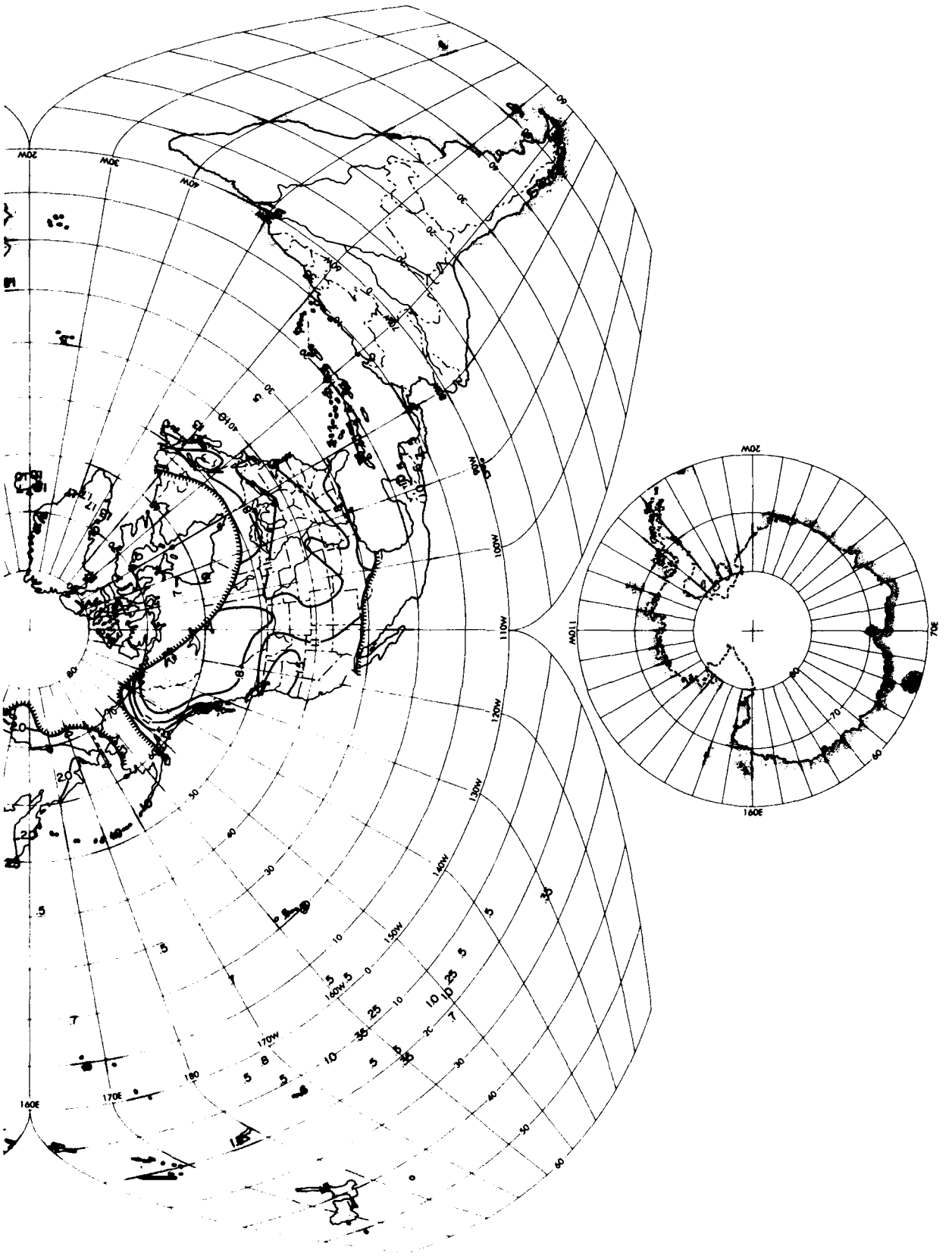

Figure 24b. Analysis of Scale Distance (r) for July, 1800 to 2000 LST (Contd)

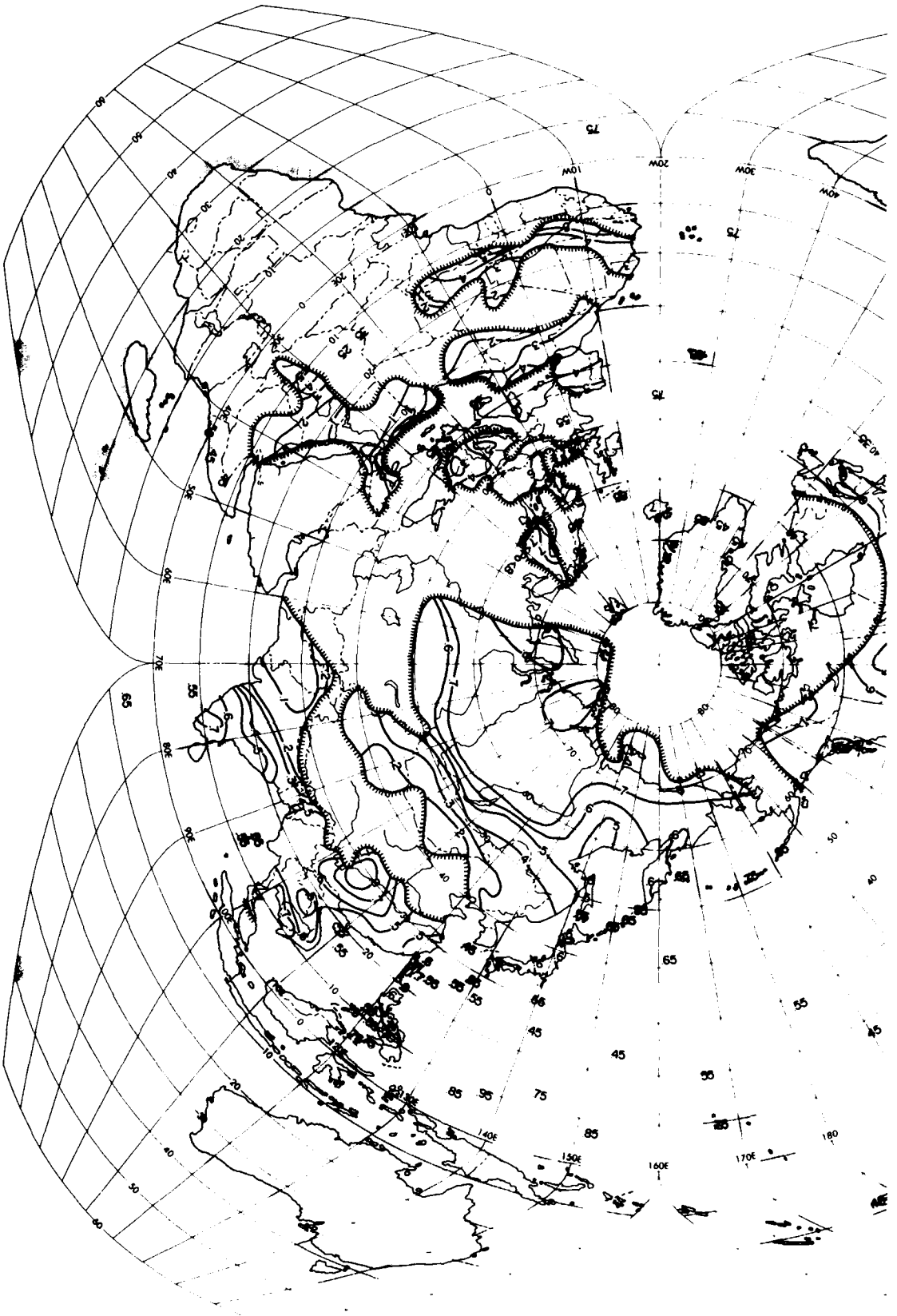

Figure 25a. Analysis of Mean Sky-Cover (P_o) for October, 0000 to 0200 LST

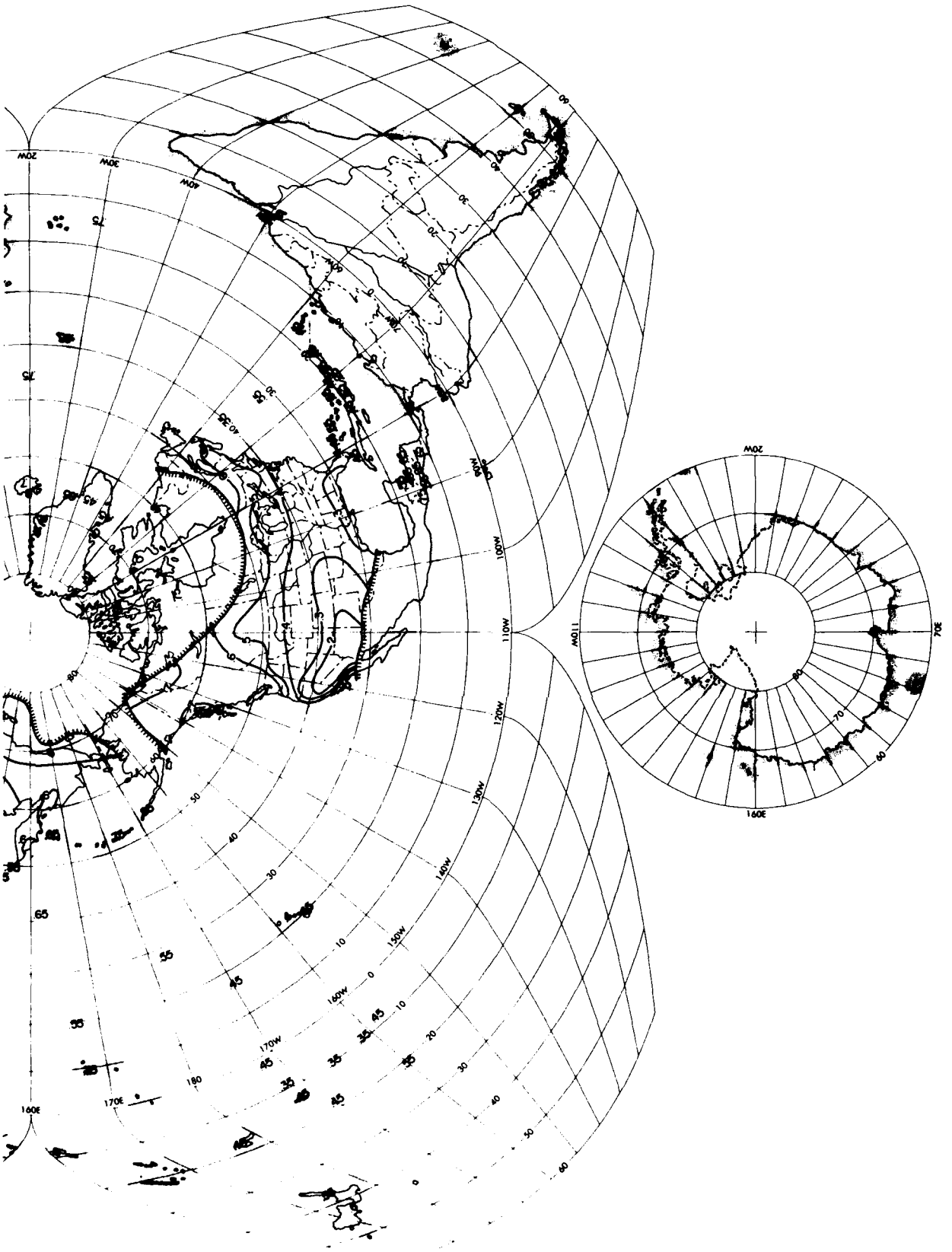

Figure 25a. *Analysis of Mean Sky-Cover (P_o) for* October, 0000 to 0200 LST (Contd)

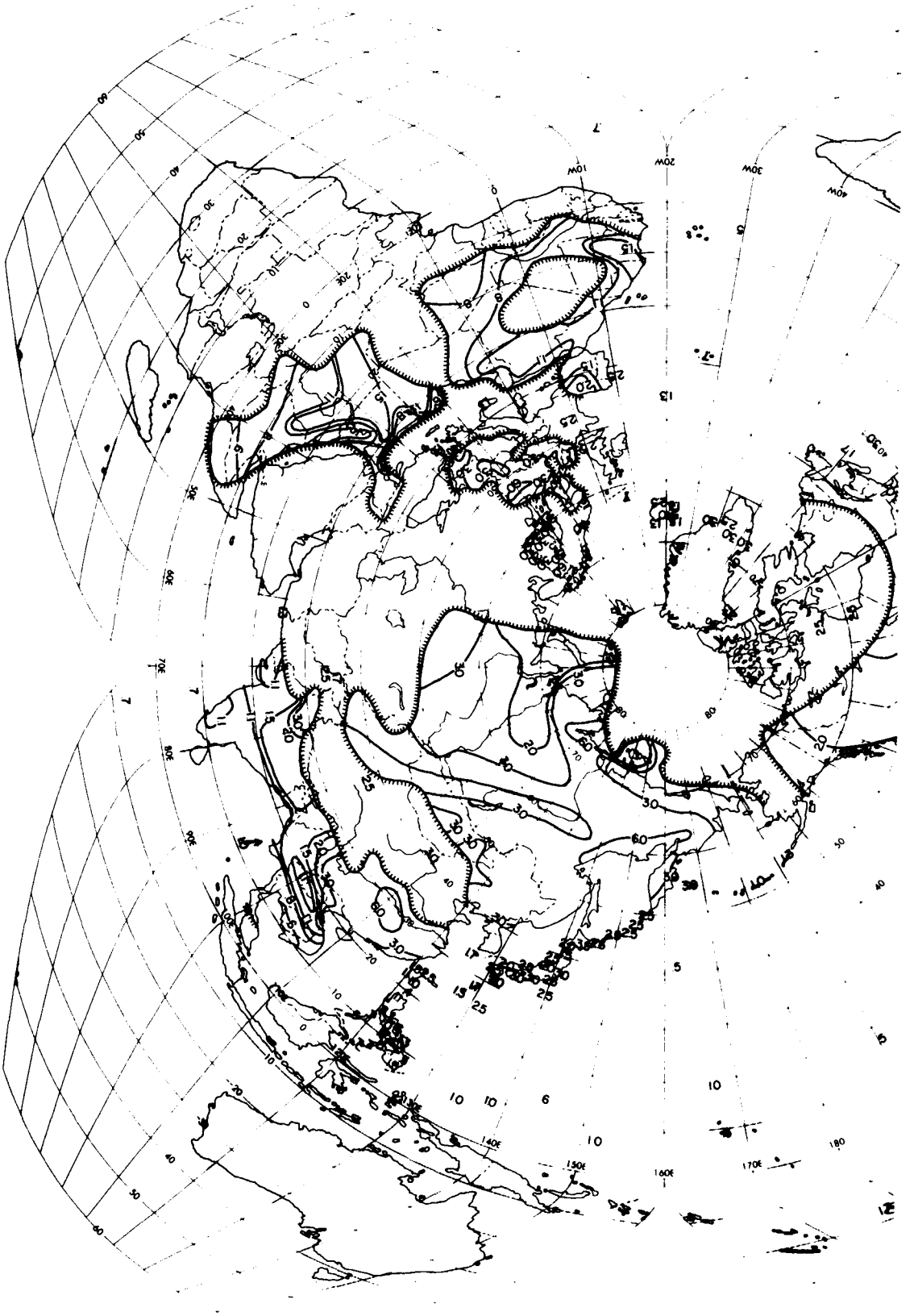

Figure 25b. Analysis of Scale Distance (r) for October, 0000 to 0200 LST

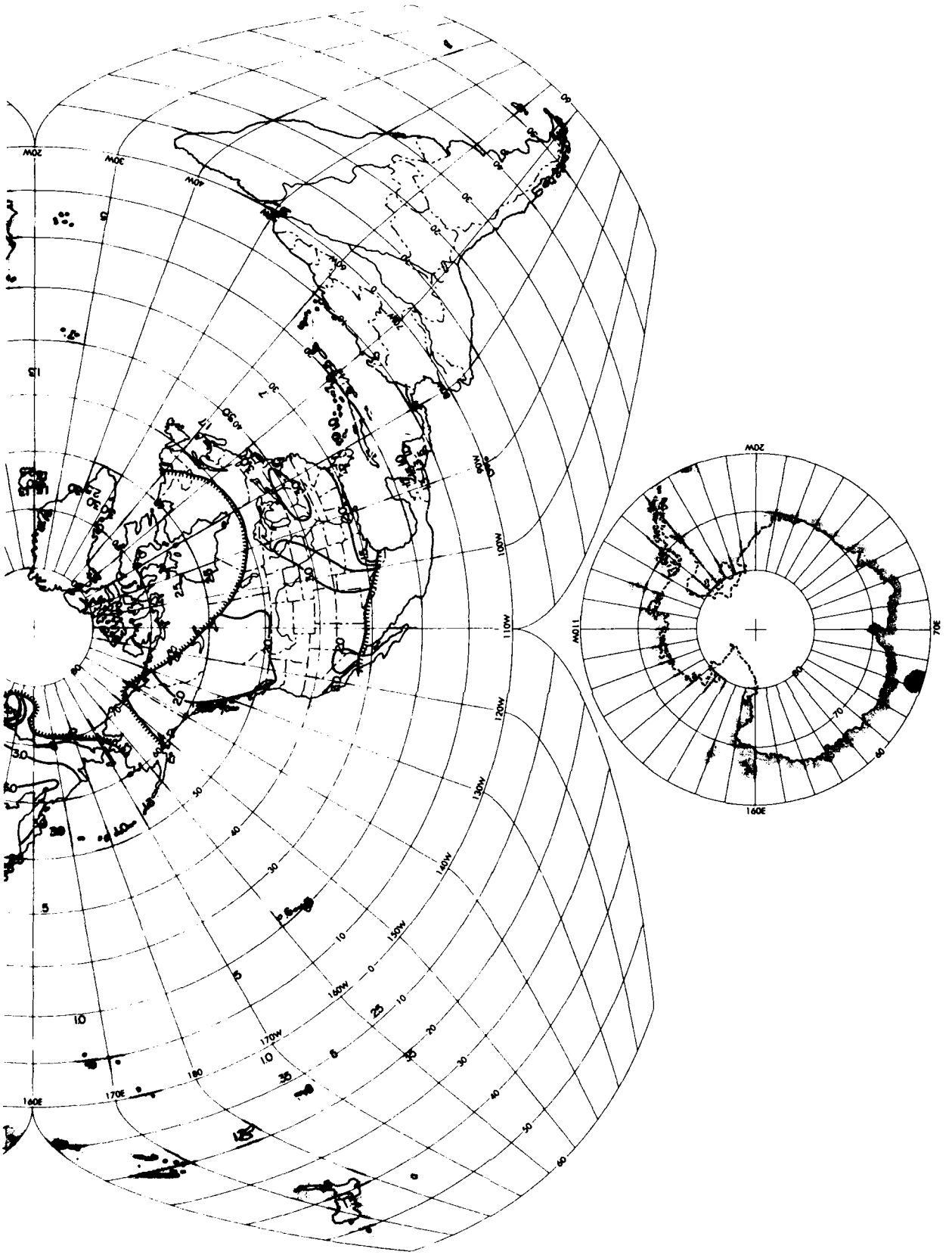

Figure 25b. Analysis of Scale Distance (r) for October, 0000 to 0200 LST (Contd)

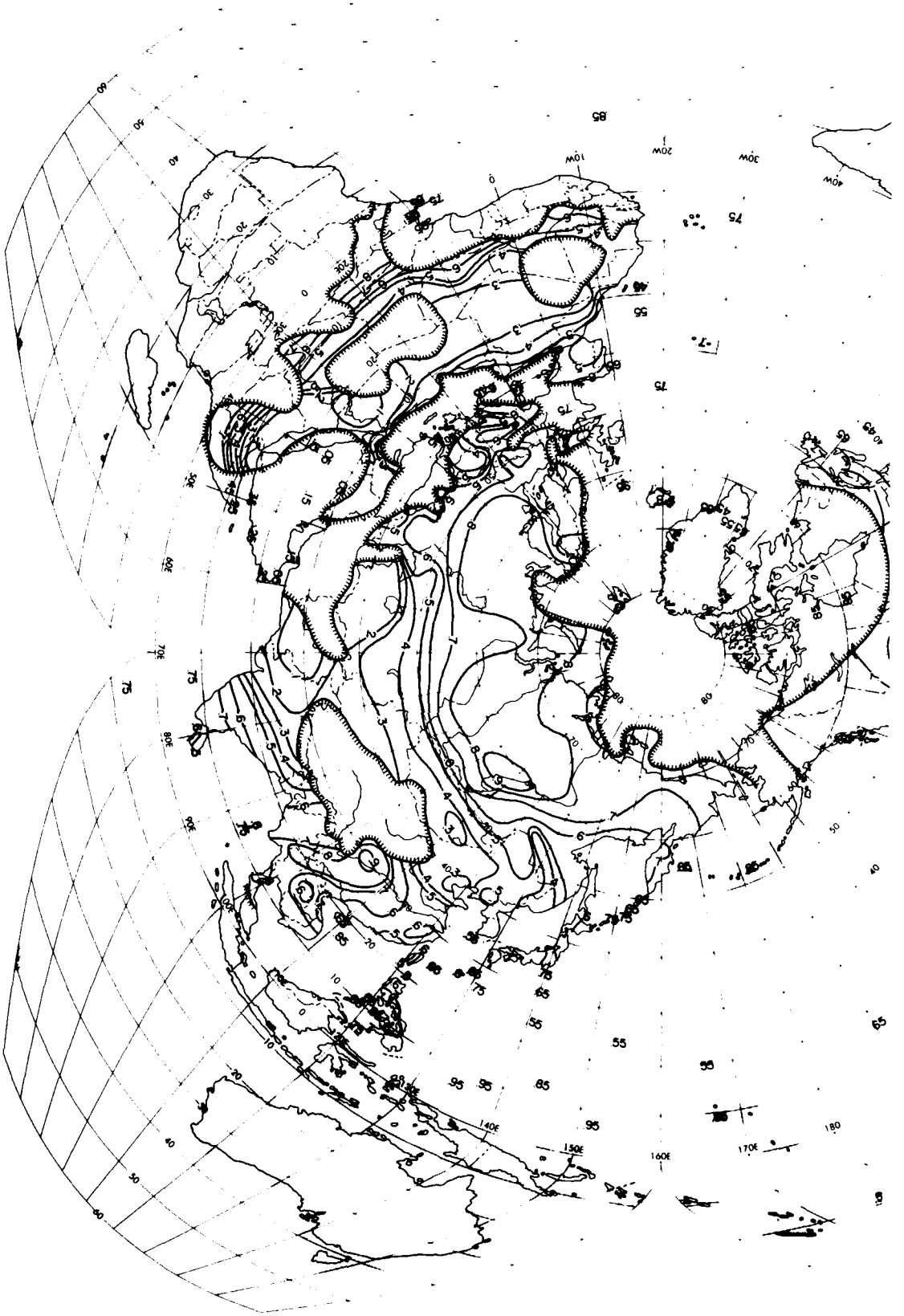

Figure 26a. Analysis of Mean Sky-Cover (P_o) for October, 0600 to 0800 LST

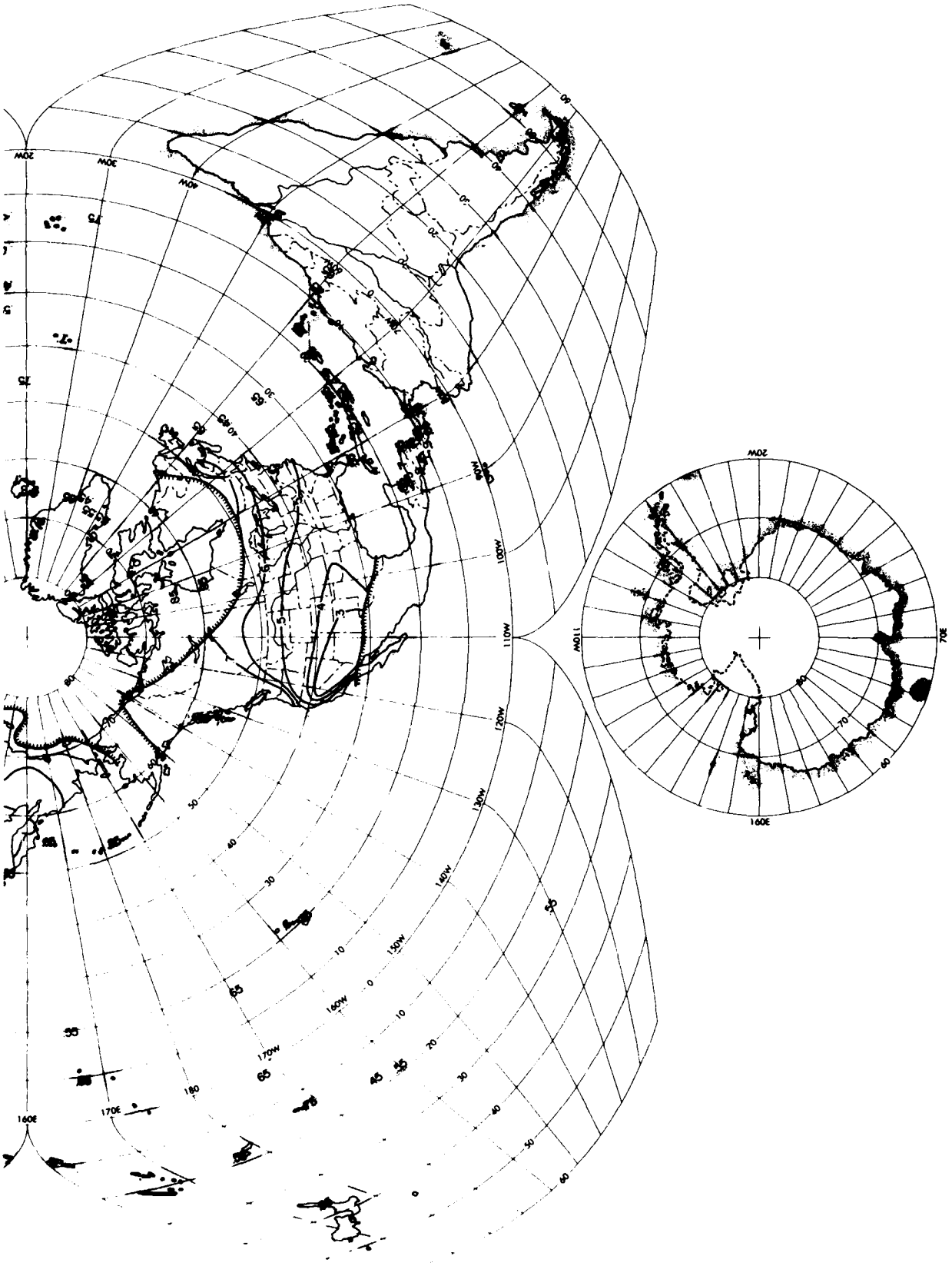

Figure 26a. Analysis of Mean Sky-Cover (P_o) for October, 0600 to 0800 LST (Contd)

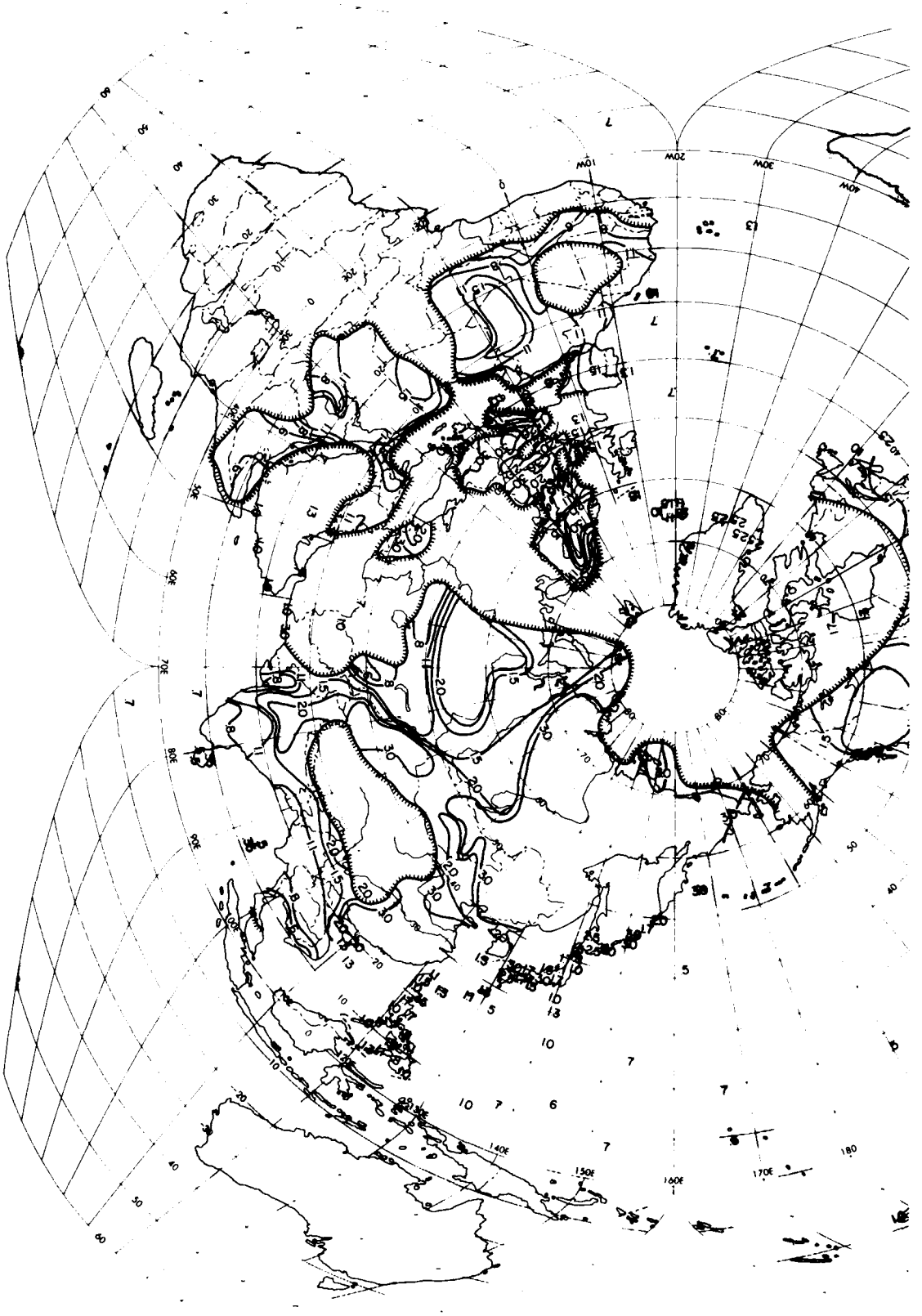

Figure 26b. Analysis of Scale Distance (r) for October, 0600 to 0800 LST

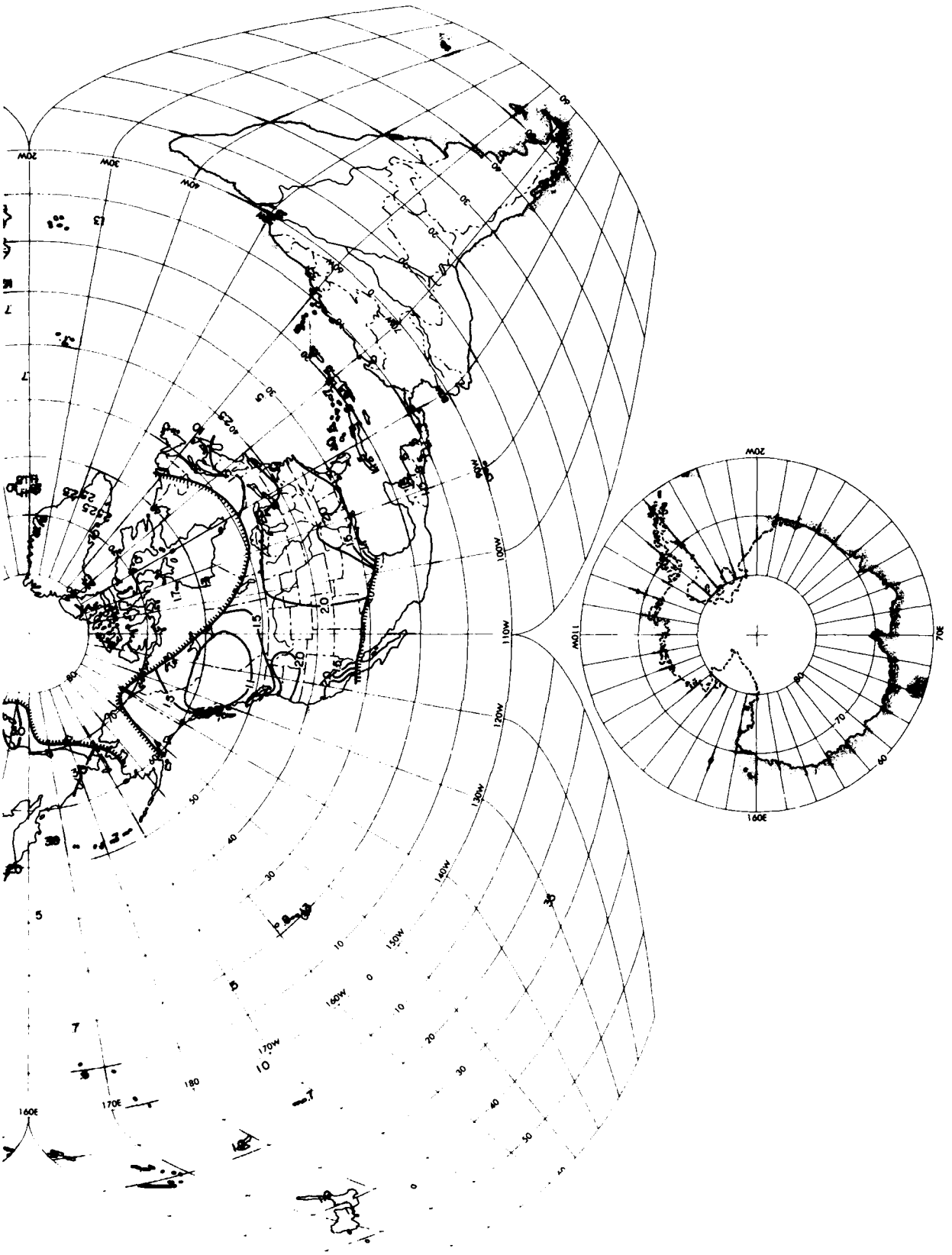

Figure 26b. Analysis of Scale Distance (r) for October, 0600 to 0800 LST (Contd)

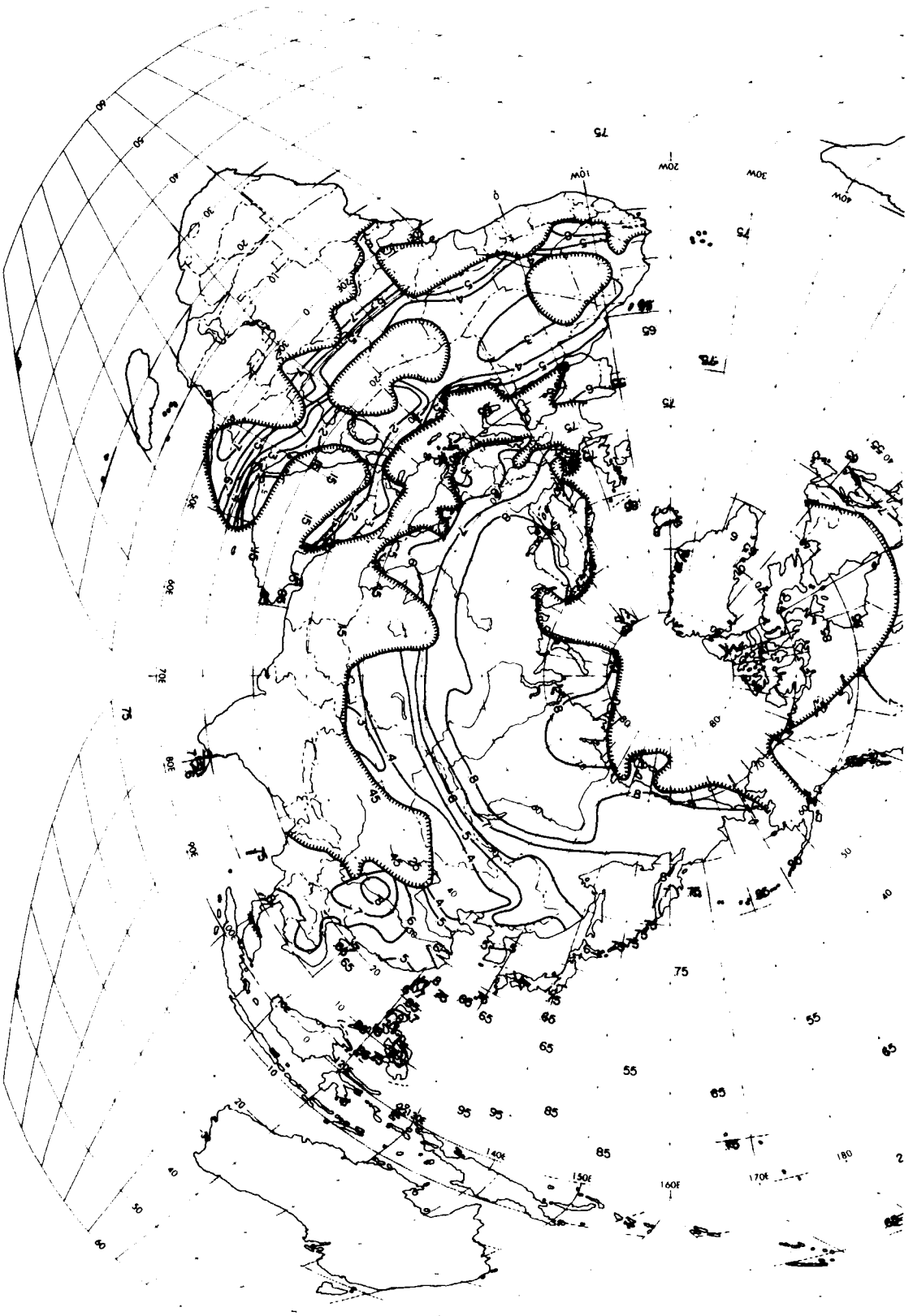

Figure 27a. Analysis of Mean Sky-Cover (P_o) for October, 1200 to 1400 LST

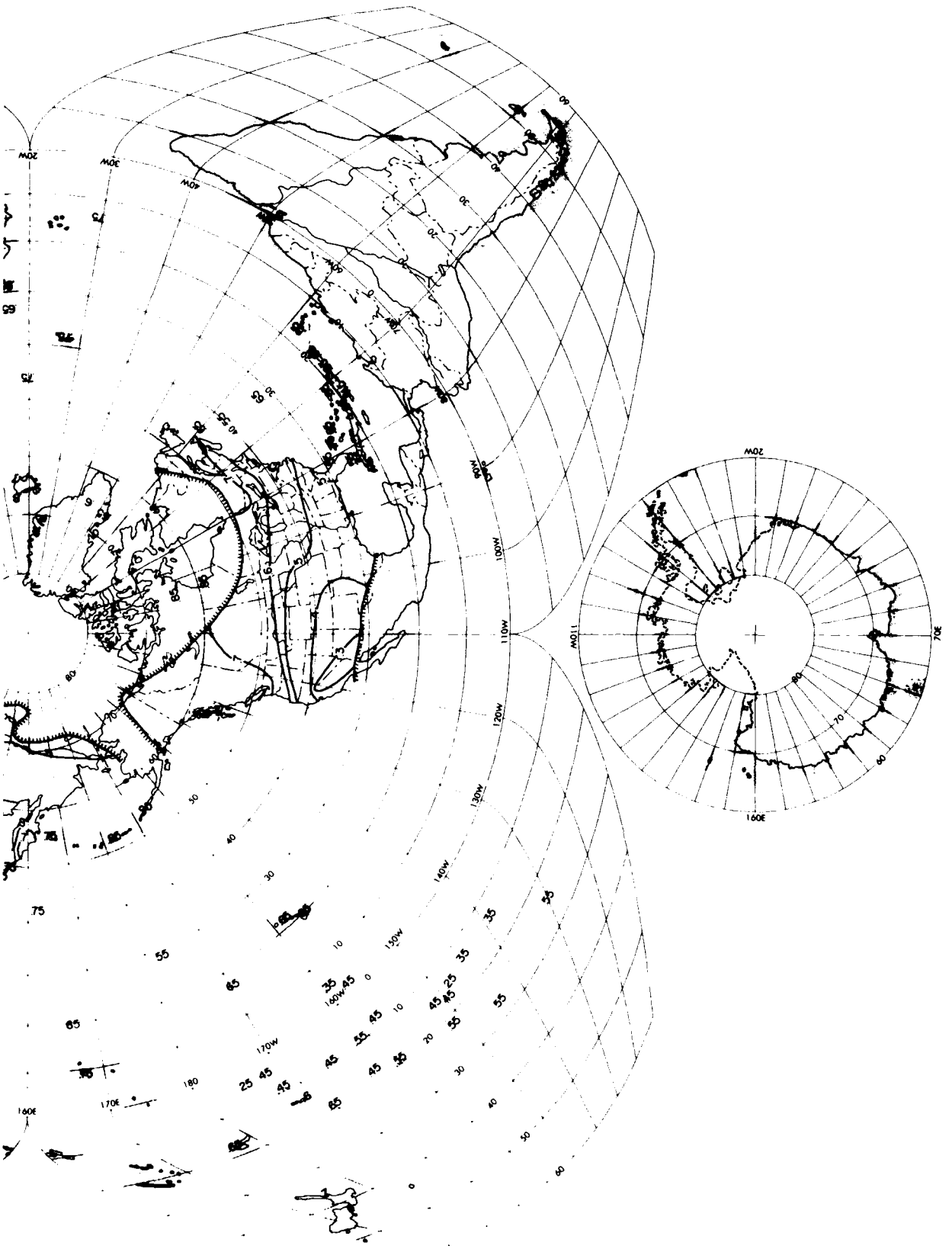

Figure 27a. Analysis of Mean Sky-Cover (P_o) for October, 1200 to 1400 LST (Contd)

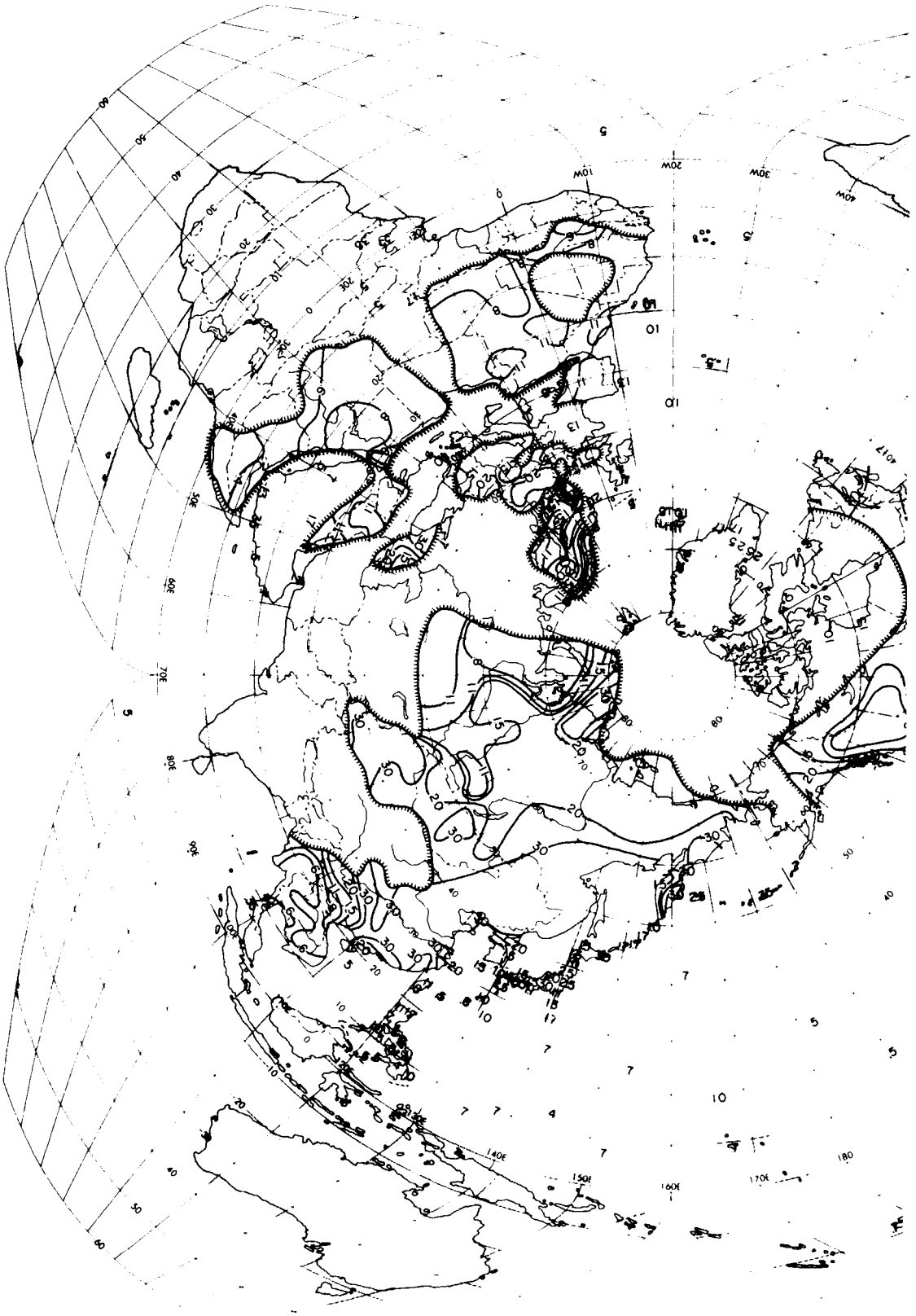

Figure 27b. Analysis of Scale Distance (r) for October, 1200 to 1400 LST

AD-A170 474 WORLD ATLAS OF TOTAL SKY-COVER(U) AIR FORCE GEOPHYSICS 2/2
LAB HANSCOM AFB MA C F BURGER 04 SEP 85
AFGL-TR-85-0190

UNCLASSIFIED F/G 4/2 NL

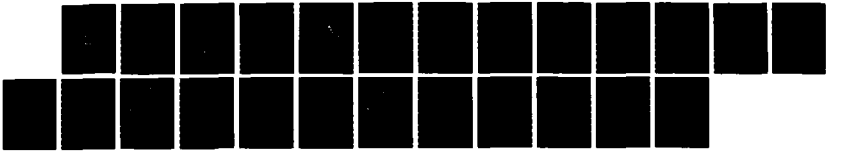

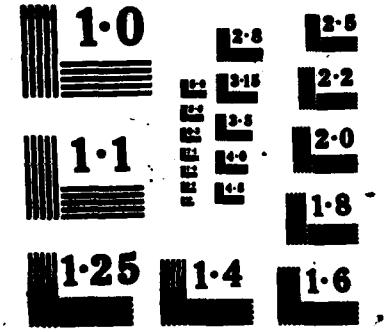
1·0
1·1
1·25
1·4
1·6
1·8
2·0
2·2
2·5
2·8
3·15
3·5
4·0
4·5

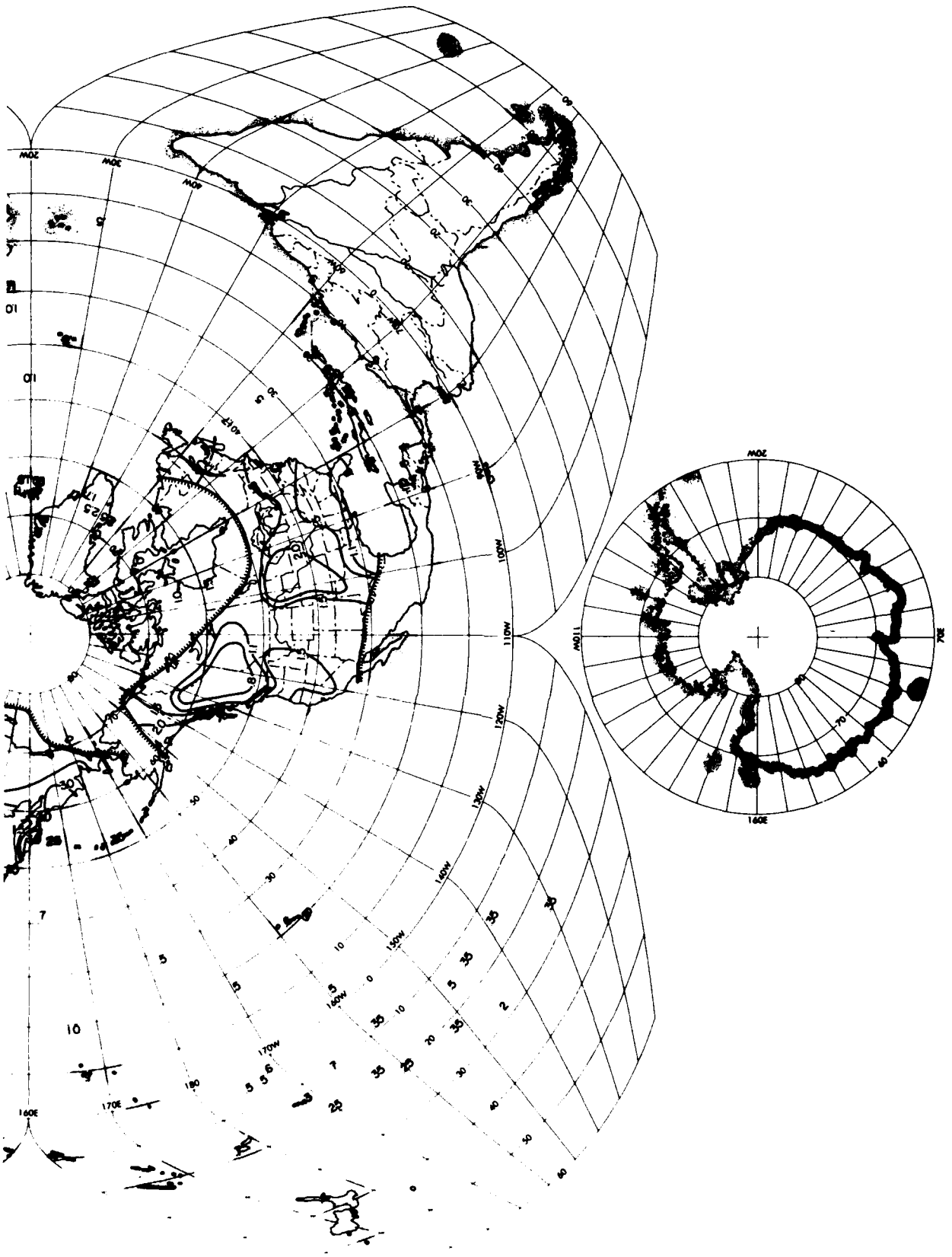

Figure 27b. Analysis of Scale Distance (r) for October, 1200 to 1400 LST (Contd)

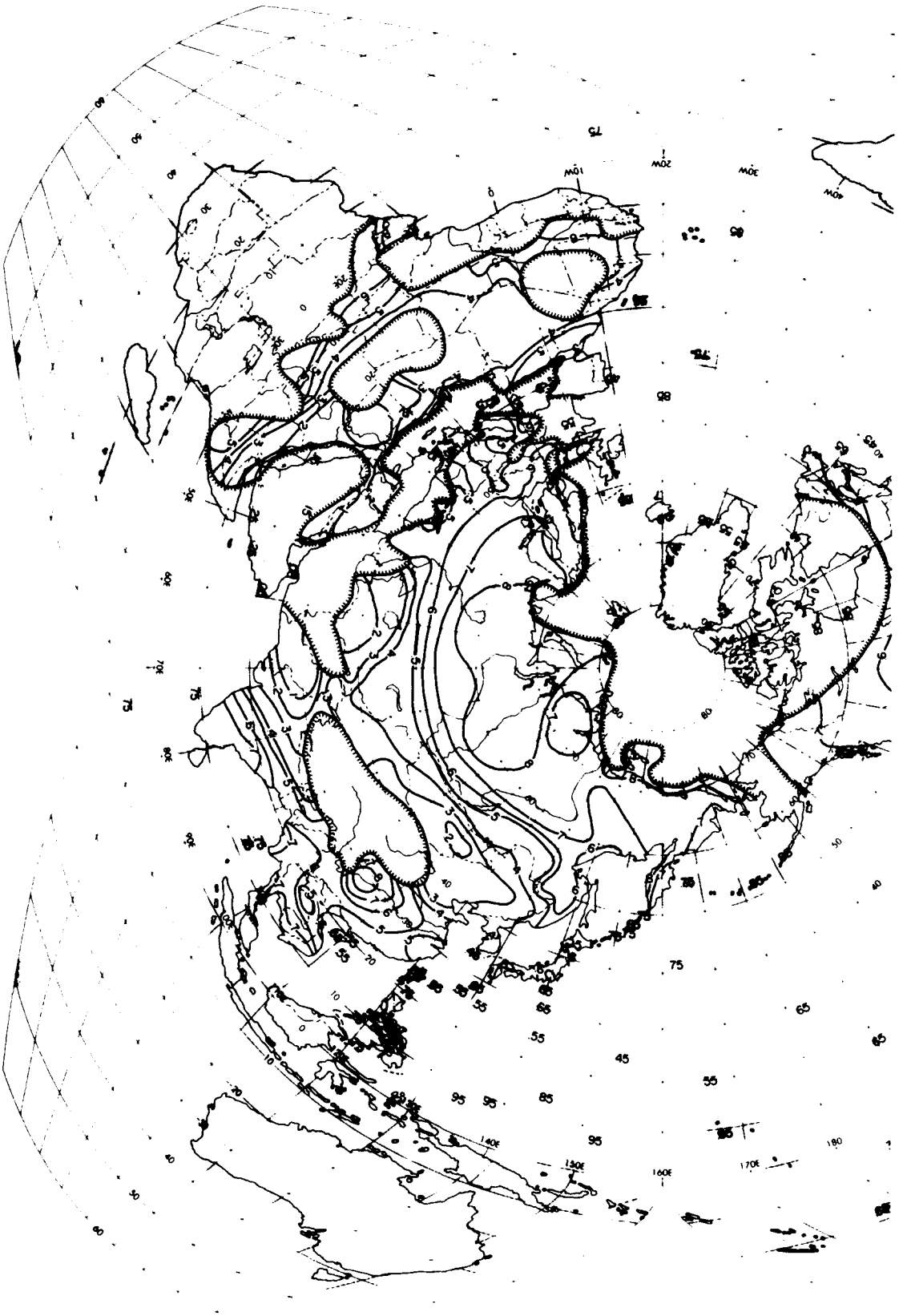

Figure 28a. Analysis of Mean Sky-Cover (P_o) for October, 1800 to 2000 LST

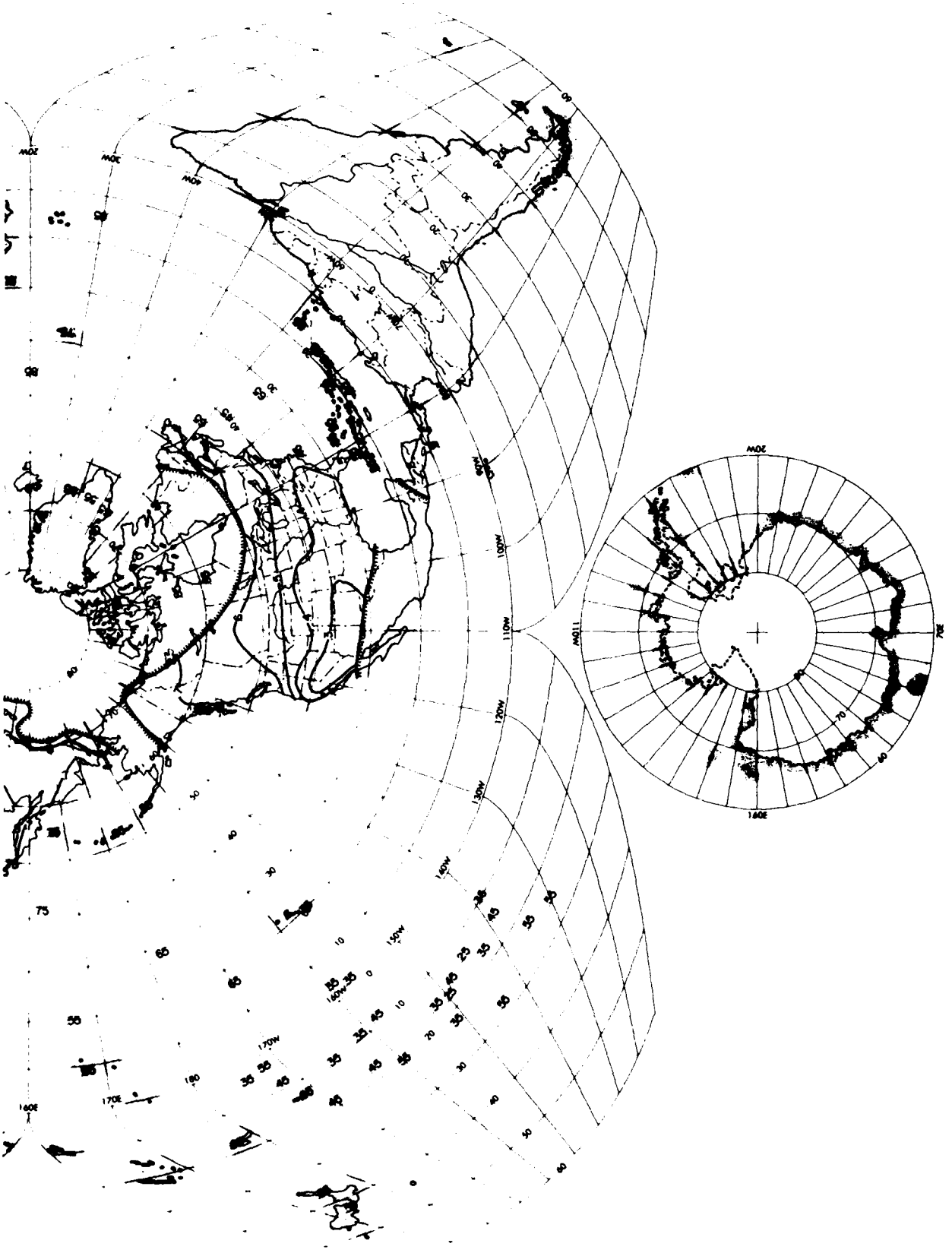

Figure 28a. Analysis of Mean Sky-Cover (P_0) for October, 1800 to 2000 LST (Contd)

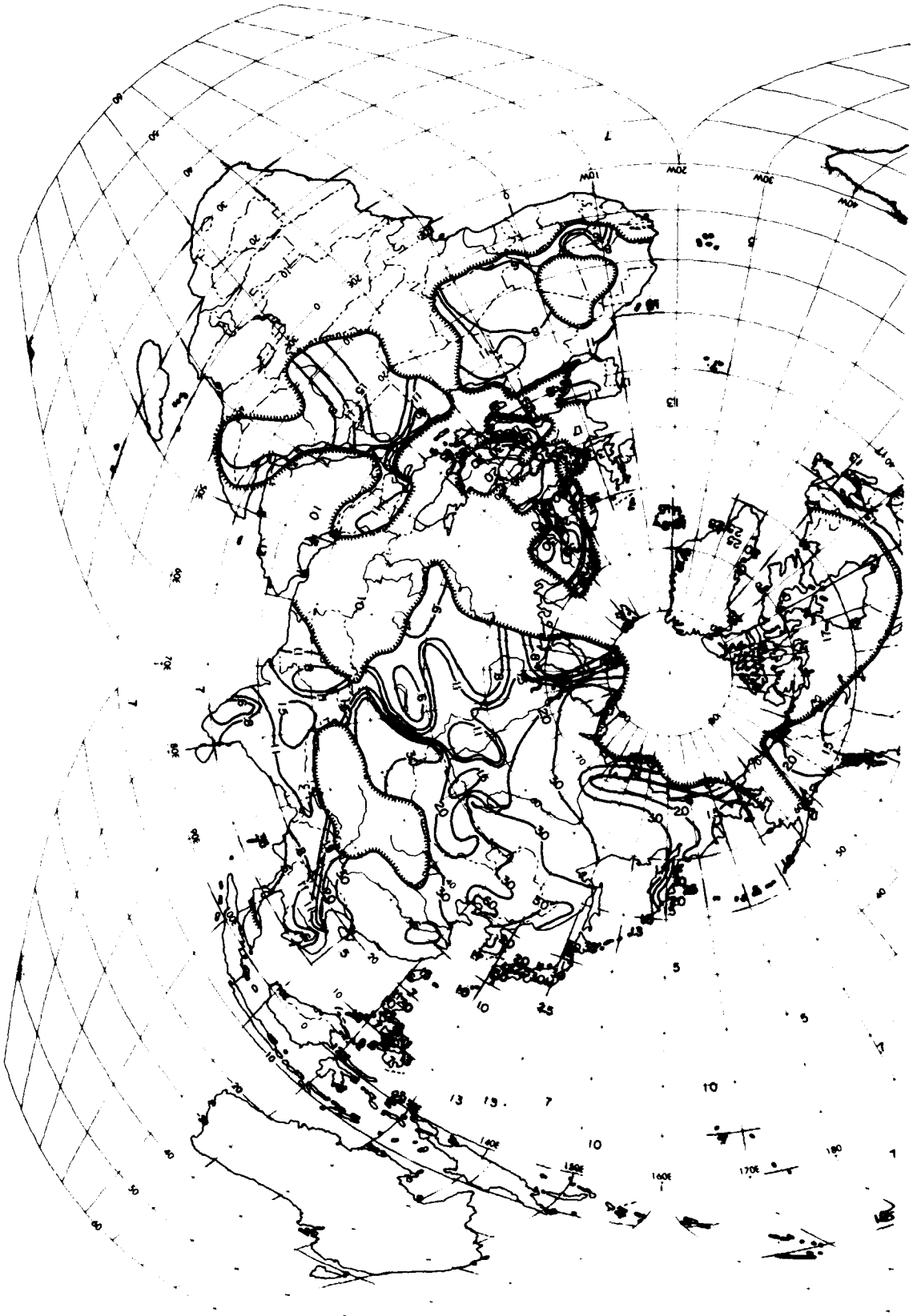

Figure 28b. Analysis of Scale Distance (r) for October, 1800 to 2000 LST

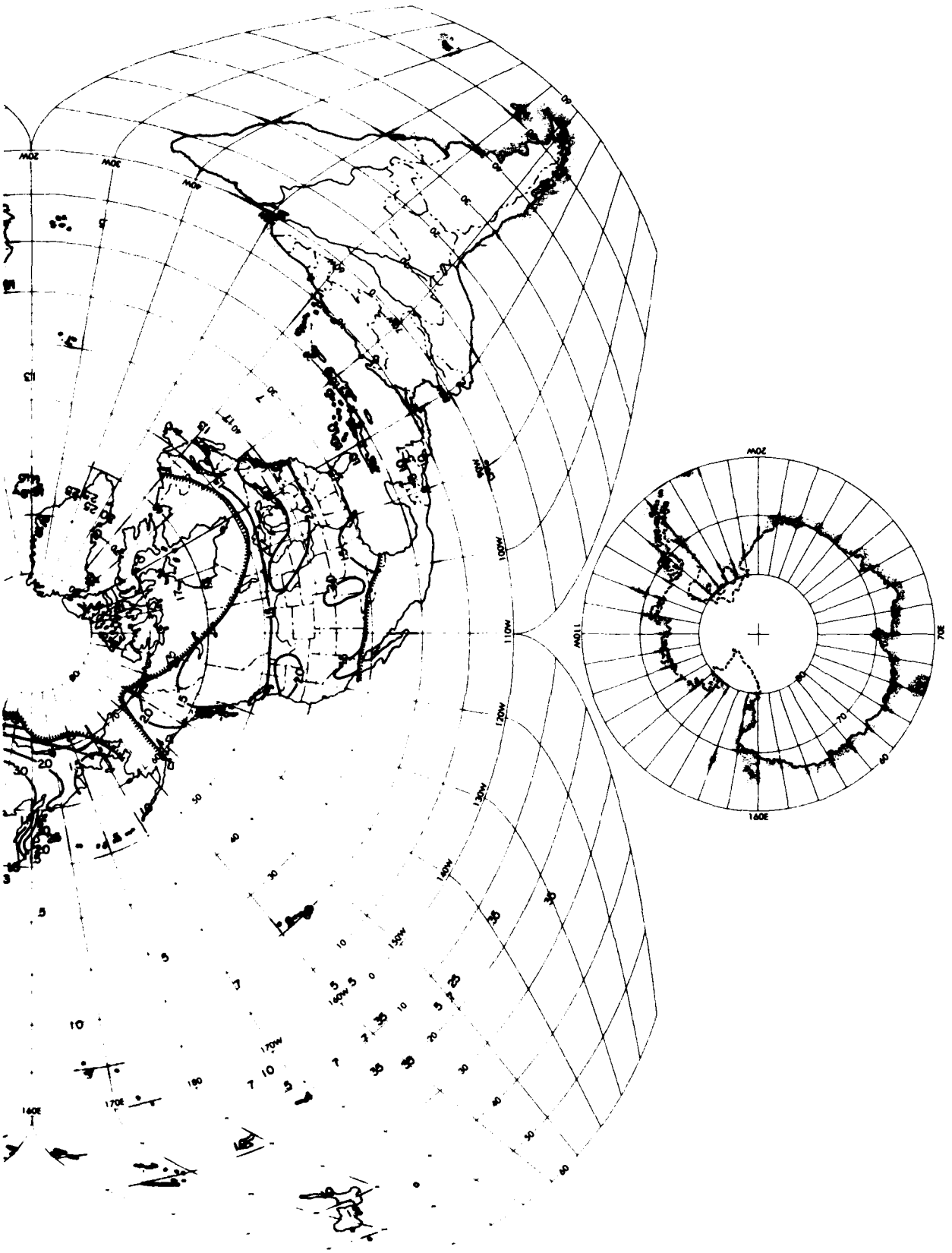

Figure 28b. Analysis of Scale Distance (r) for October, 1800 to 2000 LST (Contd)

Figure 29a. Monthly Analysis of Mean Sky-Cover (P_o) for January

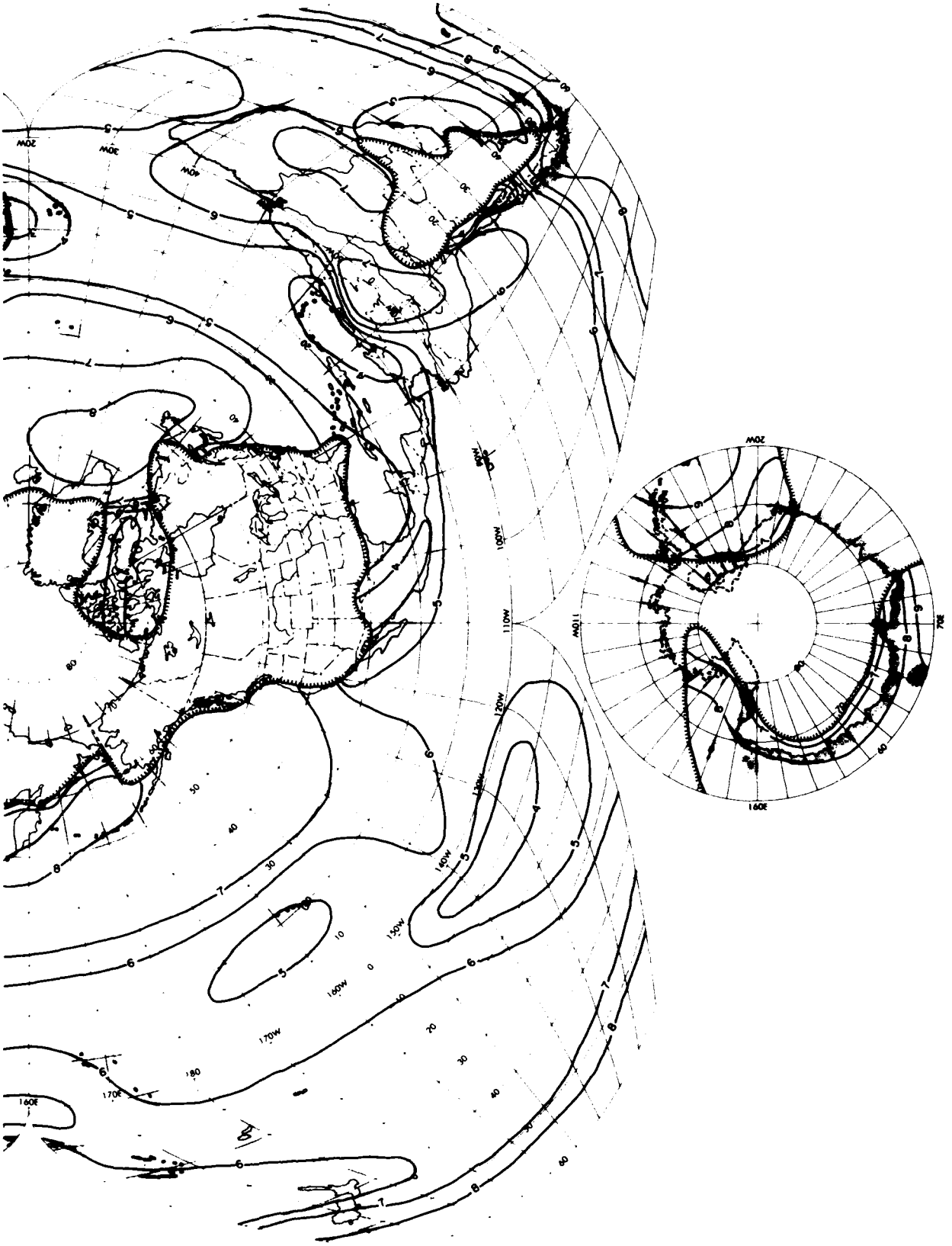

Figure 29a. Monthly Analysis of Mean Sky-Cover (P_o) for January (Contd)

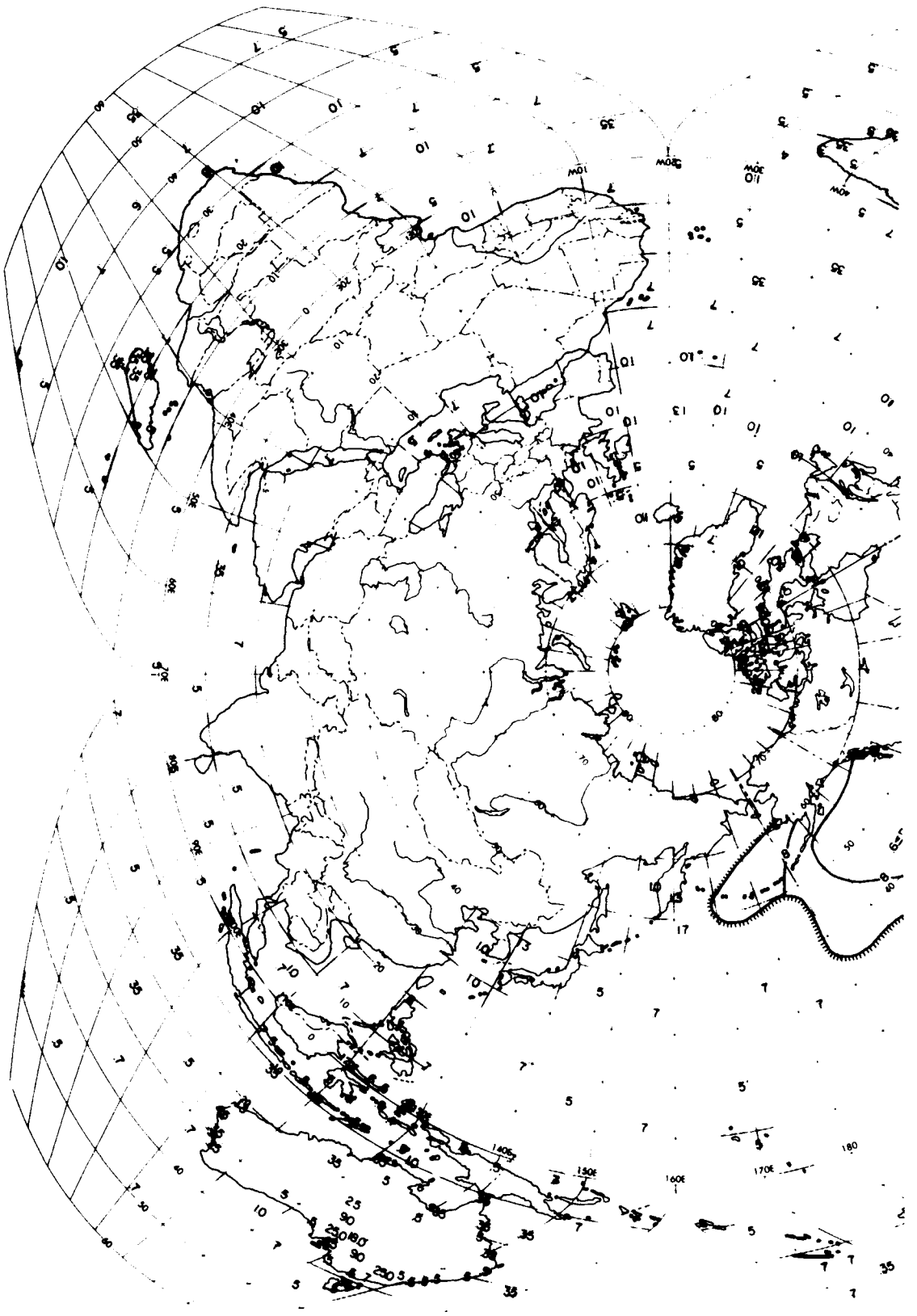

Figure 29b. Monthly Analysis of Scale Distance (r) for January

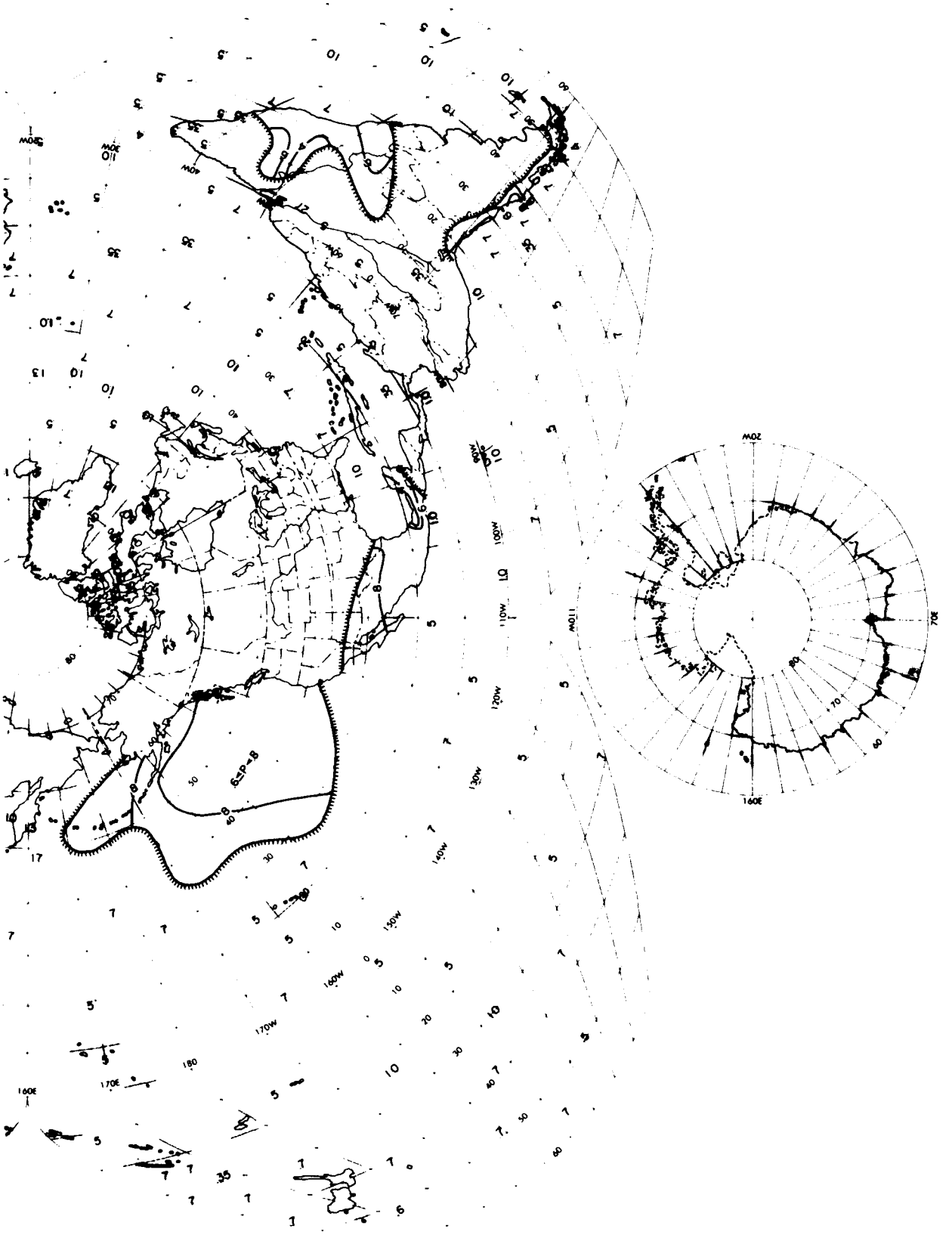

Figure 29b. Monthly Analysis of Scale Distance (r) for January (Contd)

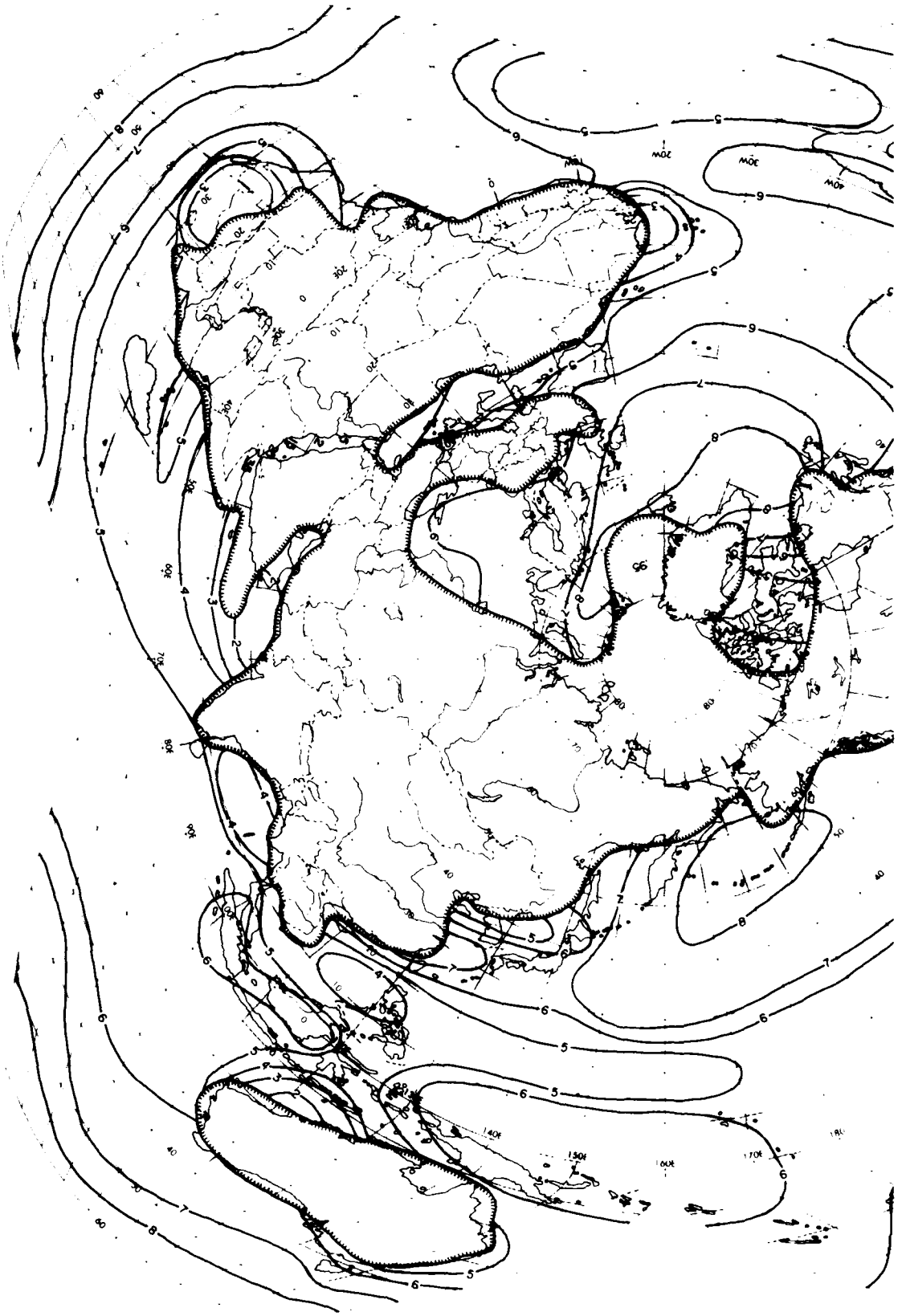

Figure 30a. Monthly Analysis of Mean Sky-Cover (P_o) for April

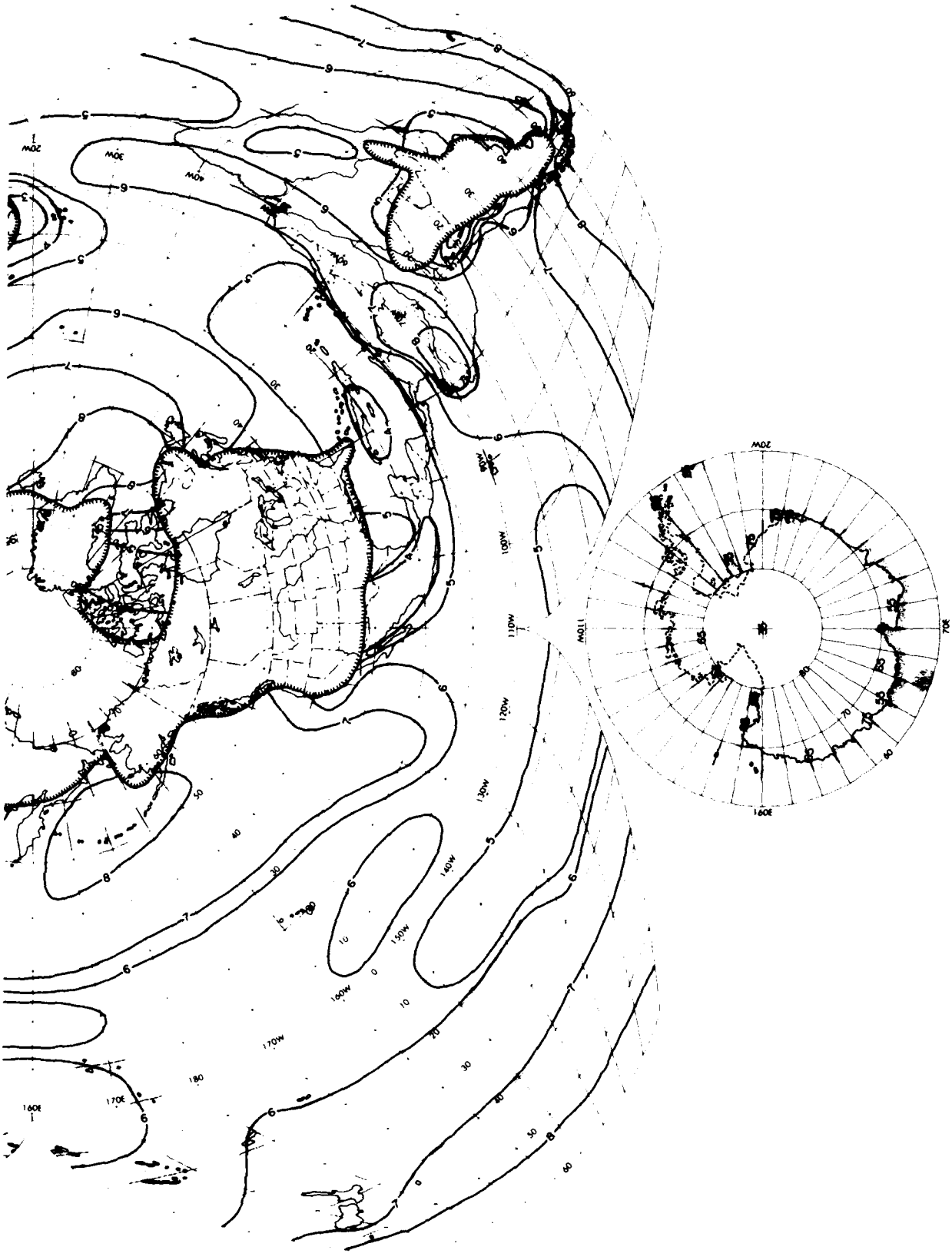

Figure 30a. Monthly Analysis of Mean Sky-Cover (P_o) for April (Contd)

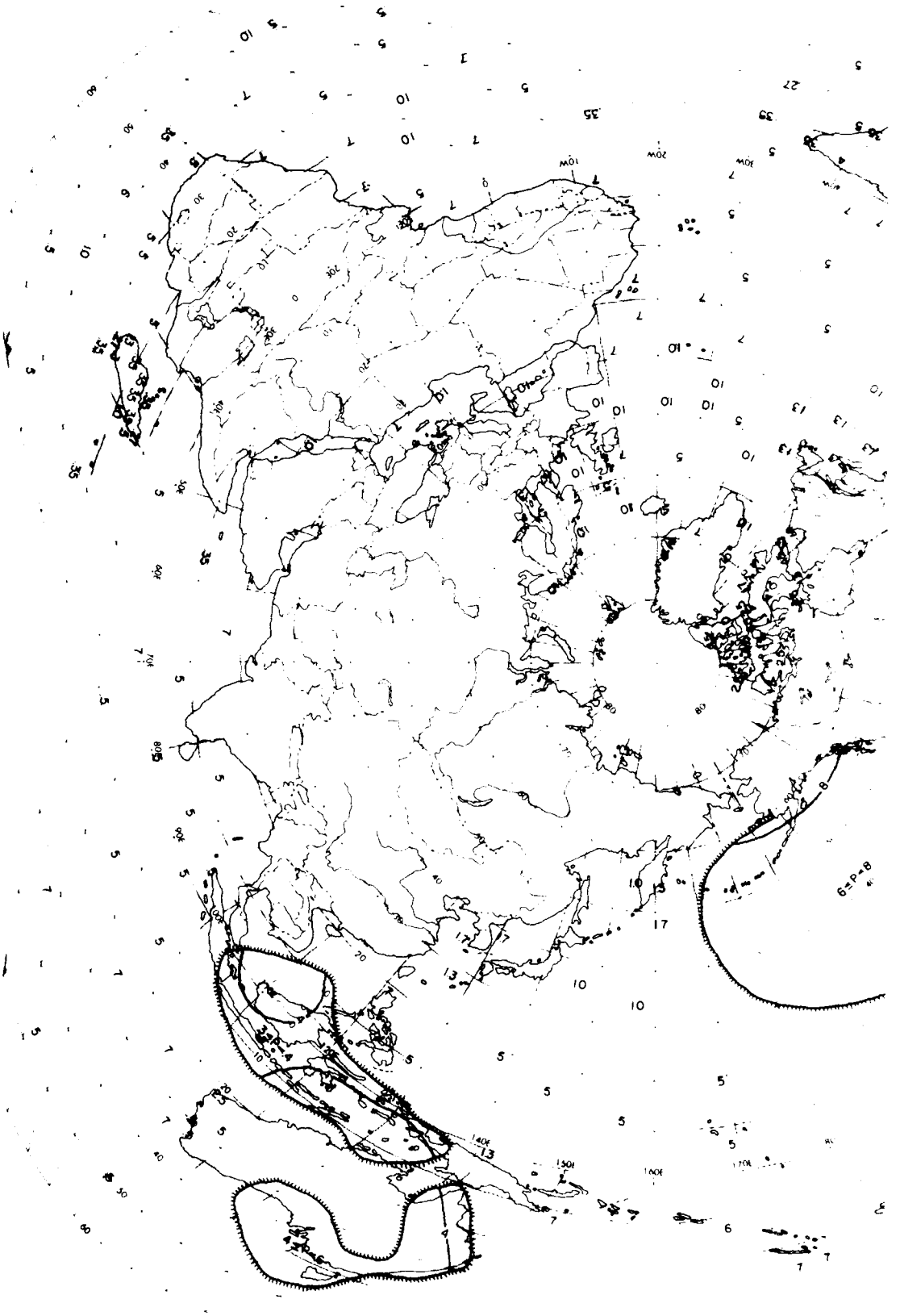

Figure 30b. Monthly Analysis of Scale Distance (r) for April

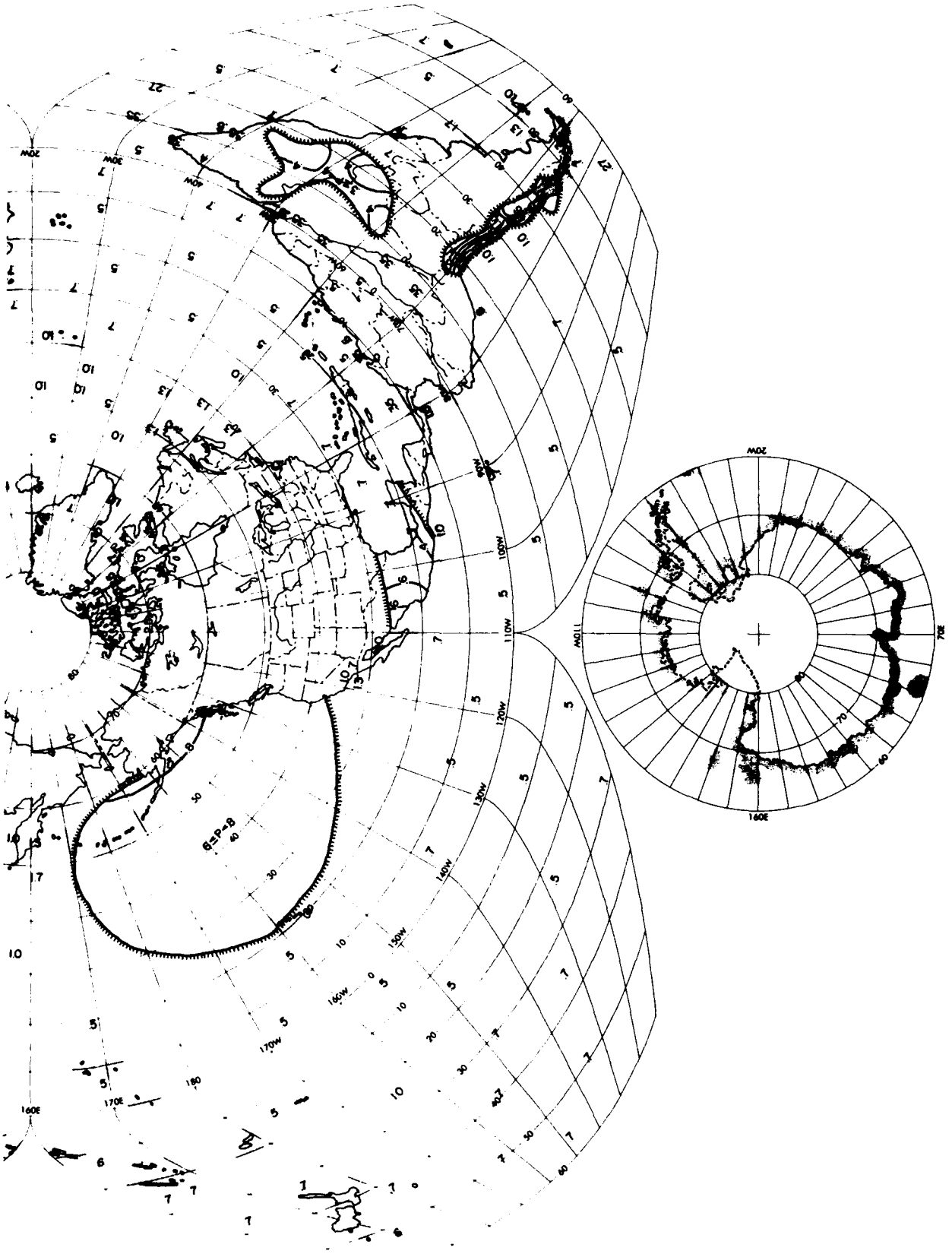

Figure 30b. Monthly Analysis of Scale Distance (r) for April (Contd)

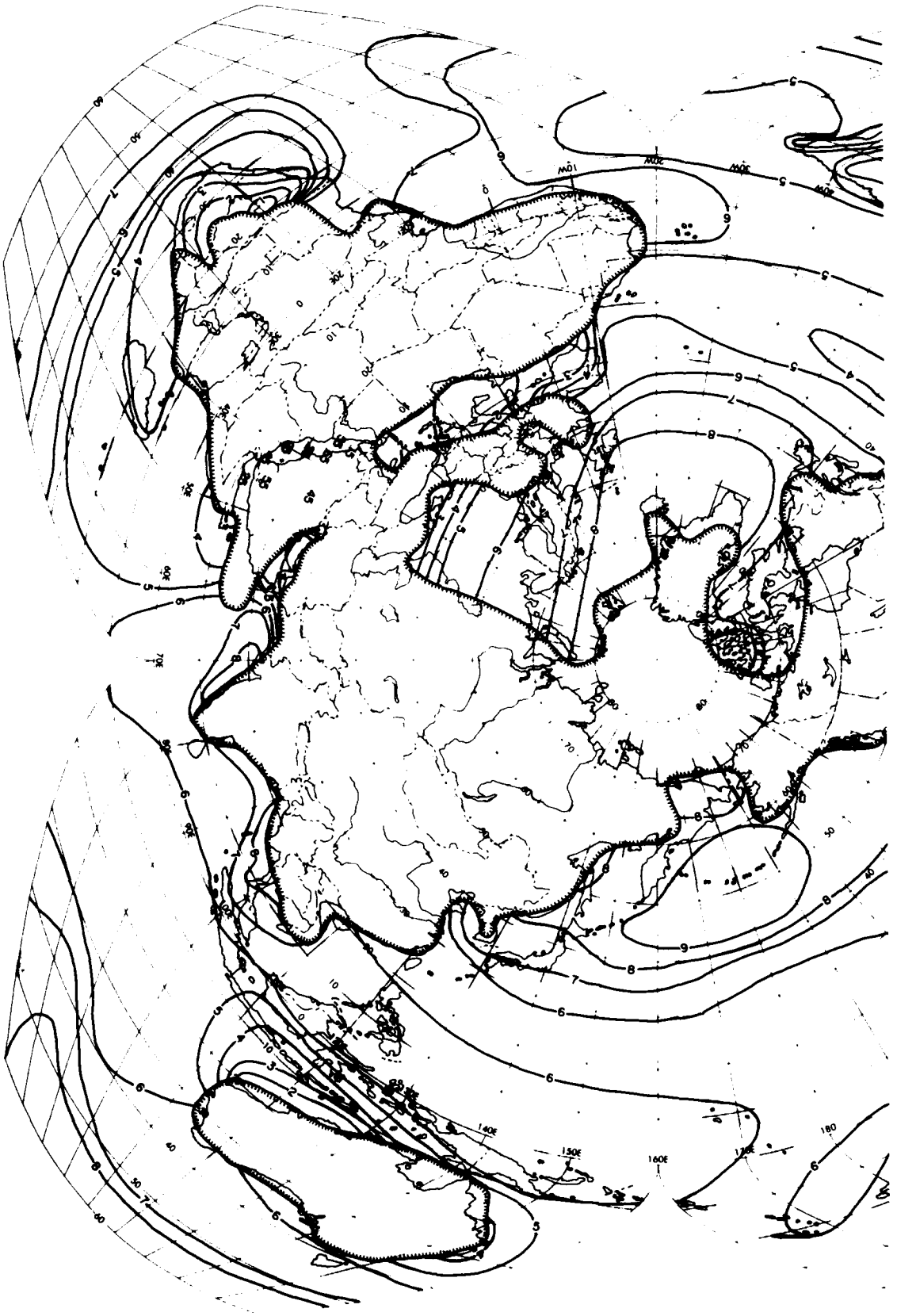

Figure 31a. Monthly Analysis of Mean Sky-Cover (P_o) for July

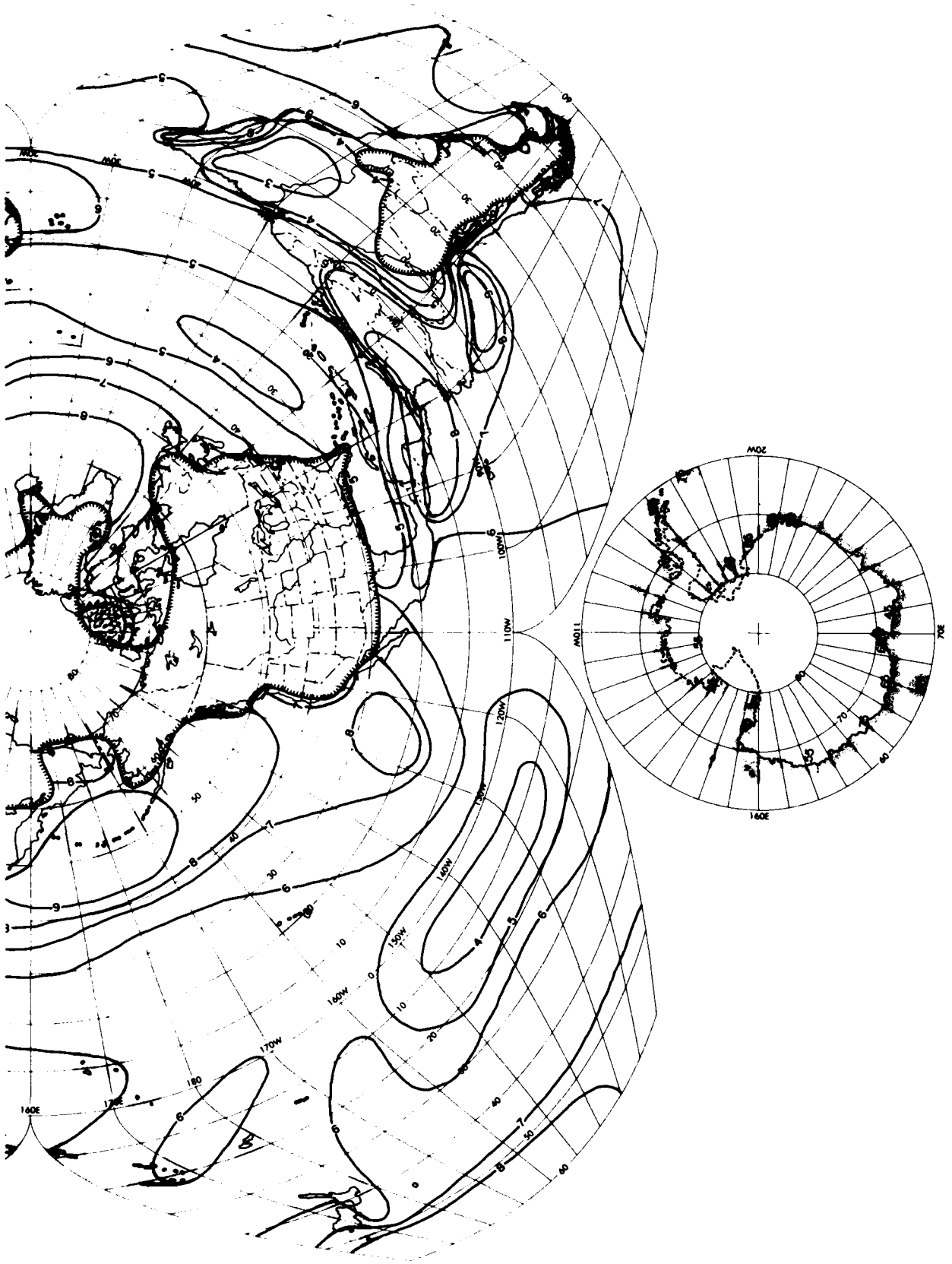

Figure 31a. Monthly Analysis of Mean Sky-Cover (P_o) for July (Contd)

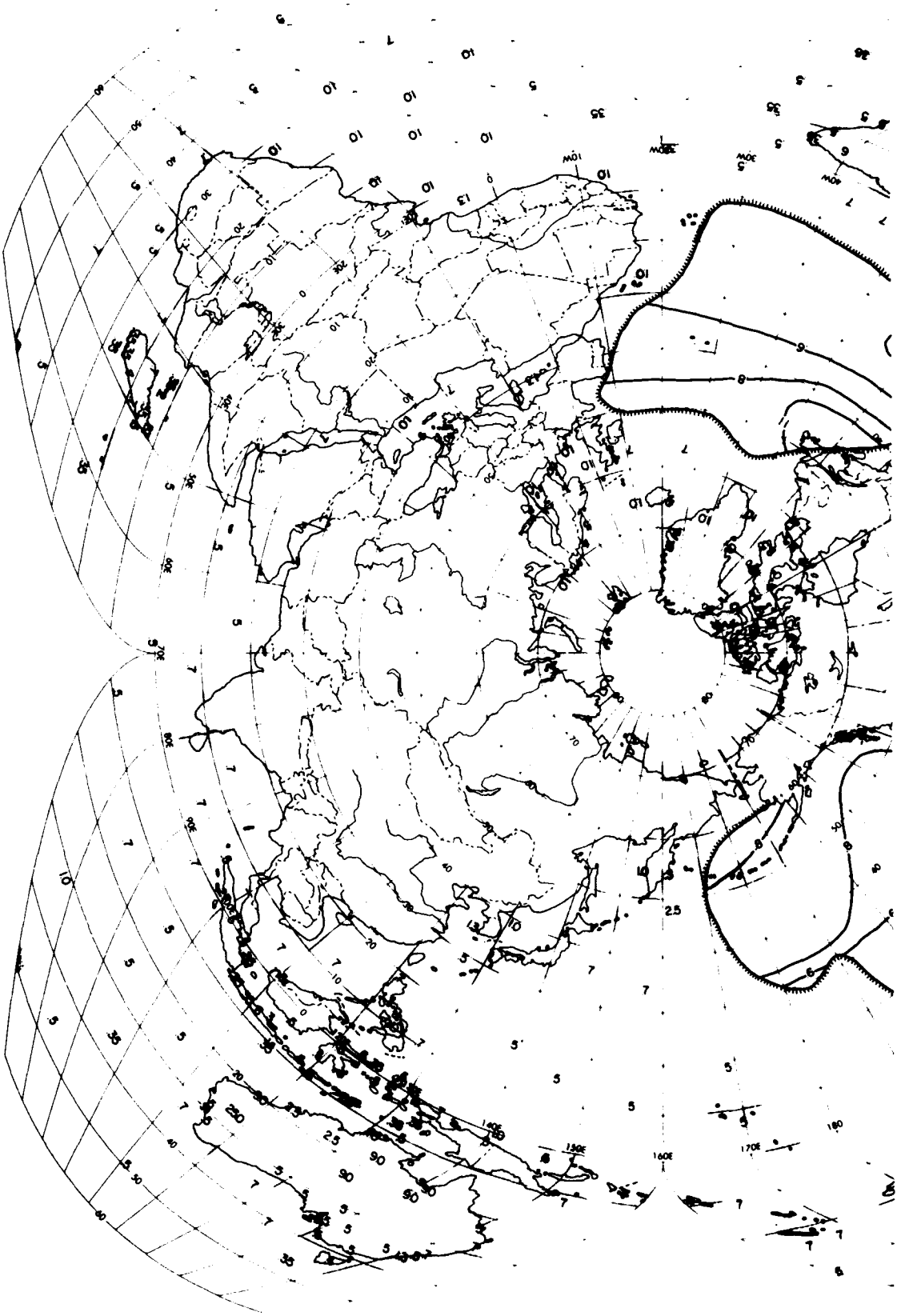

Figure 31b. Monthly Analysis of Scale Distance (r) for July

Figure 31b. Monthly Analysis of Scale Distance (r) for July (Contd)

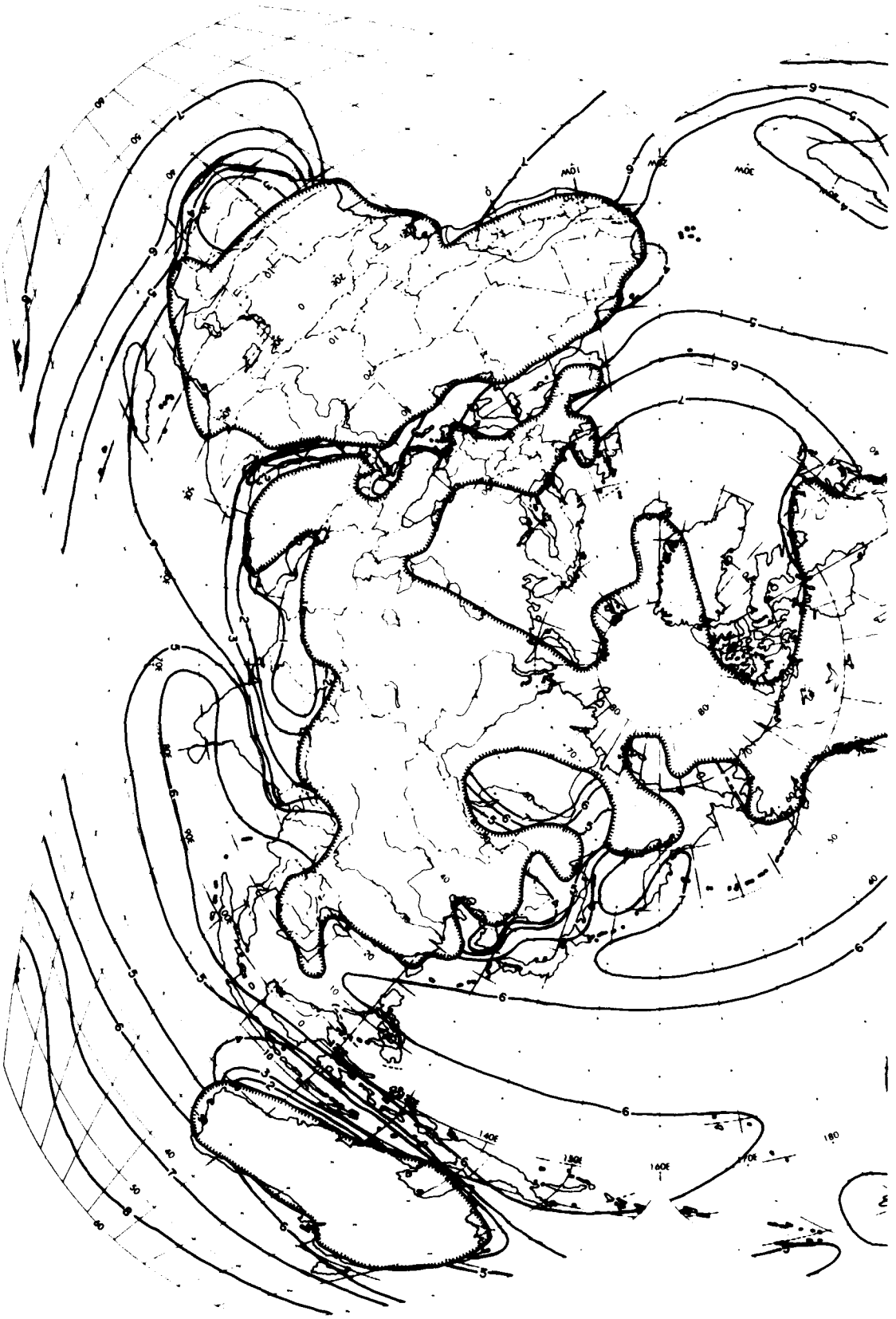

Figure 32a. Monthly Analysis of Mean Sky-Cover (P_o) for October

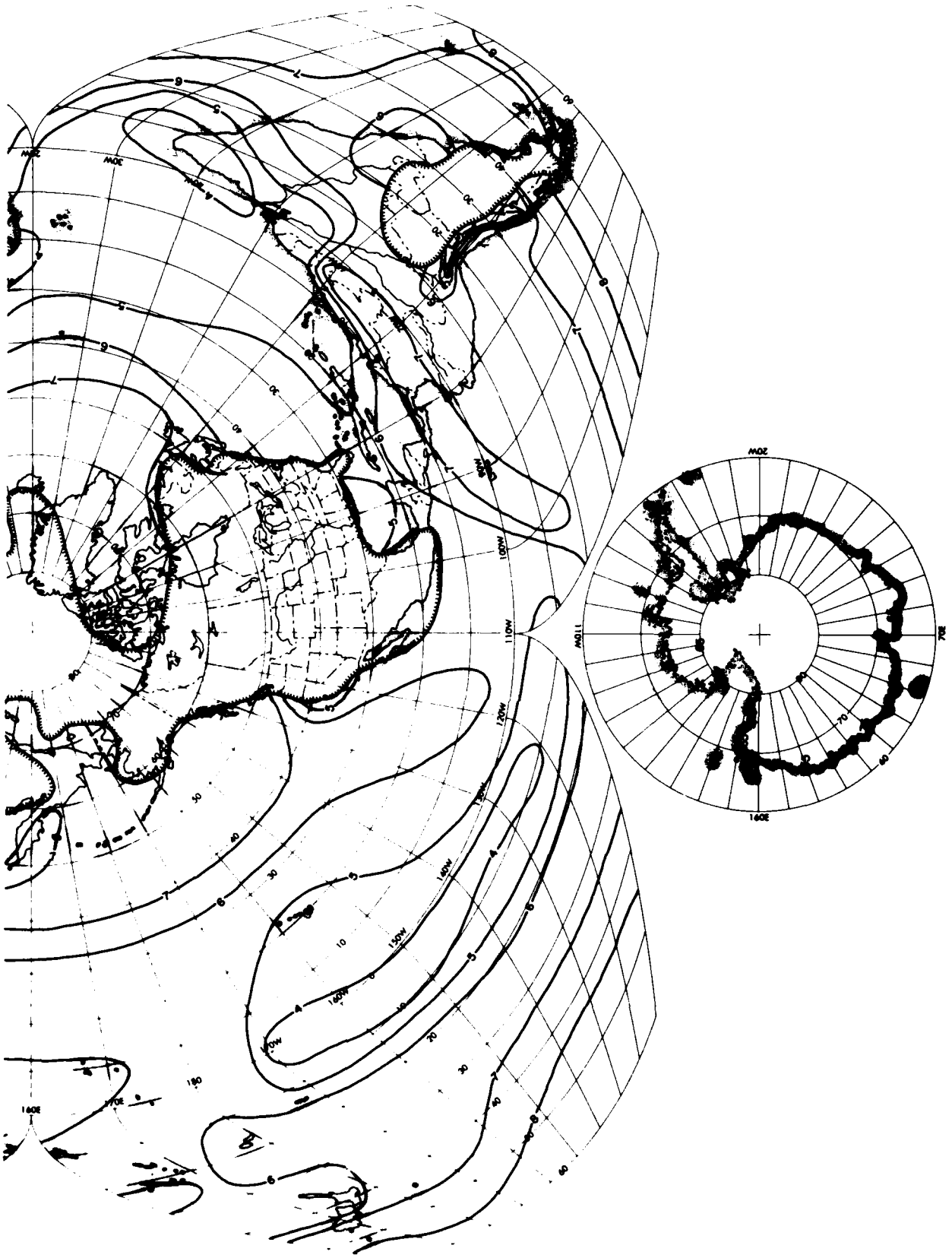

Figure 32a. Monthly Analysis of Mean Sky-Cover (P_o) for October (Contd)

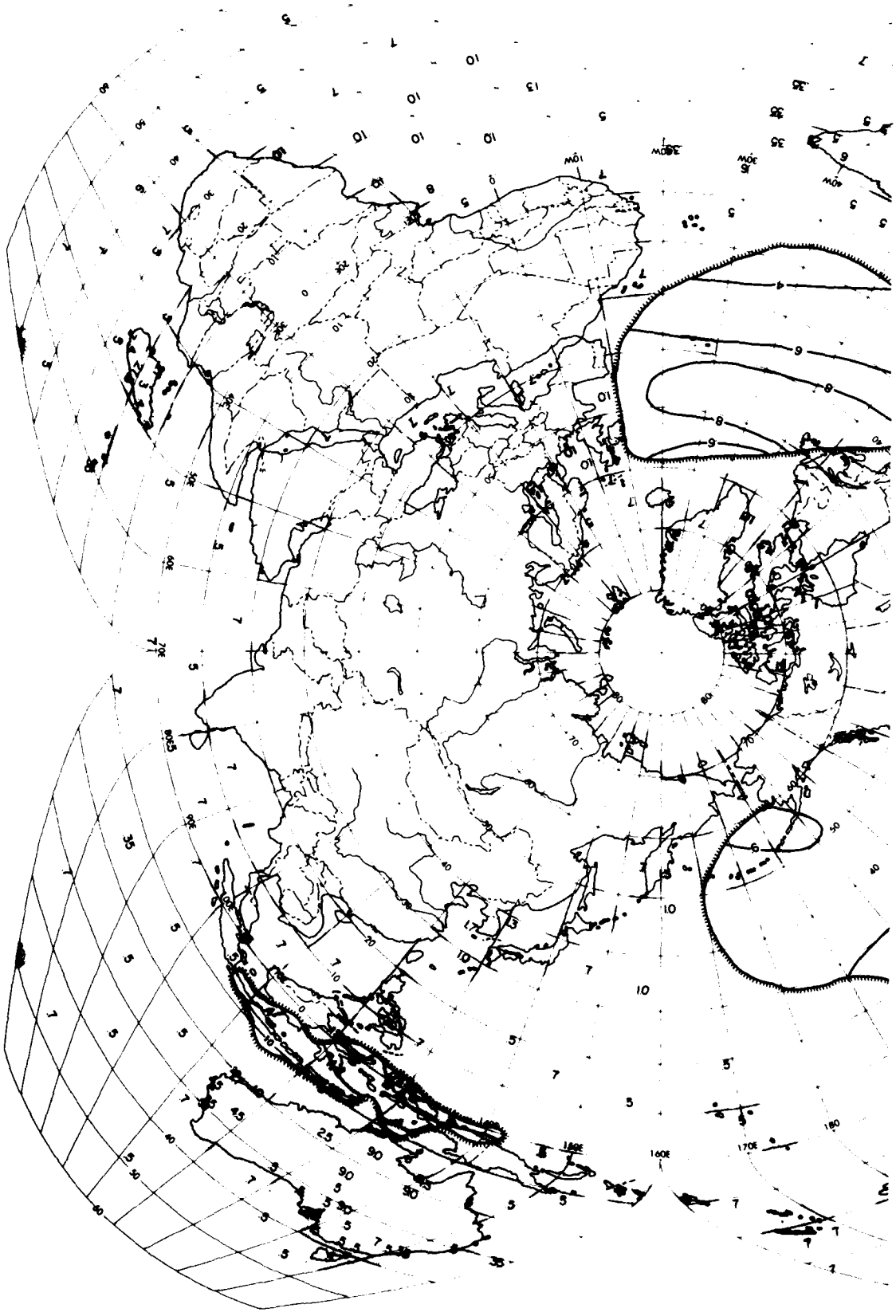

Figure 32b. Monthly Analysis of Scale Distance (r) for October

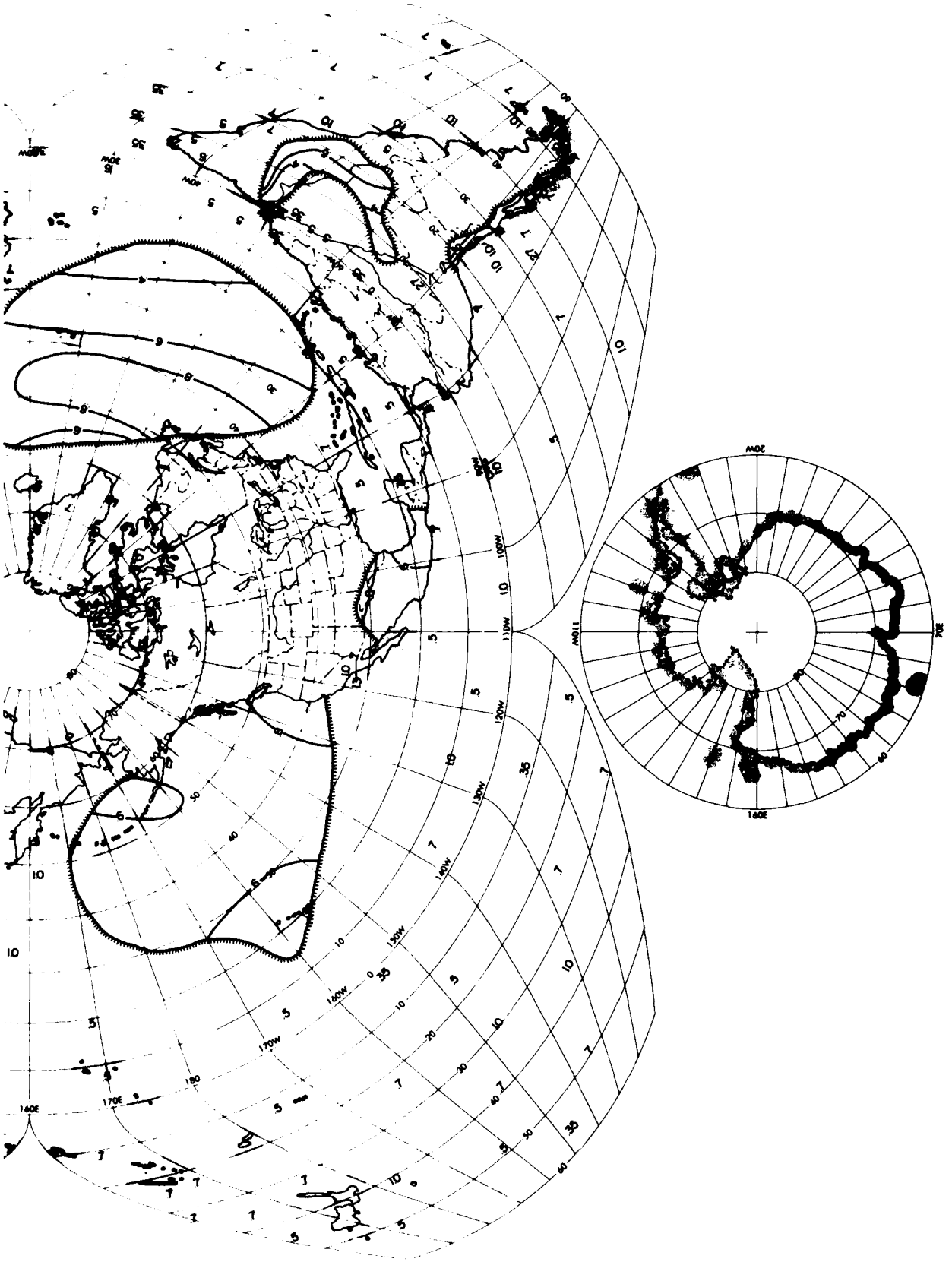

Figure 32b. Monthly Analysis of Scale Distance (r) for October (Contd)

References

1. Schiffer, R. A., and Rossow, W. B. (1983) The International Satellite Cloud Climatology Project (ISCCP): The first project of the World Climate Research Programme, Bull. Am. Meteorol. Soc. 64:779-784.

2. Berry, F. A., Jr., Bollay, E., and Beers, N. R. (1945) Handbook of Meteorology, McGraw-Hill Book Company, Inc., New York, pp. 988-996.

3. London, J. (1957) A Study of the Atmospheric Heat Balance, AFCRC-TR-57-287, Final Report, Contract No. AF 19(122)-165, New York University, ASTIN No. 11 7227.

4. Sadler, J. C. (1966) Average Monthly Cloud Cover for the Global Tropics as Determined from Satellite Observations, Preprint Pamphlet, Contract No. AF 19 (628)-3860, Hawaii Institute of Geophysics, University of Hawaii.

5. Sherr, P. E., Glasen, A. H., Barnes, J. C., and Willand, J. H. (1968) World-Wide Cloud Cover Distribution for Use in Computer Simulations, NASA CR-61226, Final Report, Contract No. NAS 8-21040, Allied Research Associates, Inc., Concord, Mass.

6. Hall, R. J. (1969) Cloud Cover of the USSR, SAMSO-TR-69-147, Vol. 1, Contract No. F04701-68-C-0200, Aerospace Corp.

7. Miller, D. B., and Feddes, R. G. (1971) Global Atlas of Relative Cloud Cover 1967-70, NOAA/NESS, USAFETAC.

8. Malberg, H. (1973) Comparison of mean cloud cover obtained by satellite photographs and ground-based observations over Europe and the Atlantic, Mon. Wea. Rev. 101:893-897.

9. Berlyand, T. G., and Strokina, L. A. (1980) Global distribution of total cloud amount, Gidrometeoizdata, Leningrad (translated by S. Warren).

10. Hahn, C. J., Warren, S. G., London, J., Chervin, R. M., and Jenne, R. (1982) Atlas of Simultaneous Occurrence of Different Cloud Types Over the Ocean, NCAR Technical Note No. TN-201+STR, Atmospheric Analysis and Prediction Division, Boulder, Colo.

11. Hahn, C. J., Warren, S. G., London, J., Chervin, R. M., and Jenne, R. (1984) Atlas of Simultaneous Occurrence of Different Cloud Types Over Land, NCAR Technical Note No. TN-241+STR, Atmospheric Analysis and Prediction Division, Boulder, Colo.

12. Henderson-Sellers, A., and Hughes, N. A. (1984) Cloud Archiving Strategies, AFGL-TR-84-0166, Final Report, Contract/Grant No. AFOSR-83-0118, University of Liverpool, Liverpool, U. K.

13. Henderson-Sellers, A., Hughes, N. A., and Wilson, M. (1981) Cloud archiving on a global scale: a discussion of principles, Bull. Am. Meteorol. Soc. 62:1300-1307.

14. Falls, L. W. (1973) The Beta Distribution: A Statistical Model for World Cloud Cover, NASA Technical Memorandum No. 64714, Marshall Space Flight Center, Ala.

15. Falls, L. W. (1974) The beta distribution: a statistical model for world cloud cover, J. Geophys. Res. 79:1261-1264.

16. Bean, S. J., and Somerville, P. N. (1981) Some new worldwide cloud-cover models, J. Appl. Meteorol. 20:223-228.

17. Somerville, P. N., Watkins, S., and Daley, R. (1978) Some Models for Sky Cover, AFGL-TR-78-0219, Scientific Report No. 2, Contract No. F19628-77-C-0080, Florida Technological University, Orlando, Fla., AD A062650.

18. Somerville, P. N., and Bean, S. J. (1979) A New Model for Sky Cover, AFGL-TR-79-0219, Scientific Report No. 5, Contract No. F19628-77-C-0080, University of Central Florida, Orlando, Fla., AD A078368.

19. Burger, C. F., and Gringorten, I. I. (1984) Two-Dimensional Modeling for Lineal and Areal Probabilities of Weather Conditions, AFGL-TR-84-0126, AD A147970.

20. Quayle, R. G. (1974) A climatic comparison of ocean weather station and transient ship records, Mariners Weather Log 18 (No. 5), NOAA, Environmental Data Service.

21. Lydolph, Paul E. (1977) Climates of the Soviet Union, World Survey of Climatology 7:363-427, Elsevier Scientific Publishing Co., Amsterdam, The Netherlands.

22. Gringorten, I. I. (1981) Mapping the Climate, AFGL-TR-81-0015, AD A102904.

U. S. GOVERNMENT PRINTING OFFICE: 1986--600-000--20,025

END

DTIC

9-86